HOKKAIDO UNIVERSITY

| | |
|---|---|
| Title | Detection of Cercospora Leaf Spot in Sugar Beet by Image-based Robust Tracking and Feature Extraction |
| Author(s) | 周, 嶸 |
| Degree Grantor | 北海道大学 |
| Degree Name | 博士(情報科学) |
| Dissertation Number | 甲第11767号 |
| Issue Date | 2015-03-25 |
| DOI | https://doi.org/10.14943/doctoral.k11767 |
| Doc URL | https://hdl.handle.net/2115/58938 |
| Type | doctoral thesis |
| File Information | Zhou_Rong.pdf |

Hokkaido University Collection of Scholarly and Academic Papers : HUSCAP

SSI-DT79125036

**Doctoral Thesis**

# Detection of Cercospora Leaf Spot in Sugar Beet by Image-based Robust Tracking and Feature Extraction

Rong ZHOU

February, 2015

Division of Systems Science and Informatics
Graduate School of Information Science and Technology
Hokkaido University

Doctoral Thesis
submitted to Graduate School of Information Science and Technology,
Hokkaido University
in partial fulfillment of the requirements for the degree of
Doctor of Philosophy.

Rong ZHOU

Thesis Committee: Shun'ichi KANEKO Professor
Satoshi KANAI Professor
Takayuki TANAKA Associate Professor

# Detection of Cercospora Leaf Spot in Sugar Beet by Image-based Robust Tracking and Feature Extraction*

Rong ZHOU

**Abstract**

This thesis proposes a novel and robust image algorithm for continuous detection of a leaf disease named Cercospora leaf spot (CLS) in sugar beet plant. The CLS is the most destructive foliar disease in sugar beet with high incidences affecting over one-third cultivation area worldwide and approaching 40% sugar losses. Therefore, these large economic factors are the driving forces to continuously detect the CLS for precise plant protection. The aim of this study is to utilize color imaging techniques for robust and continuous CLS detection under real and natural conditions (without any artificial control of ambient luminance and interference of plant growth), by which the accessed information of disease progress can be utilized for the precise plant protection.

The algorithm mainly consists of two frameworks. First is template matching based framework for robust foliar disease tracking against various illumination and living plant movements. Second is feature extraction along with SVM based framework for further disease classification from complex image backgrounds. In the first framework, we proposed an adaptive OCM method which is on the basis of robust orientation code matching (OCM), to achieve consistent and multi-scale foliar disease observation. In the second framework, two novel features with powerful discrimination ability were proposed for classifying CLS under two different conditions: without and with soil. First, a two-dimensional (2D) feature of xy-color histogram was proposed to classify CLS disease under conditions without soil concern. Second, a 3D feature of $L^*$, $a^*$, Entropy $\times$ Density was proposed for conditions involving soil background. The 3D feature attacks a key difficulty for discriminating CLS from clutter sandy soil as they resemble with each other in color. Moreover, it can handle real field conditions to classify CLS against complex visual backgrounds of healthy leaf, leaf stalk, specular reflection and soil.

We conducted experiments for CLS disease detection on two scales and two different conditions. One is detecting CLS on local region scale without soil condition by employing small-scale template tracking and the 2D xy-color histogram feature. Both indoor and field experiments showed that the proposed algorithm can obtain precise disease detection and quantification. The other is detecting disease on a single leaf scale with soil condition by applying leaf-scale template tracking and the 3D $L^*$, $a^*$, Entropy $\times$ Density feature. Field experimental results showed the effectiveness of the proposed algorithm for observing CLS develops in complex field

*Doctoral Thesis, Division of Systems Science and Informatics, Graduate School of Information Science and Technology, Hokkaido University, SSI-DT79125036, February 21, 2015.

conditions. Moreover, comparative experiments demonstrated the superior performances of the proposed two frameworks for tracking and classifying the foliar disease.

This thesis is organized into the following 5 chapters:

The first chapter initially introduces agricultural background and previous image-based studies for plant disease study. Then, we highlighted the difficulties experienced in the field of foliar disease detection, as well as the limitations of existing algorithms. Finally, we briefly described the motivation and concept of this study.

The second chapter introduces the first framework of the proposed algorithm, which is on the basis of the template matching method OCM for robust foliar disease tracking. First, we theoretically analyze the robust performance of OCM for searching foliage against illumination changes. Then, we introduce adaptive OCM for extending the OCM into foliar disease tracking issues. Lastly, we illustrate its applications for tracking disease on two scales, one is on local region scale for achieving subtle disease observation; the other is on a single leaf scale for corresponding practical field application.

The third chapter introduces the second framework of the proposed algorithm, which is based on feature extraction along with SVM for CLS classification against complex and clutter backgrounds. We proposed two powerful discrimination features for classifying CLS disease under two different conditions: one is a color-based feature of 2D xy-color histogram for conditions without soil concern; the other is a color and orientation code histogram based 3D feature combination of $L^*$, $a^*$, Entropy $\times$ Density for conditions with soil concern, which attacked CLS classification problem against clutter sandy soil background.

The forth chapter initially provides experimental information of plant treatments and imaging acquisitions under both indoor and real field conditions, respectively. Then, experimental results are shown into four parts for demonstrating the robustness and effectiveness of the proposed algorithm. First, the robustness of OCM for successful foliage tracking against various illuminations has been experimentally demonstrated and compared. Second, the necessity and effectiveness of adaptive OCM for foliar disease tracking are comparatively discussed. Third, experimental results for local-regional disease detection without considering soil background are shown under both indoor and field conditions. The mean precision value for the classification results compared with manual classifications is above 0.94 in the indoor conditions and 0.59 in the dramatically changed field conditions, respectively. Forth, results of a single leaf scale based disease detection under challenging real field conditions with complex backgrounds are shown, and the mean precision value is above 0.53. In addition, comparative experiment results show the effectiveness and relatively robust performance of the proposed 3D feature for the disease classification.

The Last chapter summaries the main contributions of the research and discusses future work.

**Keywords:** disease detection, image analysis, robustness, Cercospora leaf spot (CLS), sugar beet, image tracking, template matching, orientation code matching (OCM), image classification, pattern recognition (PR), support vector machine(SVM), color distribution, entropy, density, natural daylight, variant illumination, clutter soil background, complex field conditions

# Contents


**1. Introduction** **1**

1.1 Research background . . . 1

1.1.1 Cercospora leaf spot (CLS) in sugar beet . . . 1

1.1.2 Precision plant protection and disease monitoring . . . 2

1.2 Image-based foliar disease detection . . . 2

1.2.1 Color image processing . . . 3

1.2.2 Spectral image processing . . . 4

1.2.3 Optical sensor fusion systems . . . 4

1.3 Difficulties and limitations in foliar disease detection . . . 5

1.3.1 Difficulties in foliar disease detection . . . 5

1.3.2 Limitations of existing algorithms . . . 6

1.4 Motivation of the research . . . 6

1.5 Overview . . . 8

**2. OCM based foliar disease tracking** **10**

2.1 Orientation code matching (OCM) . . . 10

2.2 Robustness of OCM for foliage searching . . . 11

2.3 Adaptive OCM for foliar disease tracking . . . 12

2.3.1 Disease tracking on local region scale . . . 15

2.3.2 Disease tracking on a single leaf scale . . . 15

2.3.3 Discussion on initial template selection . . . 16

2.4 Summary . . . 16

**3. Feature extraction along with SVM for CLS classification** **17**

3.1 Importance of feature extraction . . . 17

3.2 Support vector machine (SVM) . . . 18

3.3 Without soil condition . . . 18

3.3.1 Feature extraction: (2D) xy-color histogram . . . 19

3.3.2 Dataset for SVM modelling . . . 22

3.4 With soil condition . . . 22

3.4.1 Feature extraction: (3D) $L^*$, $a^*$, Entropy $\times$ Density . . . 23

3.4.2 Parameter optimization . . . 24

3.4.3 Dataset for SVM modelling . . . 27

3.4.4 Edge detection based post-processing . . . 29

3.5 Summary . . . 32

**4. Experimental treatments and results** **35**
4.1 Plant cultivation and pathogen inoculation . . . . . 35
4.1.1 Indoor experiment . . . . . 35
4.1.2 Field experiment . . . . . 36
4.2 Experiment configuration . . . . . 36
4.2.1 Indoor experiment . . . . . 36
4.2.2 Field experiment . . . . . 36
4.3 Robustness of OCM for foliage searching . . . . . 36
4.4 Effectiveness of adaptive OCM for foliar disease tracking . . . . . 41
4.5 Disease detection on local region scale without soil condition . . . . . 43
4.5.1 Indoor experiment . . . . . 43
4.5.2 Field experiment . . . . . 48
4.6 Disease detection on a single leaf scale with soil condition . . . . . 54
4.6.1 Field experiment . . . . . 54
4.7 Summary . . . . . 63

**5. Conclusions** **64**
5.1 Thesis contributions . . . . . 64
5.2 Discussion and future work . . . . . 65
5.3 Conclusion . . . . . 67

**Acknowledgements** **68**

**References** **69**

**A. Publication lists** **74**
A.1 Journal Papers . . . . . 74
A.2 International Conferences . . . . . 74
A.3 Japan Conferences . . . . . 74

# List of Figures


1.1 Symptoms' development of Cercospora leaf spots in sugar beet plant. . . . . 2

2.1 Robustness of orientation code (OC) under different illuminations. (a) A beet leaf captured under two different lights/illuminations; (b) grayscale images of the leaf and (c) the corresponding OC images. . . . . 13
2.2 Illustration of adaptive template measurement. . . . . 14
2.3 Adaptive OCM for tracking local region of leaf among plant sequential images. 15
2.4 Adaptive OCM for tracking a single leaf among plant sequential images. . . . . 15

3.1 Intensity curves of a single pixel P in (a) RGB and (b) xyY color spaces, respectively, under various illumination conditions (c). . . . . 20
3.2 Comparable example of 2D xy-color histogram for templates belonging to disease, health, and background respectively under indoor condition. . . . . 21
3.3 Comparable example of 2D xy-color histogram for pixels belonging to disease, health, and background respectively under field condition. . . . . 21
3.4 Demonstration the process for calculating the orientation code histogram based feature of Entropy × Density for CLS and soil classification. (a) CLS and soil regions extracted from the center pixel (x,y); (b) $a^*$ component images for the two regions; (c) orientation code histograms and the value of Entropy × Density for the two regions. . . . . 25
3.5 Effectiveness of the proposed 3D feature combination of $L^*$, $a^*$, Entropy × Density for classifying CLS patterns against other four patterns of healthy leaf, leaf stalk, highlighted leaf surface, and sandy soil under field condition. (a) 100 pixels were extracted for the each pattern; (b) results of the proposed 3D feature combination for the five patterns; (c) and (d) are the top view and side view for the feature space visualizations respectively. . . . . 26
3.6 Optimization of the regional size *M* for Entropy×Density. (a) Fisher's criterion; (b) classification accuracy; (c) computation time. . . . . 28
3.7 Fault cases for CLS and soil discriminations by Entropy × Density due to the complex field conditions. (a) A fault example for a soil region locating at leaf boundary; (b) a fault example for a CLS region locating at heavily destroyed leaf part. . . . . 30

3.8 False positive and false negative pixels in the classification result aroused from the feature of Entropy × Density. (a) An leaf image; (b) classification result by the proposed SVM classifier; (c) ground truth; (d) false positive pixels (in red color) mainly concentrated at leaf edges; (e) false negative pixels (in red color) mainly concentrated at heavily destroyed leaf parts. (The blue areas correspond to the background region.) . . . . . 31
3.9 Edge based post-processing to filter the false positive noise. (The blue areas correspond to the background region.) . . . . . 31
3.10 Comparative results for edge detection of leaf by different detectors with various thresholds. . . . . 33
3.11 Distance value $dist(\triangle P, \triangle R)$ calculated from different $T_{Canny}$ and $N$ combinations for parameter optimization. . . . . 33

4.1 Graphic illustration of indoor experiment setup. . . . . 37
4.2 Graphic illustration of field experiment setup. . . . . 38
4.3 Comparation of matching results by OCM, SAD, SSD and NCC methods for time sequence plant images all through a day. . . . . 39
4.4 The comparative visualization results for the robustness of OCM against illumination changes. . . . . 40
4.5 Comparative 3-D plots of the similarity values around the best match position in the object scene at time 13:00 by OCM, SAD, SSD and NCC methods respectively. 41
4.6 Comparative tracking results for foliar disease at early stage by adaptive OCM and OCM respectively. . . . . 42
4.7 Comparative tracking results for foliar disease at late stage by adaptive OCM and OCM respectively. . . . . 42
4.8 Illustration of the five templates extraction and illumination conditions for seven plant frames over the experimental week period under indoor condition. (a) Extraction of five effective templates from the plant image frame on December 28, 2012 for disease development observation over time; (b) average intensity for each plant frame among all plant time sequence images. . . . . 43
4.9 Visualization results of adaptive template matching and disease classification for disease development observation with two different templates out of the five under indoor condition. (a) Result of template_1 and (b) result of template_3. (The blue areas correspond to the disease region. The gridding and red square are for position references of the template matching.) . . . . . 45
4.10 Quantitative results for the disease development of the five effective templates under indoor condition. (a) by our proposed method; (b) by manually classification. . . . . 46
4.11 Performance evaluation of our proposed method by comparison with the manual classification results for (a) precision, (b) recall, and (c) $F$-measure under indoor condition. . . . . 47

4.12 Illustration of the five templates extraction and local illumination conditions for the five templates during the five-day experimental period under field condition. (a) Extraction of five effective templates from the plant image frame on September 17, 2013 for disease development observation over time; (b) average intensity for each template during the five-day period. . . . . 49
4.13 Visualization results of adaptive template matching and disease classification for disease development observation with three different templates out of the five under field condition. (a) Result of template_1, (b) result of template_3 and (c) result of template_5. (The blue areas correspond to the disease region. The red square is for position references of the template matching.) . . . . . 51
4.14 Quantitative results for the disease development of the five templates by both (a) our proposed method and (b) manually classification under field condition. . . . 52
4.15 Performance evaluation of our proposed method by comparison with the manual classification results for (a) precision, (b) recall, and (c) *F*-measure under field condition. . . . . 53
4.16 Visualization for single leaf based continuous CLS observation for two selected single leaves over five-day period. The upper part is for an older leaf and lower one if for a younger leaf. (The blue areas correspond to the background region.) 56
4.17 Visualization for single leaf based continuous CLS observation for two selected single leaves over five-day period. The upper part is for an older leaf and lower one if for a younger leaf. (The blue areas correspond to the background region.) 57
4.18 Comparative classification results of precision, recall, and *F*-measure for showing the effectiveness of $L^*$, $a^*$, Entropy $\times$ Density compared with $L^*$, $a^*$, Entropy and $L^*$, $a^*$, Density. (a) Results of the older leaf; (b) results of the younger leaf. 59
4.19 Comparative classification results of precision, recall, and *F*-measure from different feature combinations. (a) Results of the older leaf; (b) results of the younger leaf. . . . . 61
4.20 Comparative classification results of precision, recall, and *F*-measure from two types of datasets. (a) Results of the older leaf; (b) results of the younger leaf. . 62

# List of Tables


4.1 Mean precision, recall, and $F$-measure values for the five templates under indoor condition. . . . . 48
4.2 Mean precision, recall, and $F$-measure values for the five templates under field condition. . . . . 52
4.3 Mean precision, recall, and $F$-measure values for the two templates of the older and younger single leaves over the five-day field experiment period. . . . . 55
4.4 Mean precision, recall, and $F$-measure values for the comparative classification results for showing the effectiveness of Entropy $\times$ Density over the five-day field experiment period. . . . . 58
4.5 Mean precision, recall, and $F$-measure values for the comparative classification results from different feature combinations over the five-day field experiment period. . . . . 60
4.6 Mean precision, recall, and $F$-measure values for the comparative classification results from different types of datasets over the five-day field experiment period. 63

# Chapter 1. Introduction

This interdisciplinary research linking image processing with agriculture-oriented application for detecting a foliar disease in sugar beet plant. Plant diseases are of critical importance to humans because they damage plants and reduce plant production on which human relay for fundamental food supply [1]. Therefore, continuous and accurate disease detection is in great need and as a prerequisite to provide essential disease information, by which effective plant protection such as optimal decision of fungicide spraying [2, 3], detailed analysis of plant pathology [4], efficacy evaluation of fungicide application [5] can be facilitated. However, variations and complexities from real environments caused by natural daylight, living plant growth and movements, and complex field background are of great challenge for image algorithms. Thus, this thesis proposes a novel algorithm which can cope with the variations and complexities for robust and continuous disease detection. In this chapter, we introduce this research from both aspects of agricultural needs and image-based techniques.

## 1.1 Research background

### 1.1.1 Cercospora leaf spot (CLS) in sugar beet

Sugar beet (cv. Beta vulgaris) is a commercial plant, which accounts for 20% of the world's sugar production [6]. Its large rooted with high content of sucrose is for sugar extraction. However, it is vulnerable to many pathogens which will negatively affect the sugar purity and production. Among those, Cercospora leaf spot (CLS) is the most destructive leaf disease in sugar beet with high incidences affecting over one-third of sugar beet cultivation area worldwide [7] and approaching 40% sugar reduction [8].

CLS is caused by the fungus *Cercospora beticola*, which survives on infected beet plants, in the form of residual spores (conidiophores) and stromata. Under favorable conditions (especially in high temperature and humidity), spores will germinate and penetrate leaf surface and damage the photosynthetic apparatus of the leaf. Early symptoms feature as isolated and circular leaf spots with ash-colored centers and purple to brown borders. As the disease develops, individual spots will coalesce and heavily infect leaf tissue by expanding their size [8]. The speed of the disease spread varies with different environment conditions. Fig. 1.1 shows CLS disease development observed under indoor conditions (around 23° and 40% relative humidity). Small and isolated spots were visible on leaf surface at 4 weeks after inoculation. As time pasts, the spots enlarged with its size (as seen in 7 weeks), and then some of them integrated with each other and formed as lager necrotic areas (as seen in 10 weeks). Meanwhile, from the zoom-in

subimage, an interesting phenomenon can be observed that the diffusion speed of individual spots are different with each other even if they appear on a same leaf surface. This acts as individual variability of the disease spot spreading.

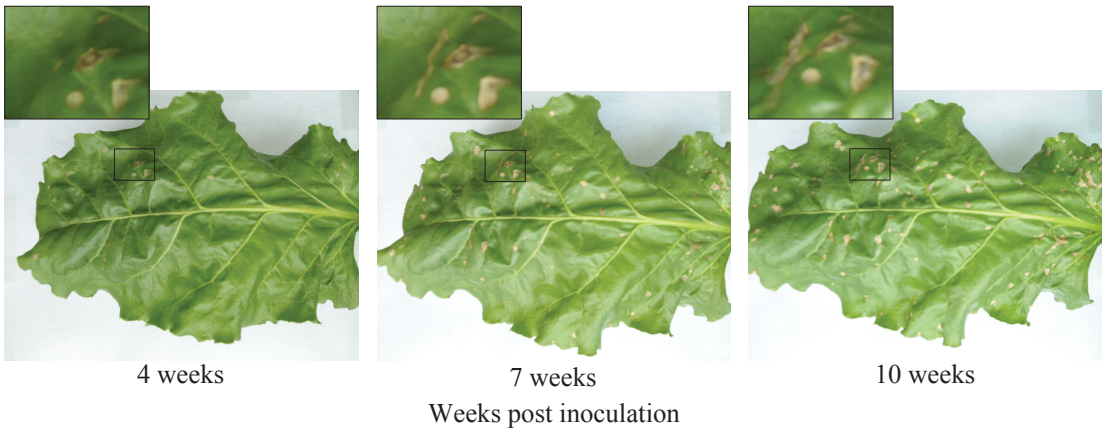



Figure 1.1: Symptoms' development of Cercospora leaf spots in sugar beet plant.

### 1.1.2 Precision plant protection and disease monitoring

Since non-chemical disease control managements such as plant resistant cultivates, crop rotation, or multiple fungicide application do not provide adequate disease prevention. Alternative fungicide spraying is the most important tool for managing disease spread [9]. Usually, optimal and profitable decisions for the timing and frequency of the adaptive fungicide spraying are made in terms of disease severity and local weather conditions [3], by which both economic losses and chemical usage can be reduced for precision plant protection. Therefore, information of disease severity assessment is a fundamental premise for the decision-making process of fungicide sprays [10, 11].

The traditional way for CLS severity assessment is manual field monitoring. It is a process that specialists or trained assessors first walk into field with time intervals, and then assess the disease severity by naked eye observation based on a certain rating criterion, such as a single leaf scale based [3] or a whole plant scale based [12]. However, this human eye and hand operation based filed monitoring has limitations of laborious, discontinuous, some degree of subjective with large-scale field, and imprecise with subtle disease variations. Especially, the discontinuous monitoring may cause high possibilities to late fungicide sprays and over-extended spray intervals, resulting in inefficient plant protection.

## 1.2 Image-based foliar disease detection

To overcome these problems, an automatic, consistent, reproducible and precise disease detection method is desirable and essential for precise plant protection [13, 14]. In recent years,

image sensing techniques have been extensively explored for plant disease study because of their merits of noninvasive, rapid, continuous, and precise measurement capacities [4, 15]. Especially, visible spectrum sensing (400–700 nm) such as RGB color image, as well as some invisible spectrum sensing techniques of multispectral imaging (separate the wavelengths into numerous bands) and hyperspectral imaging (finer spectral resolution), are currently gaining much interest for their well-demonstrated results in detecting, diagnosing, categorizing, and quantizing plant diseases.

In [16], authors provided a comprehensive overview for currently used technologies that can assist in detecting diseases in plants under field conditions, in which both visible and spectroscopic imaging techniques can be accessible. In [13], authors presented a detailed review for three approaches used in estimating plant disease severity, two of them are image-based techniques: visible digitalization imagery and hyperspectral imaging. The review introduced the backgrounds, applications and future needs of the both imaging methods for disease assessment. A review in [15] outlines the advances of optical sensors for sensing plant diseases on different scales for precision crop protection.

### 1.2.1 Color image processing

Digital cameras are inexpensive and widely used imaging devices, by which visible sensing-based RGB color images can be easily accessed for various applications. By color image processing, many human visual work can be automated and elaborated. The human eye is thought to percept and distinguish about 10 million different colors while digital cameras are capable of 16.8 million ($2^{8+8+8}$, 8 bit per color in R,G,B component) colors.

For plant disease study, a pioneering study in 1980 [17] introduced the digital image analysis in plant pathology, and demonstrated the applicability of image processing for disease assessment. Several studies afterwards demonstrated color image analysis to be superior to human visual raters in accuracy and repeatability [18, 19, 20]. Over the past three decades, extensive studies utilized color image processing for detecting and analyzing diseases in various plants. [21] used RGB and photosynthetic efficiency (PE) images for early prediction of the disease outbreak in cabbage leaf by comparing the pixel-wise image registration schemes of penalized likelihood warping with robust point matching methods. This method can handle the leaf warping and slit overlapping problems during leaf growth processes. [22] developed a disease segmentation algorithm for diverse crop disease identification by determining the threshold value according to the position of a set of local maxima in the histogram. This algorithm can cope with large intensity distributions of the image set. Furthermore, [23] conducted a continuous study using a support vector machine (SVM) to classify different disease causing agents in cotton crops. A set of features, such as shape, textures, and fractal dimension, were extracted from disease regions and a best classification model with a classification rate of 93.1% was achieved via cross-validation. To improve the accuracy and stability of a classifier model for disease classification, [24] developed an SVM-based multiple classifier system (MCS) with color, texture, and shape features to categorize different leaf diseases in wheat plants. An improved accuracy

rate of 96.16% was demonstrated for the performance of the MCS compared with that of other pattern recognition methods. Authors in [25] employed artificial neural network along with color and texture features for detecting and classifying three foliar diseases in Phalaenopsis seedling based on color images. In [26], the research uses elementary color analysis to built a multivariate decision model for discriminating asymptomatic and symptomatic seeds of soybean for the grain inspection and grading. Author in [27] presented a survey on digital image processing techniques for detecting, quantifying and classifying plant diseases, the paper summarized and sorted related researches according to their different research objects, purposes, and image techniques.

### 1.2.2 Spectral image processing

Spectral imaging is an optical sensing technique that measures a wide range of the electromagnetic spectrum in discrete spectral wave bands. It forms as similar as color image, but each pixel acquires many bands of light intensity data from the spectrum, instead of just the three bands of the RGB color image [28]. Compared with the color image, it can discern massive amount spectral information but needs enormous storage and is more expensive. Besides, a normalisation process is commonly required to adjust spectral reflectance with ambient illumination.

Spectral image processing is a relatively new technique, and its applications in plant disease study is particular recent. One of the earliest studies using the spectral image in 2003 [29] was to detect yellow rust disease in wheat fields by a spectrograph mounted on a self-made buggy, a discriminating model was proposed for diseased and healthy spectra differentiation, with a classification accuracy of 96%. Over the past ten years, spectral imaging has been shown as a convincing way for foliar disease detection, by detecting specific spectral reflectance for a particular disease of a given plant species [30]. And it has also been explored in many researches for investigating various plant diseases' spectrum information.[31] employed multispectral radiometer for the identification of panicle blast in rice, and showed that further airborne multispectral scanners may be effectively extended by the spectral range selected. [32] used hyperspectral imaging to detect disease at an early stage and distinguish different pathogens caused leaf diseases in sugar beet plants. [33] also introduced a hyperspectral imaging for detection, differentiation and quantification of diseases in sugar beet based on small-scale analysis, which could facilitate detailed description and understanding of disease development. Researchers in [34] investigated the sensitivity of disease detection from different view angles of canopy by multispectral image analysis and suggested a range of view angles from 40° to 60° to improve early detection of disease symptoms.

### 1.2.3 Optical sensor fusion systems

Furthermore, some researchers designed imaging systems by combining different optical sensors with their complementary advantages to provide more comprehensive disease analysis.

But the optical sensor fusion systems are usually costly and not easy to operate.

[35] evaluated the performance of four proximal optical sensors (RGB color imaging, spectrophotometer, spectral imaging and chlorophyll fluorescence imaging) for detecting tulip breaking virus (TBV) in tulips. [36] designed a multi-sensor fusion disease detection system based on hyperspectral and multispectral fluorescence imaging sensors for detecting diseases in arable crops under field condition. [37] employed a multi-sensoral approach involves airborne hyperspectral imaging, HyMap sensor and spectroradiometer to detect disease in sugar beet fields at different growth stages respectively. [38] developed a tractor mounted cost-effective optical sensor fusion system by combining hyperspectral and fluorescence imaging to detect and recognize yellow rust disease of winter wheat in the field conditions. The combined measurements showed the discrimination between diseased and healthy plants with accuracy of 94%, demonstrating a great potential for developing fusion optical sensors based tractor system for recognizing diseased plants in field.

## 1.3 Difficulties and limitations in foliar disease detection

### 1.3.1 Difficulties in foliar disease detection

For practical application of foliar disease detection in real environments without any artificial control of ambient luminance and interference of natural plant growth, such as in transparent greenhouses or real fields, environmental variations and complexities will disturb the robustness of image algorithms. Therefore, prior to designing a image algorithm, difficulties aroused from the real environments need to be considered and resisted for achieving robust and consistent disease observation:

I. Illumination changes and irregulations.

- Changeable illumination is a crucial and primary issue leading brightness intensities of plant images captured under natural sunlight conditions vary from time to time.
- In addition, illumination irregulations of shadow, highlight, and specular reflection also exist in the images due to irregular light reflection on leaf/stalk surface.

Therefore, algorithm should be primarily robust and insensitive to the changes and irregulations in illumination/lights. That is to say, robust patterns and features which are irrelevant to the illumination variations should be learned and extracted to keep consistency for disease observation along time.

II. Leaf growth and movements.

Plant is a living organism, so incessant growth and movements exist in non-rigid plant.

- Plant growth is a irreversible process increasing the size of the plant. The growth process acts as scale changes of leaf objects among plant sequential images.

- Simultaneously, leaf movements caused by internal circadian clock and external environment interactions (such as drought, wind and rain) perform as composite motions of the leaf objects including translation, rotation, occlusion and even shape deformation in the images.

These variations of the leaf objects cause difficulties for aligning identical leaf patches/parts from the sequential plant images, leading inconsistency for disease observation. Therefore, image algorithm should also be capable to tolerate the variable leaf growth and movements.

III. Complex field backgrounds.

Under real field conditions, excepting for plant disease, image scene contains complex backgrounds with healthy leaves, leaf stalks, specular reflection and sandy soil.

- For detecting disease from the complex backgrounds, a initially key problem of clutter sandy soil which resembles reddish brown color with CLS disease will greatly upgrade the difficulties for the CLS classification from the image scene. Additionally, soil color is varying with different wetness in soil over time.
- Besides, highlighted leaf stalk and specular reflection due to glossy leaf surface sharing similar light-brown color with the inner of spots are also parts of problems for the disease classification.

The complexities and color resembling problems give rise to difficulties for CLS disease detection under real field conditions. Therefore, image algorithm should be capable to deal with the challenging disease classification issues.

### 1.3.2 Limitations of existing algorithms

With difficulties illustrated above, however, most of the prior research work in this filed focused only on detecting disease:

- under well-controlled environment with artificial luminance;
- and/or from static images with zoom-in or small quadrats of leaves;
- and/or without considering soil background.

These lead algorithms lacking robustness against the variations and complexities, thus limiting their further applications for long-term, consistent, and comprehensive disease detection under natural and real environments.

## 1.4 Motivation of the research

In this study, we intent to:

- explore a robust image algorithm for continuous CLS detection in sugar beet under natural daylight conditions without any artificial interference and invasion of plants;
- use RGB color images captured by easily accessed digital cameras with our long-term target to develop a cost-effective, easy-operated and portable disease evaluation system, which can be used in practical field by both specialists and farmers;
- utilize plant-level image sequences to provide comprehensive disease progress temporally and spatially for each individual plant;
- attack the challenging classification problem between CLS and soil to promote the algorithm for real field application.

For achieving the continuous CLS detection from the plant-level image sequences, algorithm should meet two fundamental capabilities. First is continuity, which can align identical leaf parts through neighbouring frames for consistent foliar disease tracking. Second is discriminability, which can further classify CLS disease against the image backgrounds. However, as being discussed in previous section, the existed difficulties often disturb the robustness of image algorithms to achieve the continuity and discriminability. In this study, we propose a novel matching-based disease detection algorithm, which mainly consists of two frameworks and addressed those difficulties.

First, a robust template matching scheme called orientation code matching (OCM) [39, 40], which has shown its excellent performance in a wide range of applications such as visual control [41, 42], medical imaging [43], surveillance [44], intelligent transport system [45], optical flow computation [46], stereo vision sensor [47] and other practical applications, is initially introduced in this study as the first framework to track foliar disease of plant. To continuously observe and study disease progress on leaves in both temporal and spatially coherent manners, it is always difficult to handle the changes in both external environment (illumination variations and camera vibration) and internal plant circadian growth and movements (leave translation, small scale, rotation, and occlusion). However, the problems are simplified by using the OCM method, which is capable of providing robust and continuous disease detection over time based on its gradient quantization principle. Meanwhile, the template-based scheme enables site-specific and multi-scale disease observation.

Second, a pattern recognition approach of SVM [48] was further employed for the disease classification since its unique solution and robust tolerance for training dataset. For achieving substantially discriminative power, feature extraction prior to the SVM plays a pivotal role. Not only this, a lower dimensional feature space but as good representation for the appearance of specific instances from input images will get more accurate and efficient performances [49, 50]. Therefore, feature extraction with low dimensions and powerful discriminability for CLS discrimination is one of core work in this study. Because soil resembles CLS in color causing great interference for their discrimination, in this study, we proposed two feature spaces with respects to two different conditions: with and without soil concern. First is for conditions without soil concern, we proposed a color-based feature of two-dimensional (2D) xy-color histogram. The

feature is a luminance-independent feature that can robustly detect CLS against illumination changes over time, and pixel-wise disease quantification can be additionally obtained based on its precise classification performance. Second is for conditions with soil concern, a 3D feature combination $L^*$, $a^*$, Entropy $\times$ Density was proposed. The feature has powerful discrimination capability to classify CLS disease from complex field backgrounds. In particular, the feature attacked the key classification problem of the CLS and soil discrimination for real field application.

In other words, this study provides a way to observe and quantify disease progress temporally and spatially from color-based plant sequential images, the accessed disease progress information can then assist precise plant protection such as optimal fungicide decision and better pathology understanding.

## 1.5 Overview

The first chapter initially introduced agricultural background and previous image-based studies for plant disease study. Then, we highlighted the difficulties experienced in the field of foliar disease detection, as well as the limitations of existing algorithms. Finally, we briefly described the motivation and concept of this study. By using the two frameworks based algorithm, robust, consistent and accurate foliar disease detection can be achieved against challenging variations and complexities under real and natural conditions.

The second chapter introduces the first framework of the proposed algorithm, which is on the basis of the template matching method OCM for robust foliar disease tracking. First, we theoretically analyze the robust performance of OCM for searching foliage against illumination changes. Then, we introduce adaptive OCM for extending the OCM into foliar disease tracking issues. Lastly, we illustrate its applications for tracking disease on two scales, one is on local region scale for achieving subtle disease observation; the other is on a single leaf scale for corresponding practical field application.

The third chapter introduces the second framework of the proposed algorithm, which is based on feature extraction along with SVM for CLS classification against complex and clutter backgrounds. We proposed two powerful discrimination features for classifying CLS disease under two different conditions: one is a color-based feature of 2D xy-color histogram for conditions without soil concern; the other is a color and orientation code histogram based 3D feature combination of $L^*$, $a^*$, Entropy $\times$ Density for conditions with soil concern, which attacked CLS classification problem against clutter sandy soil background.

The forth chapter initially provides experimental information of plant treatments and imaging acquisitions under both indoor and real field conditions, respectively. Then, experimental results are shown into four parts for demonstrating the robustness and effectiveness of the proposed algorithm. First, the robustness of OCM for successful foliage tracking against various illuminations has been experimentally demonstrated and compared. Second, the necessity and effectiveness of adaptive OCM for foliar disease tracking are comparatively discussed. Third, experimental results for local-regional disease detection without considering soil background are

shown under both indoor and field conditions. The mean precision value for the classification results compared with manual classifications is above 0.94 in the indoor conditions and 0.59 in the dramatically changed field conditions, respectively. Forth, results of a single leaf scale based disease detection under challenging real field conditions with complex backgrounds are shown, and the mean precision value is above 0.53. In addition, comparative experiment results show the effectiveness and relatively robust performance of the proposed 3D feature for the disease classification.

The Last chapter summaries the main contributions of the research and discusses future work.

# Chapter 2. OCM based foliar disease tracking

In this chapter, we introduce the first framework of the proposed algorithm. To achieve the continuity in foliar disease observation against of environmental variations, we employed a robust template matching method called orientation code matching (OCM) as basis for foliar disease tracking from plant-level image sequences over time. OCM has been theoretically and experimentally proved as a robust object matching method which can search objects from a variety of challenging scenes in the presence of irregularities and ill-conditions, such as illumination changes, partial occlusion and background variations [39, 40]. By utilizing its advantages in robust object searching, in this study, we extended it into adaptive OCM for tracking plant disease by considering accumulated disease changes along time. The chapter is organized as follows: first, we give the definition of the OCM with its gradient quantization and similarity evaluation processes; then, we demonstrate its robust performance for foliage searching under various illuminations. Meanwhile, the robustness of OCM compared with other convenient template matching methods are discussed; next, we describe the adaptive OCM for tracking foliar disease by adaptively replacing template to follow the non-rigid plant and disease changes; finally, we demonstrate the applications of the adaptive OCM for foliar disease tracking on two different scales.

## 2.1 Orientation code matching (OCM)

OCM has been proposed as a robust image registration algorithm. It is defined as matching the orientation codes between two images which are to be compared for similarity evaluation. For digital images, the orientation codes are obtained with quantized gradient angle of each pixel by applying some operator like for Sobel operator to compute the horizontal and vertical derivatives. If a discrete image is presented as $I(x, y)$ then its gradient angle $\theta_{x,y}$ could be obtained from:

$$\theta_{x,y} = \tan^{-1}(\frac{\nabla I_x}{\nabla I_y}) \tag{2.1}$$

where $\nabla I_x = \frac{\partial I}{\partial x}$ and $\nabla I_y = \frac{\partial I}{\partial y}$ are the horizontal and vertical gradient of pixel location $(x, y)$. Here, we use the Sobel kernels for calculating approximations of the horizontal and vertical gradient, which is based on convolving the image with two small, separable, and integer valued 3×3 kernels in horizontal and vertical directions and is therefore computationally efficient for real-time system application:

$$\nabla I_x \approx \begin{pmatrix} -1 & 0 & 1 \\ -2 & 0 & 2 \\ -1 & 0 & 1 \end{pmatrix} * I(x,y) \tag{2.2}$$

$$\nabla I_y \approx \begin{pmatrix} 1 & 2 & 1 \\ 0 & 0 & 0 \\ -1 & -2 & -1 \end{pmatrix} * I(x,y) \tag{2.3}$$

where $*$ denotes the two-dimensional convolution operation.

Then, orientation code (OC) is defined by quantizing $\theta_{x,y}$ using a preset sector angle $\Delta\theta$:

$$c_{i,j} = \begin{cases} [\frac{\theta_{i,j}}{\Delta\theta}] : & |\nabla I_x| + \left|\nabla I_y\right| > \Gamma \\ L : & otherwise \end{cases} \tag{2.4}$$

A separate code L ($= \frac{2\pi}{\Delta\theta}$) is assigned for low contrast regions, for which it is not possible to compute the gradient angels. For all experiments, we used 16 ($N = 16$) orientation codes ($\Delta\theta = \frac{\pi}{8}$), which have been found to be the best through experiment evaluation. The threshold value $\Gamma$ plays an important role in suppressing the effect of noise and has to be selected according to the problem at hand. Small value of 10 was used for $\Gamma$ which proved adequate for most of our experiment. A dissimilarity measurement is defined as the summation of the difference between the orientation codes of the corresponding pixels of the two regions being matched. The cyclic property of orientation codes is used for finding the difference. If $O1(i, j)$ and $O2(i, j)$ represent the orientation codes of template image from reference scene and subimage from object scene, then the dissimilarity function between them is given by:

$$D = \frac{1}{M} \sum d(O1(i, j), O2(i, j)) \tag{2.5}$$

where $M$ is the total number of pixels used in matching process and $d(\cdot)$ is the error function based on an absolute difference criterion defined as follows:

$$d(m,n) = \begin{cases} min(|m-n|, N-|m-n|) : & m \neq N \cap n \neq N \\ 0 : & m = n = N \\ \frac{N}{4} : & m = N \oplus n = N \end{cases} \tag{2.6}$$

To account for the differences in the quantization width, we normalize $D$ by using maximum of error function $\frac{N}{2}$ and refer to the result as dissimilarity $D_{nor} = \frac{D}{\frac{N}{2}}$. Thereafter the normalized similarity $S$ is defined by using the normalized dissimilarity $D_{nor}$ as follows:

$$S = 1 - D_{nor} \qquad (0 \leq S \leq 1) \tag{2.7}$$

## 2.2 Robustness of OCM for foliage searching

The objective of this study is to detect disease under real and natural conditions, such as transparent greenhouses or real fields, so plant images are captured under natural daylight. Therefore,

high robustness of the disease observation algorithm against various illumination conditions is required. A conventional template matching technique such as sum of absolute differences (SAD) [51] or sum of squared differences (SSD) [52], which measures the similarity simply based on the aggregation of the brightness difference between template image and subimage, is not invariant even if slight changing of illumination. Besides, normalized cross correlation (NCC) [53] is known to be invariant against global changes in illumination by a constant magnifier and offset, but it is also regarded to be very sensitive to local fluctuation in illumination, which is unevenly distributed illumination in a scene, such as specular reflection of gloss on the leaf surface. In contrast, OCM demonstrates strong robustness against both global and local illumination changes because the gradient operation, such as the Sobel operation, is defined in a local domain and maintains invariable phase angle even under irregular illumination.

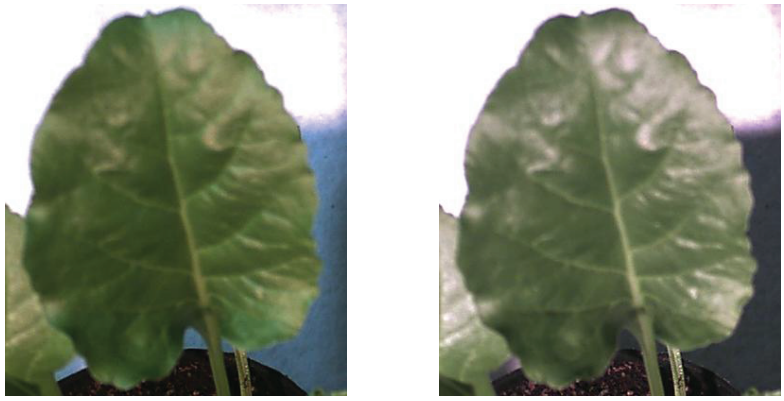
Figure 2.1 (a) shows two color images which were taken for a young beet leaf at same position under two different illuminations. Illumination in right image is brighter than left one. Fig. 2.1 (b) is the grayscale images of them. We see the grey values of images are highly relevant with illumination changes. Comparatively, Fig. 2.1 (c) shows the orientation code images (scaled to 256 grey levels), it can be seen that orientation codes (OC) can extract intrinsic features for an object which are irreverent and robust against illumination changes. Moreover, we see OC image can highlight the edges of leaf veins than that in grayscale image. The local and fine edge representation of the leaf object provides more rich and detailed information for similarity measurements of leaves. This property is also superior to other color and texture features based similarity measurements for leaf object searching. Because the surface appearance of leaves characteristics as similar green pigments and approximately uniform texture distribution, small disparities can be revealed by the color and texture features thus easily leading mismatching results.

Moreover, we conducted a contrastive experiment to illustrate the superior robustness of OCM for searching leaf object against various illumination changes by comparison with SAD and NCC. The comparative visualization results are presented in section 4.3.

## 2.3 Adaptive OCM for foliar disease tracking

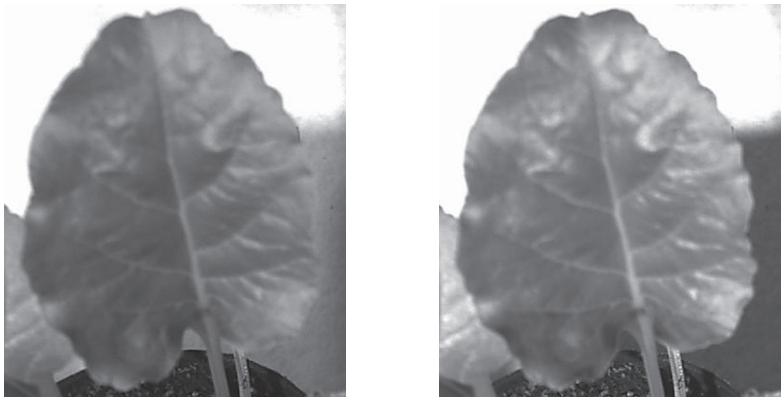
Because disease development and plant growth will cause accumulated changes for template matching, therefore, we extend OCM into adaptive OCM in which template searched by OCM is adaptively replaced frame by frame in order to follow the trend of disease and growth changes, and get the closest similarity between two chronological neighborhood frames.

For calculating the adaptive template, suppose $T_{p,q}^{t-\Delta t}$ is the template at time $t-\Delta t$ among plant images sequence, where $(p,q)$ indicates the upper-left position of the template. Then, the template searches its best match position $T_{p+u,q+v}^{t}$ in the next chronological image at time $t$ inside a predefined-sized search window. If $O_{p,q}^{t-\Delta t}$ and $O_{p+x,q+y}^{t}$ are the corresponding orientation code images for the images involved in the template matching, then the best matched position $(p+u,q+v)$ at time $t$ is calculated as follows:



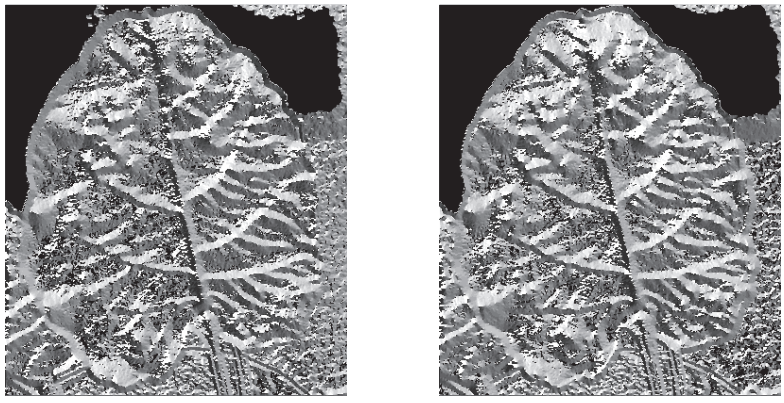
Light 1 Light 2

(a)



Grayscale image under light 1 Grayscale image under light 2

(b)



OC image under light 1 OC image under light 2

(c)

Figure 2.1: Robustness of orientation code (OC) under different illuminations. (a) A beet leaf captured under two different lights/illuminations; (b) grayscale images of the leaf and (c) the corresponding OC images.

$$(u,v)_{p,q} = arg \min_{x,y}(D_{p,q}(x,y)) \tag{2.8}$$

$$D_{p,q}(x,y) = \frac{1}{M}\sum_{i,j} d(O^{t-\Delta t}_{p,q}(i,j), O^{t}_{p+x,q+y}(i+x, j+y)) \quad \forall (p+x, q+y) \in W \tag{2.9}$$

where $\Delta t$ is the image capturing interval. $W$ is a search window, centred at the former template position, whose size is pre-selected to accommodate the maximum expected displacement of template within plant images. An illustration for the process of the adaptive template measurement is given in Fig. 2.2. The reason for setting a search window is that the motion and growth of a plant between two adjacent frames of plant images usually do not have severe variance. Consequently, the setting of the search window will not only improve the accuracy of the matching result but also save computation time. Subsequently, the best matched region $T^{t}_{p+u,q+v}$ at time $t$ will also be the adaptive template for searching its identical object from next frame at time $t + \Delta t$, and other frames are done in the same manner along time.

Furthermore, for demonstrating the effectiveness of the adaptive OCM for foliar disease tracking compared with the OCM, comparative experiments were implemented. The comparative results and discussions are shown in section 4.4.

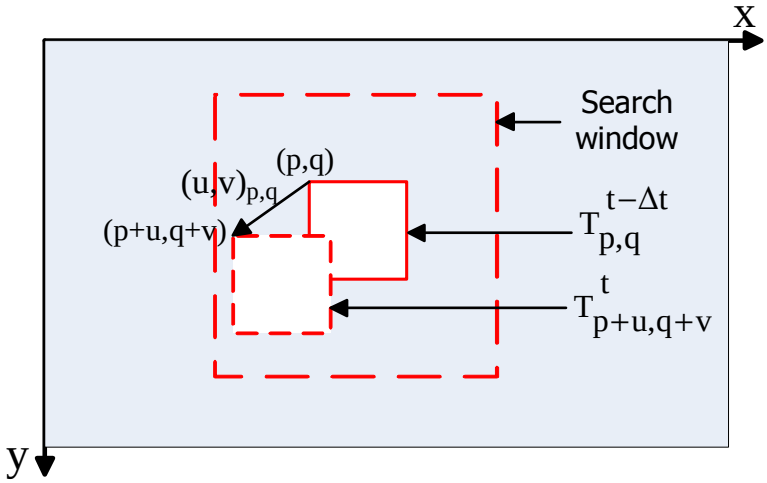



Figure 2.2: Illustration of adaptive template measurement.

In addition, on the basis of template-based regulation, the adaptive OCM can be applied for multi-scale disease tracking by extracting various sizes of templates from initial plant frame. This enables to take insights of disease development on different scales for different application purposes. In this study, we introduce the adaptive OCM for tracking foliar disease on two scales, one is on local region scale for subtle disease analysis and quantification; the other is on a single leaf scale for corresponding to one of practical disease rating criteria. Meanwhile, individual and site-specific variability of disease progress within a whole plant can be reflected by extracting multiple templates from the initial frame.

### 2.3.1 Disease tracking on local region scale

Applying the adaptive OCM on local region scale is to extract small-scale template on leaf surface from the initial plant frame, then the disease information within the small-scale template can be tracked and observed. The local region scale based disease tracking enables to observe subtle disease changes along time which not only provides precise disease spread information for fungicide sprays, but also assists in understanding and analyzing disease pathology (e.g., a detailed description of disease pigment and morphological changes). Fig. 2.3 illustrates the process of the adaptive OCM for tracking foliar disease on local region scale among plant sequential images. In this study, both indoor and field experiments were implemented at this scale. The size of the search window is set to $50 \times 50$ pixels in indoor experiment and $200 \times 200$ pixels in field experiment. The larger size of the field experiment is due to more drastic leaf motions affected by natural environment interactions, such as wind, draught and rain.

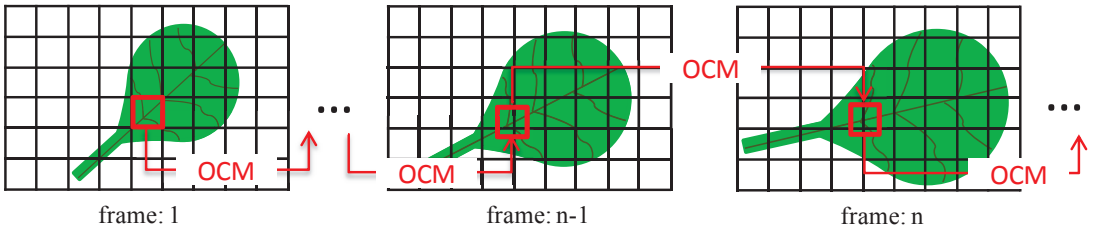



Figure 2.3: Adaptive OCM for tracking local region of leaf among plant sequential images.

### 2.3.2 Disease tracking on a single leaf scale

As an intent for real application of the proposed algorithm, we enlarge the size of template into single leaf scale for corresponding to one of practical CLS rating criteria: a single leaf scale based CLS rating system [3]. Fig. 2.4 illustrates the adaptive OCM for a single leaf based disease tracking from the sequential images. We applied this process in real field experiment and the size of the search window is $200 \times 200$ pixels.

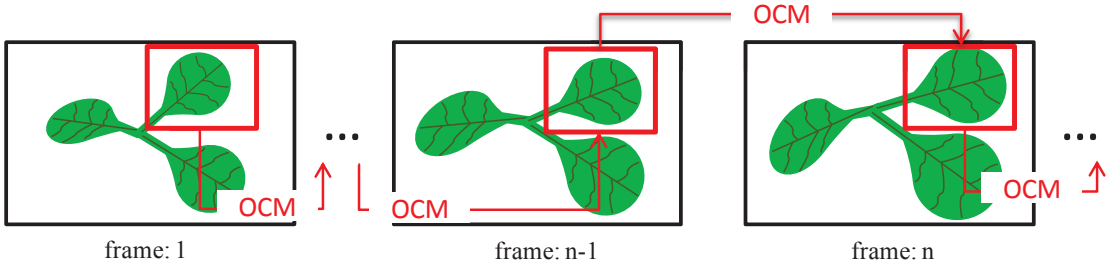



Figure 2.4: Adaptive OCM for tracking a single leaf among plant sequential images.

Note that the application of the adaptive OCM for foliar disease tracking is not limited to the two scales. According to different application purposes, variable template sizes can be defined

to analyse disease progress at different scales.

### 2.3.3 Discussion on initial template selection

In this study, the disease progress was observed on the basis of template-based matching method. Therefore, initial template selection from the first plant frame of the image sequence is a premise step for the continuous disease observation. However, in Fig. 1.1, we can see that due to the living disease, the sizes of individual disease spots are different even in a same leaf. Meanwhile, the positions of the spots appearing on the leaf surface are non-uniform and unpredictable. Besides, the spreading speed of individual disease is distinct from each other even under the same cultivated condition. Furthermore, the rhythmical oscillation of upward and downward leaf circadian movements are variant from different leaf growth stages [54]. For example, young leaves usually get more active movements than mature ones which easily lead large shape deformation in plant sequential images. Because of the complexities and variances from both living disease and plant, it is not easy to optimize the size and automate the position of the initial template.

Therefore, in this study, we preliminarily selected the initial template by manually initializing its size and position according to different application purposes. Meanwhile, to demonstrate the adaptive OCM for observing disease development at different scales, we extracted templates at two scales as mentioned in above section: one is on the local region scale for small-scale disease understanding, the template extraction processes in both indoor and field experiments are illustrated in section 4.5.1 and section 4.5.2. The other is on a single leaf scale for corresponding to practical single leaf based disease rating criterion, the related template extraction process is explained in section 4.6.1. Especially, in field condition, leaves are apt to get large shape deformation or move out of the camera view due to drastic environmental interactions. Therefore, we also state the restrictions in the relevant template extraction processes.

However, we should point out the open problem for developing ideal scales (i.e. template size) for different application purposes and environment conditions, which is also mentioned as future research priority in a review [13] for evaluation of plant disease severity by image analysis method.

## 2.4 Summary

This chapter introduced the first framework of the proposed algorithm: adaptive OCM for foliar disease tracking. We first introduced the OCM which is as basis of the tracking process. We then analysed its high robust performance for object searching against illumination changes through discussing its gradient quantization concept. Meanwhile, we demonstrated the superiorities of OC image in illumination invariance and fine leaf edge presentation. Finally, we introduced the extended adaptive OCM to accommodate the OCM for non-rigid foliar disease tracking. We first gave the definition of the adaptive OCM, then provided two instances as demonstrations of its wide applications for multi-scale disease observations.

# Chapter 3. Feature extraction along with SVM for CLS classification

By employing the template matching based adaptive OCM scheme, continuous locations for identical leaf parts can be accessed as the matched templates by OCM over time. Then, information within each temporally matched template can be utilized for further plant disease classification and analysis. In this chapter, a machine learning method of support vector machine (SVM) [48] is utilized as the second framework of the proposed algorithm, for forward CLS classification by its generalization ability in pattern classification [55]. Thereafter the information of disease amount and spread speed during disease development can be accessible for further decision-making of fungicide application.

Prior to conducting SVM classifier, feature extraction is a primary and crucial stage which will have directly effect on the performance of classifiers. By exploiting the power of SVM, we integrate the two tasks of feature extraction and classifier training into a single consistent framework and make the feature extraction more effective for the classification. In this chapter, we first explain the significance of the feature extraction and analyze the abilities that good features should have for classification. Then, we give a brief review of the SVM. Next, we introduce the proposed two features for CLS classification under two different conditions: one is a color based feature called two dimensionality (2D) xy-color histogram for the CLS classification without soil condition/concern; the other is a color and orientation code histogram based 3D feature combination of $L^*$, $a^*$, Entropy $\times$ Density for the CLS classification with soil condition. Both features are proposed with powerful CLS discrimination and low dimensionality abilities, leading better classification performance and avoiding possible overfitting problem.

## 3.1 Importance of feature extraction

Feature extraction is a primary and key process in pattern recognition and classification [56]. Usually, applying some weak or empirical features, such as simple pixels values or histogram will limit the upper bound of final recognition performance [57]. Therefore, once we extract powerful features which fully charactering the intrinsic nature of each pattern will boost classifier's performance. A good feature representation for classifiers should have following capabilities:

I. Robust to illumination changes.

   In real-world applications, variable illuminations often encounters that lead changes in intensity brightness of image from time to time. Specially, images captured under unpre-

dicted natural daylight conditions are even hard to get overall knowledge for leaning and training. Therefore, features and patterns that are irrelevant and insensitive to the illumination changes should be extracted to keep robust and consistent of the algorithms for object's classification [58, 59].

II. Discriminative power.

Another quality indicator of the feature extraction for image classification is the discriminative power. The discriminative features should describe the essence of different visual patterns that is reliable in identifying same pattern and distinguishable in different patterns, by which better classification accuracy can be achieved compared with those weak and empirical features [60].

III. Low dimensionality.

Although SVM is less sensitive to the 'curse of dimensionality' [50] than other non-SVM techniques, we shouldn't underestimate the overfitting problem arisen when the number of features is large and the number of training samples is comparatively small. Therefore, features are with low dimensionality but most informative for the pattern classification should be extracted for overcoming the risk of overfitting and reducing computation complexity.

## 3.2 Support vector machine (SVM)

According to the principle of structural risk minimization, SVM provides a solution for nonlinear two-class classification problems by mapping the training vectors into a higher-dimensional space via a nonlinear mapping function, and an optimal separate hyperplane can be constructed by the maximum margin between two sets of vectors [48]. When the classification problem involves more than two classes, several methods are available to extend a dichotomous SVM classifier into multiclass classification. In this study, we use the one-against-one approach [61], where a voting strategy is applied for classification. The process is to construct $k(k-1)/2$ classifiers, where $k$ is the number of classes, and each classifier is trained with data from a pair of classes. Finally, the classification decision is made by a maximum vote of the class assignments. The radial basis function (RBF) kernel was used in this study with its advantages of good generalization, strong tolerance to input noise, and online learning ability [62].

## 3.3 Without soil condition

This study focuses on CLS disease detection from beet plant images, thus features of the visual patterns in the image scene should be studied and extracted for classifying CLS. However, the brown-reddish color of CLS resembling that in soil will interfere their discrimination and cause a great challenge in color image classification. In this study, we proposed two different features for classifying CLS under two different environment conditions. First under conditions without soil concern, such as sheltering soil from image scene or extracting templates of lo-

cal leaf patches on the leaf surface, for obtaining precise CLS classification and quantification results without soil disturbance. Second is under conditions with soil concern, such as extracting larger-scaled templates containing clutter sandy soil background, for coping with real field application.

This section introduce the process for the first feature extraction. The second one is introduced in the subsequent section.

### 3.3.1 Feature extraction: (2D) xy-color histogram

A 2D xy-color histogram feature is firstly introduced in this study to classify CLS disease pixels from healthy and background ones without considering soil. We use a luminance-chromaticity CIE xyY color space rather than RGB color space because the former can separately represent the luminance and chromaticity of the color. A CIE xy chromaticity diagram indicates the chromaticity of a color in a horseshoe curve by eliminating the luminance component of the color, providing a more stable performance of object color information against illumination changes [63]. Fig. 3.1 (a) and (b) show the intensity curves of a single pixel P in RGB and xyY color space, respectively, from different plant image frames under different various illuminations (Fig. 3.1 (c)). The illumination conditions were controlled by placing a diffuse incandescent lamp (180 W, RF110V180WH, Iwasaki Co., Japan) at different heights and viewing angles above the plant. We observe that the R, G, and B intensities of P change over a large range because of light changes, whereas the x and y intensities are more stable because of eliminating of the luminance information (intensity of Y) of the object.

On the basis of the above color analysis, a 2D xy-color histogram is defined as a feature of SVM input for disease classification. For a template $I(i, j)$ which is extracted from the plant image frame, its 2D xy-color histogram is given as follows:

$$H_{\mathrm{x,y}} = P\left\{I_{\mathrm{x}}(i, j) = \mathrm{x}, I_{\mathrm{y}}(i, j) = \mathrm{y}\right\} \quad \forall (i, j) \in \mathit{template} \tag{3.1}$$

where $(0 \leq I_{\mathrm{x}}(i, j) \leq 1)$ and $(0 \leq I_{\mathrm{y}}(i, j) \leq 1)$ are the x and y color intensities in xyY color space.

Fig.3.2 demonstrates a comparable example of the 2D xy-color histogram for templates corresponding to disease, healthy and background, respectively under indoor condition (a white cardboard as background to eliminate the soil and pot resemble the color of CLS).

Furthermore, when the proposed color-based feature is extended into real field condition, we cannot use an artificial cardboard as background to eliminate soil for CLS classification. For applying the proposed feature in the field condition, we preliminary focus on detecting CLS of the templates locating at the inside of leaves. Besides, we transform the pattern of white background in indoor condition into that of specular reflection in field condition. Fig. 3.3 illustrates the 2D xy-color histogram for 400 pixels of each pattern (disease, health, and specular reflection) selected from a single leaf under field condition.

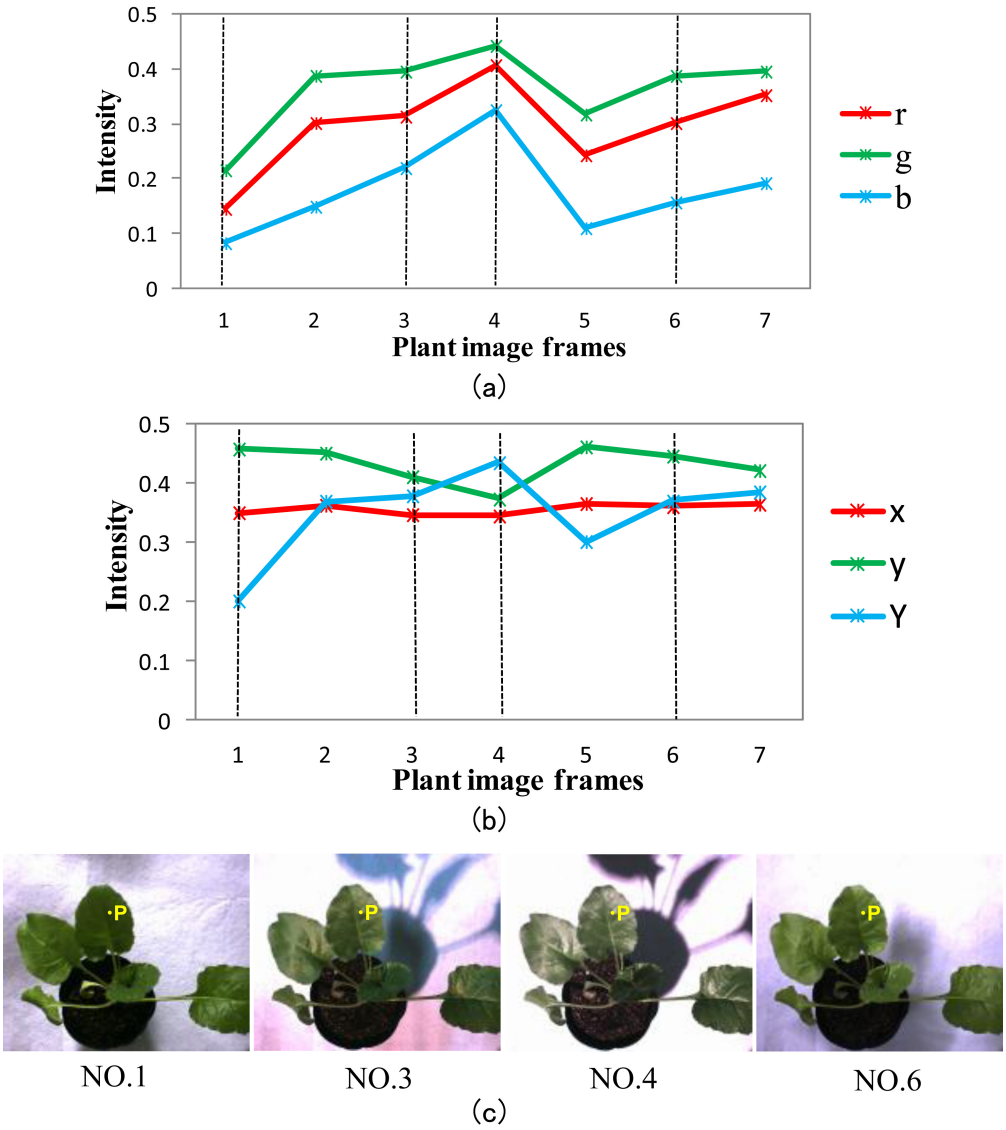



Figure 3.1: Intensity curves of a single pixel P in (a) RGB and (b) xyY color spaces, respectively, under various illumination conditions (c).

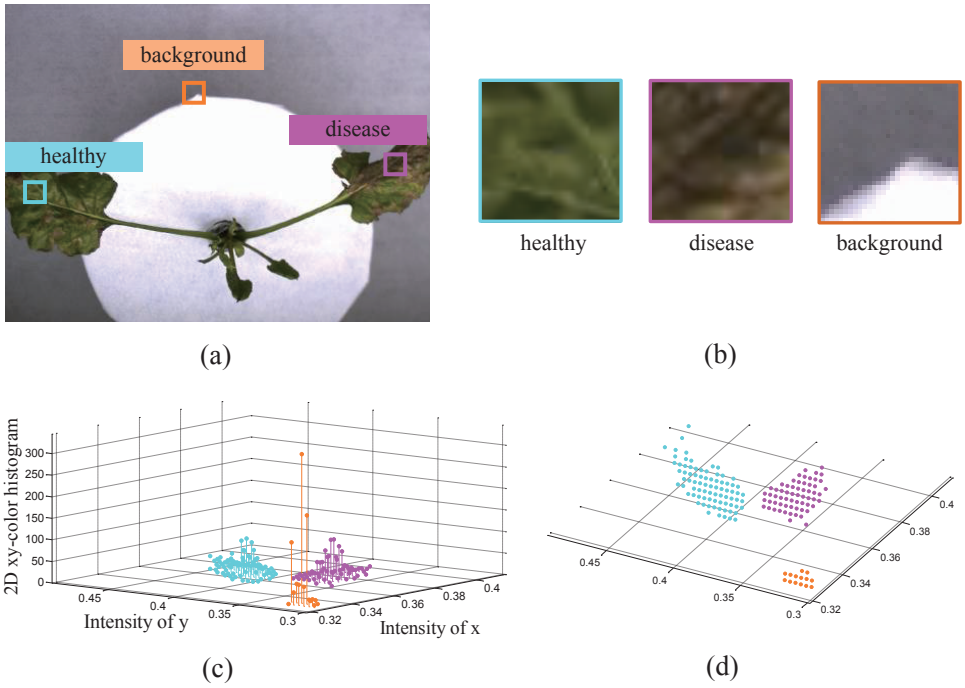



Figure 3.2: Comparable example of 2D xy-color histogram for templates belonging to disease, health, and background respectively under indoor condition.

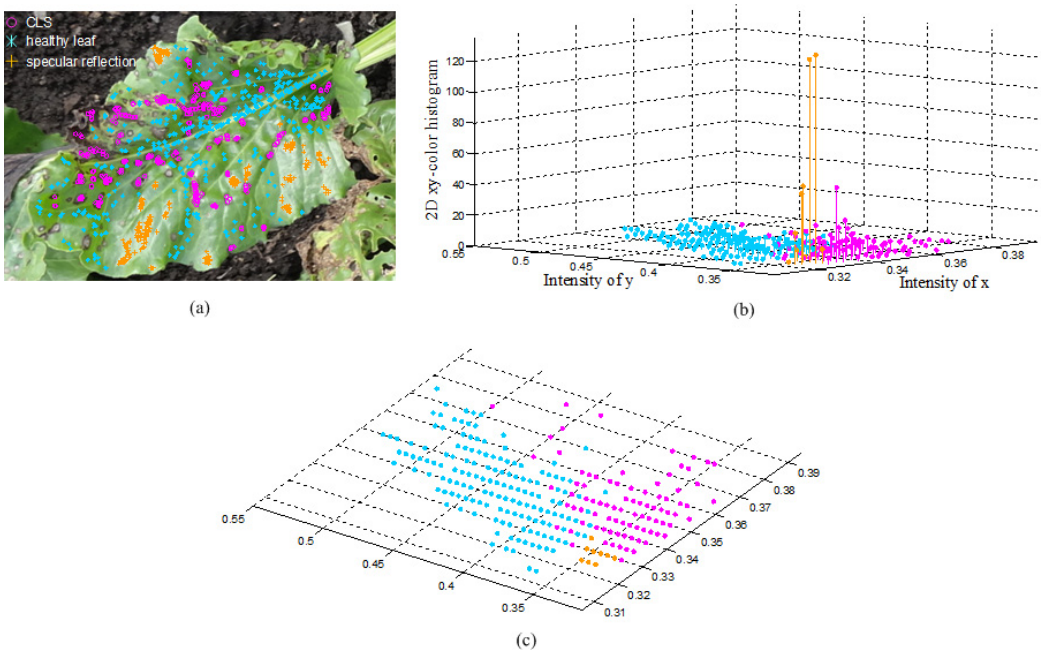



Figure 3.3: Comparable example of 2D xy-color histogram for pixels belonging to disease, health, and background respectively under field condition.

We observe that the 2D xy-color histogram shows a strong discriminative ability to classify the three different patterns under both conditions. Therefore, the color intensities of x and y of an image pixel were chosen and extracted as features for the SVM classifier.

### 3.3.2 Dataset for SVM modelling

As applications for the proposed 2D xy-color histogram feature, we implemented experiments under both indoor and field conditions. The dataset making processes for the SVM modelling with relevance to each condition are introduced in following two subsections:

#### Indoor experiment

To optimize the parameters and evaluate the performance of the SVM classifier, a training sample and testing sample were constructed by following these steps under indoor condition: first, plant images captured in one day (01:00-24:00) were randomly chosen, and 12 plant images captured every 2 h were chosen as the image sets for the training and testing samples; then, 400 pixel-level x and y color intensities were extracted for each of the three patterns (health, disease, and white background) per image (i.e. $400 \times 3$ pixels/image); finally, all image data were divided into two sets: one is the training data at times of 3:00, 7:00, 11:00, 15:00, 19:00, and 23:00, and the other is the test data at times of 1:00, 5:00, 8:00, 13:00, 17:00, and 21:00. Classification accuracies (the proportion of correctly classified pixels in relation to all classified pixels) of 99.44% and 99.07% were obtained for the training and testing samples, respectively, with optimal parameters of $c = 4$ and $\sigma^2 = 2$ by cross validation.

#### Field experiment

In field experiments, 1600 pixels were randomly selected for each of the three patterns (health, disease, and specular reflection) from the foremost image among the five-day time sequence images. Then, half of the selected pixels were used as training samples and the other half ones were for test samples. Finally, classification accuracies of 92.42% and 91.88% were obtained for the training and testing samples respectively, with parameters of $c = 256$ and $\sigma^2 = 16$.

## 3.4 With soil condition

This subsection introduces the process of feature extraction with soil condition. Moreover, the complexity of real field conditions were additionally taken into account. We attempt to proposed a feature for handling the complex field conditions, thereby to promote the proposed algorithm for real field application.

### 3.4.1 Feature extraction: (3D) L*, a*, Entropy × Density

In this study, for the natural and clutter field backgrounds, we firstly categorized pixels of a plant image into five patterns: CLS, healthy leaf, leaf stalk, highlighted leaf surface/specular reflection, and sandy soil. Then, a 3D feature combination of L*, a*, Entropy × Density is proposed as SVM inputs for CLS recognition out of other patterns. The first two features are the pixel-wise color based features, which are mainly for separating the five patterns into counter-directional color distributions of partial red and partial green, according to their brightness distributions in L*a*b* color space. For an pixel located at $(x, y)$, the first two features are calculated as follows:

$$L^*_{x,y} = I_{L^*}(x, y) \tag{3.2}$$

$$a^*_{x,y} = I_{a^*}(x, y) \tag{3.3}$$

where $I_{L^*}(\cdot)$ and $I_{a^*}(\cdot)$ are the grey component of L* and a* in L* a* b* space. Here we use L*a*b* color space [64] is because it approximates human perception for colors and is constructed so as to be perceptually uniform.

However, CLS is hardly discriminated from sandy soil by the first two features because they resemble with each other in partial red color. Therefore, the third feature Entropy× Density is additionally introduced for their discrimination. This is a region-wise orientation code histogram based feature, which is originally used for scalable image searching research in [65]. Inspired by the research, in this study, we made adjustments for it and extended it for CLS and soil classification. Fig. 3.4 (a) shows two regional images with M×M size extracted at the centering pixel $(x, y)$ belong to CLS and soil respectively. If only consider their pixel color, we see they resemble in brownish red color. However, their differences can be discovered in both shape and color aspects within their surrounding regional space. First, for regional shape difference, we see CLS region is featuring as scatted circular spot. Contrastively, soil region is with homogeneous shape/texture distribution. Second, for regional color difference, CLS region is in brown color surrounded by green leaf. However, soil region has similar chromaticity in red color. On the basis of these regional shape and color differences, we firstly transformed the RGB color image (Fig. 3.4 (a)) into a* component image (Fig. 3.4 (b)) that is an axis of L*a*b* color space representing red/green opponent colors. From Fig. 3.4 (b), we can see more distinct differences between the CLS and soil regions in both circular/homogeneous shape and contrast/uniform color differences. Then, we calculate orientation code histogram (Fig. 3.4 (c)) for the $a^*$ component image as $h_{x,y}(i)$ $(i = 0, 1, \ldots N)$ from which Entropy and Density are then derived and formulized to represent the above mentioned regional differences. Entropy, which represents the richness of an image, is firstly used to evaluate the variety of edge directions of an object in shape:

$$Entropy = -\sum_{i=0}^{N-1} P_{x,y}(i) \log_2 P_{x,y}(i) \tag{3.4}$$

where $P_{x,y}(i) = \frac{h_{x,y}(i)}{M^2 - h_{x,y}(N)}$ is the frequency of occurrence for each effective orientation code $i$ ($i = 0, 1, \cdots N-1$), except for $i = N = 16$ that is regarded as non-effective orientation codes for pixels with low contract. CLS region with scatter circular shape causes large variety edge directions. Therefore, it will have larger value of Entropy than that of soil region with less variance of edge direction. Next, Density is utilized to represent the second regional difference of color contrast and given as:

$$Density = 1 - \frac{h_{x,y}(N)}{M^2} \tag{3.5}$$

$D_{x,y}$ is calculated as the proportion of effective codes in the image region. The high contrast of red/green color in CLS region causes a greater number of effective codes which lead to larger value of Density for the region. Oppositely, soil region gets lower value of Density due to its low color contrast and thus lead to a smaller number of the effective codes. Therefore, for combining the both regional shape and color differences, we use a multiplicative operation to integrate Entropy and Density into Entropy×Density for the CLS and soil discrimination, of which CLS region will get larger value than soil region.

For demonstrating the effectiveness of the 3D feature combination of $L^*$, $a^*$, Entropy × Density for CLS classification, Fig. 3.5 (a) shows a plant-level image captured under field condition, and we randomly extracted 100 pixels for each of the five patterns. Fig. 3.5 (b) shows the visualization result of the proposed feature combination for CLS classification against the rest patterns. It can be seen that CLS can be distinctly discriminated from other clutter backgrounds. Especially, CLS can be well separated from the sandy soil. Furthermore, Fig. 3.5 (c) and (d) show both top and side views for Fig. 3.5 (b) respectively, in which the effectiveness of the first two features for color separation and the third feature for further CLS and soil discrimination can be seen orderly and clearly. Note that here we only employee a low-dimensional feature space (i.e., three-dimensional) to get a strong discrimination capability for the issue of CLS classification from the clutter background, which advantages in avoiding a potential open problem of the 'curse of dimensionality' for machine learning [50].

Furthermore, for demonstrating the effectiveness of the multiplicative integration for Entropy × Density, a comparative experiment was implemented for showing the disease classification results by three types of feature combinations: $L^*$, $a^*$, Entropy × Density; $L^*$, $a^*$, Entropy; and $L^*$, $a^*$, Density. The superior performance of the proposed feature combination $L^*$, $a^*$, Entropy × Density can be seen in the comparative experiment results of Fig. 4.18 and Table 4.4 in section 4.6.

### 3.4.2 Parameter optimization

Because the third feature Entropy×Density is a region-based feature, the regional size of $M$ will have effect on the discriminative performance between CLS and soil. Therefore, it needs to be discussed and optimally decided. In this study, we utilized three criteria for the parameter optimization: Fisher's linear discrimination criterion, classification accuracy, and computational time.

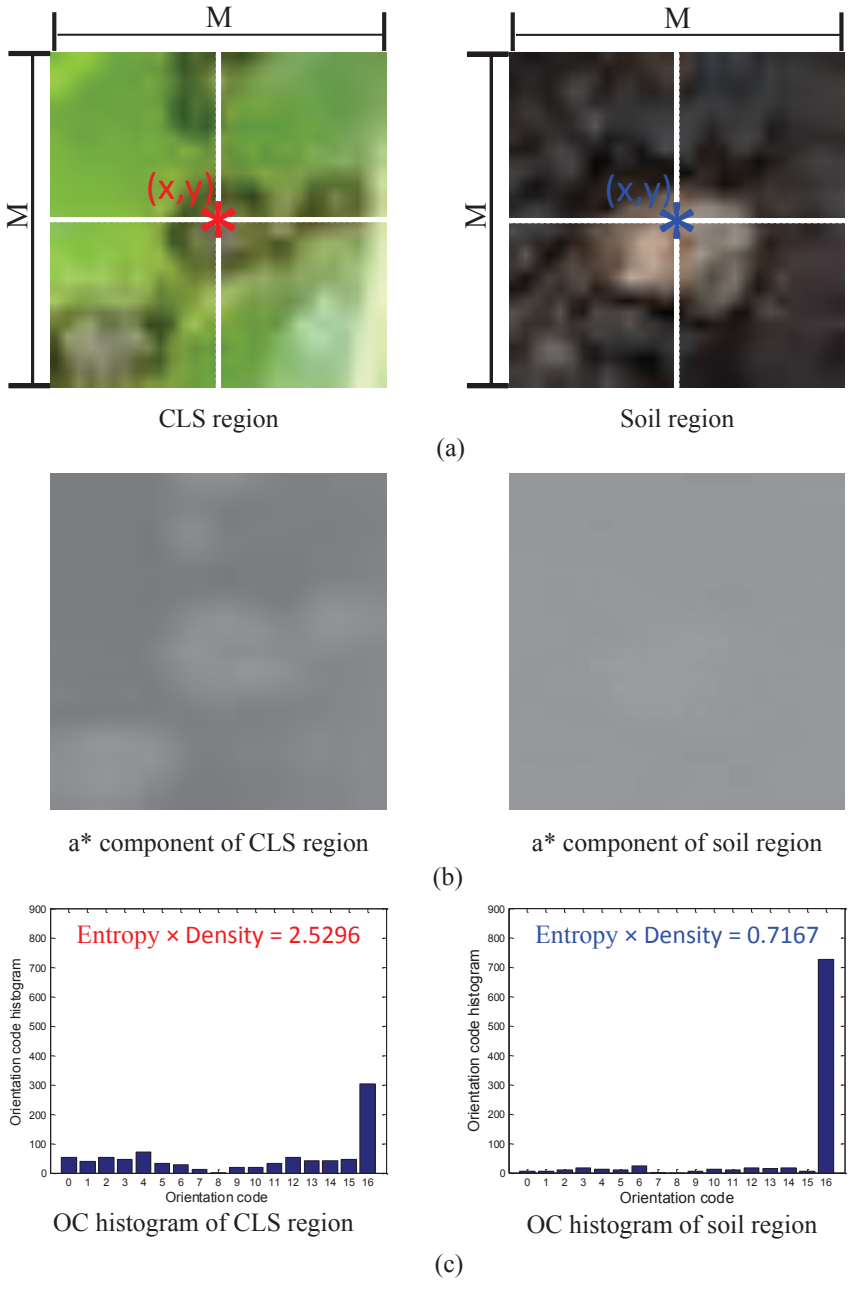



Figure 3.4: Demonstration the process for calculating the orientation code histogram based feature of Entropy × Density for CLS and soil classification. (a) CLS and soil regions extracted from the center pixel (x,y); (b) $a^*$ component images for the two regions; (c) orientation code histograms and the value of Entropy × Density for the two regions.

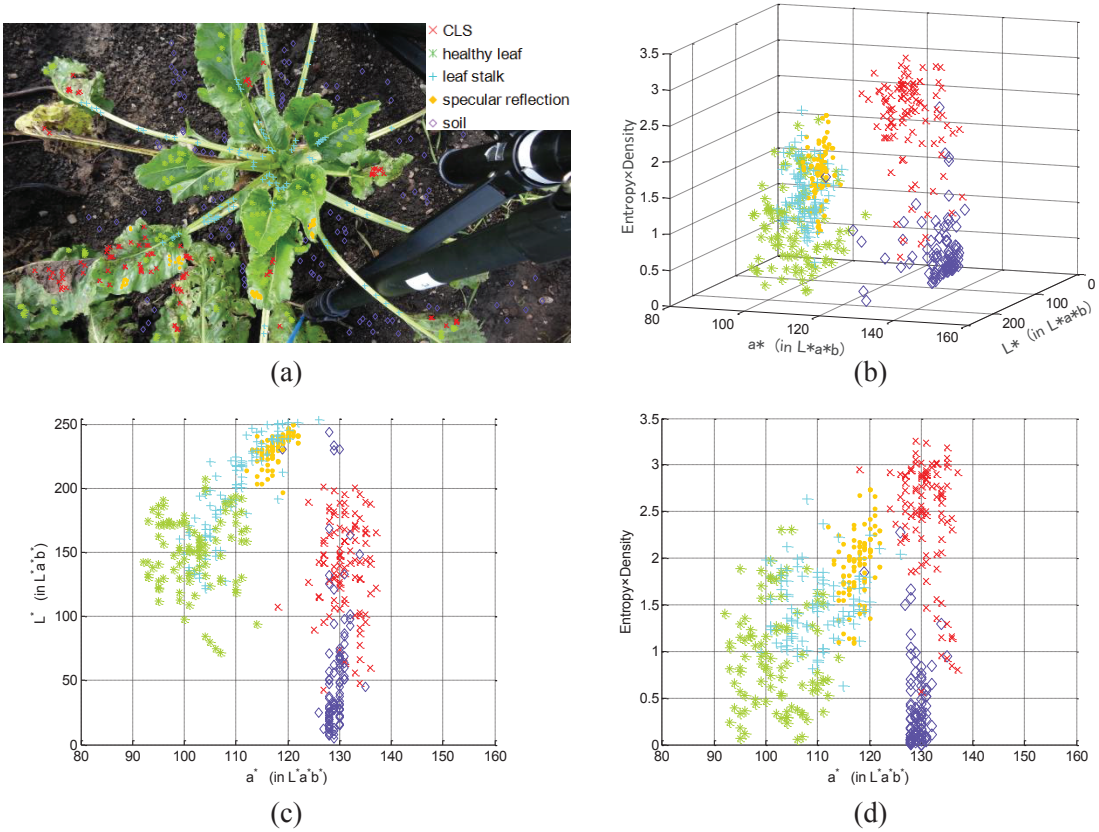



Figure 3.5: Effectiveness of the proposed 3D feature combination of $L^*$, $a^*$, Entropy $\times$ Density for classifying CLS patterns against other four patterns of healthy leaf, leaf stalk, highlighted leaf surface, and sandy soil under field condition. (a) 100 pixels were extracted for the each pattern; (b) results of the proposed 3D feature combination for the five patterns; (c) and (d) are the top view and side view for the feature space visualizations respectively.

From the side view in Fig. 3.5 (d), we see that the discrimination for the two patterns between CLS and soil by the one dimensional feature of Entropy×Density is equivalent to a liner discrimination problem, and different regional sizes can be regarded as different classifiers. Therefore, we firstly use the Fisher's criterion [66], which is maximized over all linear classifiers/projections and defined as:

$$J_F = \frac{|M_1 - M_2|}{S_1^2 + S_2^2} \tag{3.6}$$

where $M_i = \frac{1}{n_i} \sum_{x_k \in X_i} x_k$ $(i = 1, 2)$ and $S_i^2 = \sum_{x_k \in X_i} (x_k - M_i)^2$ $(i = 1, 2)$ represent a mean and a variance for each of the two patterns $X_1$ and $X_2$. Here $X_1$ denotes as CLS and $X_2$ as soil. Secondly, we additionally calculated the classification accuracy for the classifier under each regional size:

$$Acc = \frac{Acc_1 + Acc_2}{2} \tag{3.7}$$

where $Acc_i = \frac{\#\{x_k | x_k \geq T,\ x_k \in X_i\}}{\#\{X_i\}}$ $(i = 1, 2)$. $T$, as a boundary threshold for two patterns' discrimination, is visually selected depends on different applications at hand. In this experiment, we used the threshold value of 1. Thirdly, the computational time is also evaluated as a trade-off consideration between classification performance and time cost. Here the executing time is for calculating Entropy × Density value for the total 500 pixels from the five patterns. The computer used for the testing is Intel (R) 3.10 GHz with 4GB RAM. The algorithm is implemented in MATLAB (version R2009a).

For the criteria's calculation, 100 pixels from each pattern of CLS and soil were randomly selected, and Fig. 3.6 shows results for the three criteria calculated under a wide range of regional sizes from 5×5 to 60×60 at 5 unit intervals. In Fig. 3.6 (a) for the Fisher's criterion, we see that it firstly increases from the size of 5 until reaches its largest value at the size of 30, and then goes down with a negative tendency. For the classification accuracy in Fig. 3.6 (b), it initially gets a significant rise from 5 to 15 and follows with a small fluctuation from 15 to 30, and then reaches the highest value at 30 as same as the Fisher's criterion. After the peak value, it gets into a decreased tendency. Fig. 3.6 (c) shows the results of the computation time for the process of the feature calculation. Obviously, the larger the regional size, the longer computation time it takes. On the basis of the three criteria's results, we could give a recommendation that it is proper to select the regional size from a range of 15 to 30 with the trade-off consideration between classification performance and time cost. In this study, we use the regional size of 30 to obtain the best classification accuracy.

### 3.4.3 Dataset for SVM modelling

After the feature definition and parameter optimization, we extracted dataset for training SVM classifier, and then evaluated its performance as following steps: first, we randomly extracted 500 pixels for each of the five patterns (CLS, healthy leaf, leaf stalk, highlighted leaf

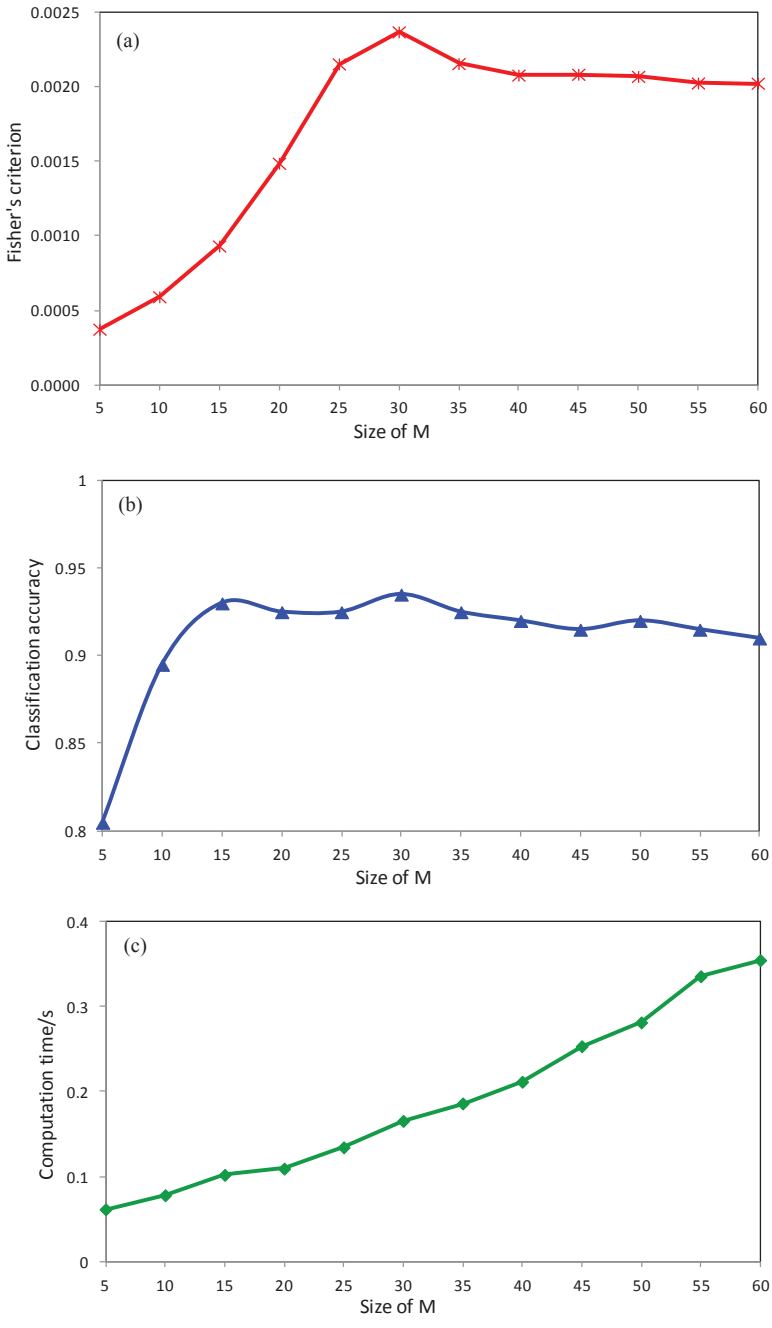



Figure 3.6: Optimization of the regional size $M$ for Entropy×Density. (a) Fisher's criterion; (b) classification accuracy; (c) computation time.

surface, and sandy soil) from a plant image captured at the first day of the five-day experimental period; second, we labeled the five patterns into three classes: disease (CLS), leaves (healthy leaf, leaf stalk, highlighted leaf surface), and soil (sandy soil); third, the dataset were divided into two parts as training and testing sets for SVM modeling and evaluation. In this study, we used LIBSVM [67] for the classification; finally, classification accuracies (the proportion of correctly classified pixels in relation to all classified pixels) of 98.48% and 97.44% were obtained for the training and testing datasets, respectively, with RBF kernel along with optimized parameters of $c = 64$ and $g = 0.00390625$ by cross validation.

### 3.4.4 Edge detection based post-processing

This section introduces a post-processing process for filtering false positive noise aroused from the third feature of Entropy $\times$ Density in order to improve the precision of the classification results. Meanwhile, all parameters involved in this procedure are discussed and optimized.

#### False positive noise

In Fig. 3.5 (d), we have seen the effectiveness of the orientation code histogram based feature of Entropy$\times$ Density for CLS and soil classification. However, there are two main fault cases for their discriminations due to the complex field conditions. One case is from the soil pixel (Fig. 3.7 (a)) which locates at the boundary position between leaf and soil will have various shape richness and higher color contrast as similar as the CLS region, causing larger value in Entropy$\times$Density and forming as false positive (type I error) noise in a classified image. The other case is from the CLS pixel (Fig. 3.7 (b)) which locates at heavily destroyed leaf parts will have little shape richness and color contrast as similar as the soil region, giving rise to smaller values in Entropy$\times$Density and being as false negative pixels (type II error) in the classified image.

Fig. 3.8 (a) shows a single leaf image extracted from the plant image captured in the field experiment and Fig. 3.8 (b) is the classification result for it by the proposed SVM classifier. Serving as a comparation, Fig. 3.8 (c) shows the ground truth manually made by human naked eyes observation under the guidance of disease specialists. Then, Fig. 3.8 (d) and (e) show the false positive and false negative pixels of the classified results, respectively. We can see that the false positive pixels mainly locate at leaf edges, and the false negative ones mainly locate at the heavily destroyed leaf parts. For the type II error, it is not easy to recover the false negative pixels from the parts of heavily destroyed leaf surface. However, for the type I error, we can filter the noise by utilizing their position property at leaf edges.

#### Edge detection based post-processing

By utilizing the edge location of false positive noise, we introduce an edge detection based post-processing for filtering the noise from the type I error. Fig. 3.9 shows the concept and

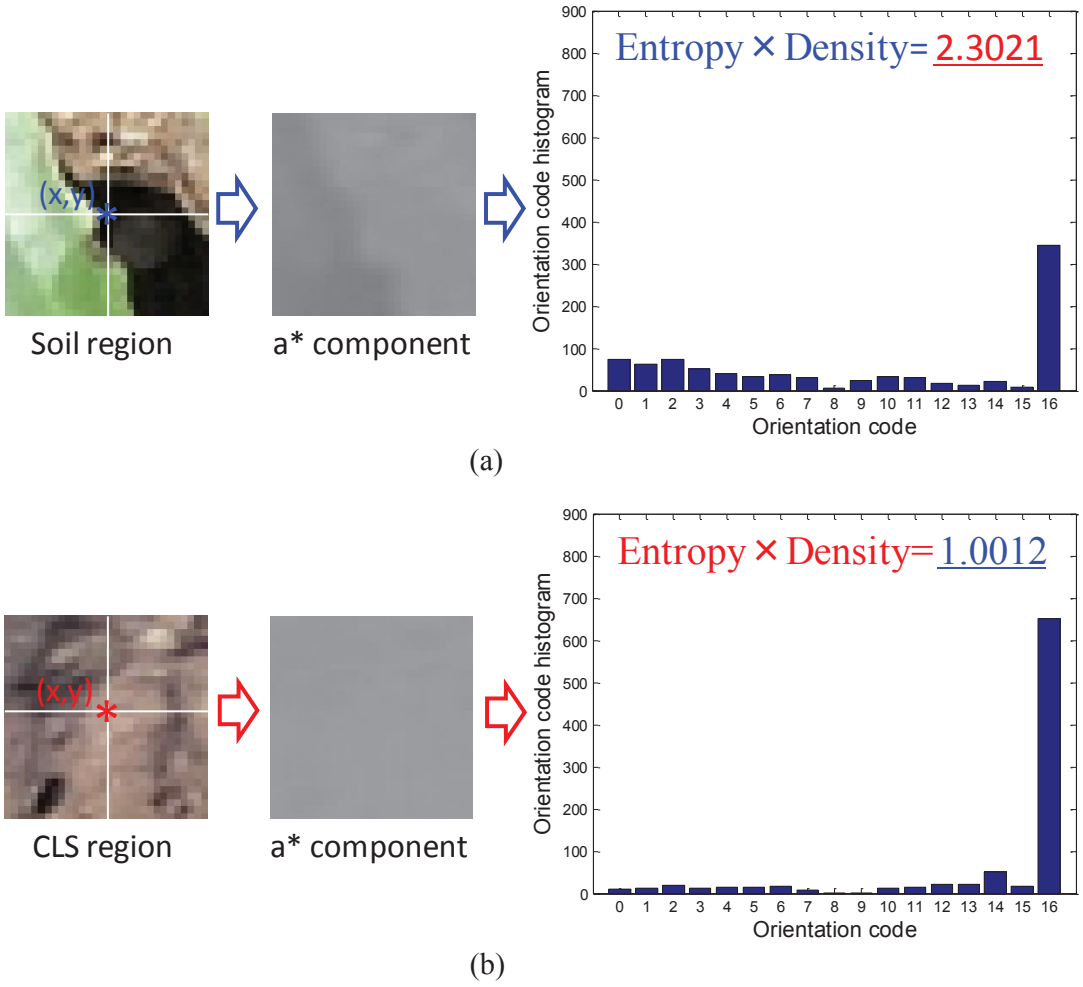



Figure 3.7: Fault cases for CLS and soil discriminations by Entropy × Density due to the complex field conditions. (a) A fault example for a soil region locating at leaf boundary; (b) a fault example for a CLS region locating at heavily destroyed leaf part.

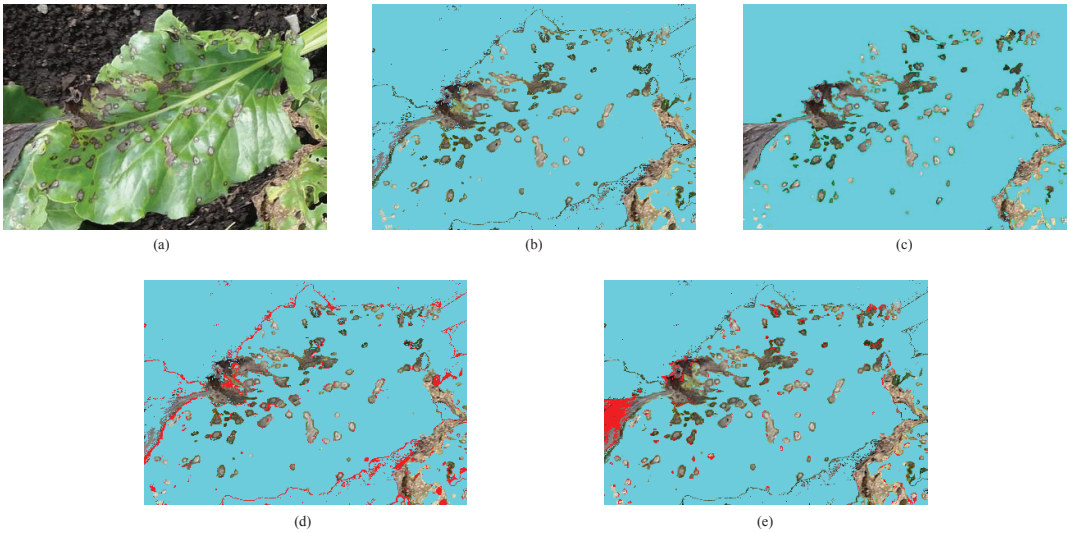



Figure 3.8: False positive and false negative pixels in the classification result aroused from the feature of Entropy × Density. (a) An leaf image; (b) classification result by the proposed SVM classifier; (c) ground truth; (d) false positive pixels (in red color) mainly concentrated at leaf edges; (e) false negative pixels (in red color) mainly concentrated at heavily destroyed leaf parts. (The blue areas correspond to the background region.)

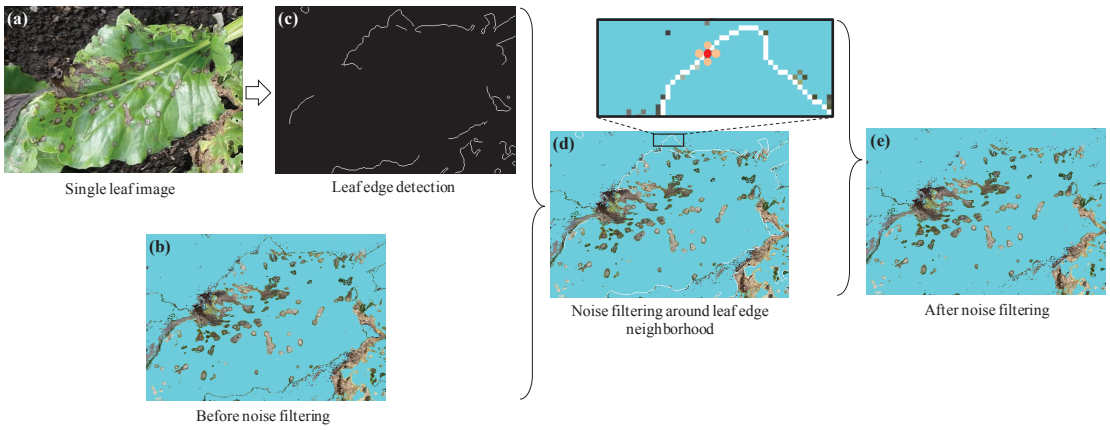



Figure 3.9: Edge based post-processing to filter the false positive noise. (The blue areas correspond to the background region.)

process of the post-processing. Here we take the single leaf image in Fig. 3.9 (a) as an instance, and Fig. 3.9 (b) is corresponding SVM classification result before the noise filtering. Firstly, we detected edges in Fig. 3.9 (a) by applying an edge detector as shown in Fig. 3.9 (c); Then, we composited Fig. 3.9 (b) and Fig. 3.9 (c) into one image in Fig. 3.9 (d) to locate leaf edges in the classification image. Meanwhile, for each detected edge pixel, we removed it along with its connected neighbouring pixels for tolerating a small position bias between noise and edges (demonstrated in the zoom-in subimage). Finally, we can see in Fig. 3.9 (e) that the false positive noise was significantly reduced and filtered after the post-processing.

**Parameter optimization**

The post-processing mainly comprises two components: one is the edge detector used for edge detection, and the other is the neighbourhood centring at the edge pixels used for noise filtering. In this section, we will discuss and optimize three important parameters involved in processing the components: (1) type of the edge detector (Canny, Sobel, etc.); (2) gradient threshold of the edge detector (0∼1); (3) type of the neighborhood (4-nerighborhood or 8-neighborhood).

First, for deciding the type of the edge detector, we compared four frequently used edge detectors of Canny, Sobel, Prewitt, and LoG for the leaf object under real field. Fig. 3.10 shows the comparative results for each of the detector under various thresholds. We see that among four differential operators, Canny detector provides the largest SNR (signal noise ratio) for detecting the outer contour of the leaf and also obtain continuous boundary. Therefore, we choose Canny as the detector for the edge detection. Then, for optimizing the gradient threshold and the neighborhood type, we use two statistical measurements of precision and recall [68] as basis for the optimization. Often, there is an inverse relationship between precision and recall after noise filtering [69]. Therefore, the optimization of the last two parameters should make the largest increase of the precision, at same time the decrease of the recall should be smallest. Suppose $P_{before}$ and $P_{after}$ indicate the precision value before and after the post-processing, and $R_{before}$ and $R_{after}$ are in same way for recall value. The optimization function for the gradient threshold of Canny detector $T_{Canny}$ and the neighborhood type $N$ should be as:

$$(T_{Canny}, N) = arg\ max(dist(\triangle P, \triangle R)) \tag{3.8}$$

where $dist(\triangle P, \triangle R) = |\triangle P| - |\triangle R|$ are the distance between changes of the precision $\triangle P = P_{after} - P_{before}$ and the recall $\triangle R = R_{after} - R_{before}$ by the post-processing. Fig. 3.11 shows the results for the distance value under different $T_{Canny}$ and $N$ combinations. It can be seen that the maximal value of the distance occurs at $T_{Canny} = 0.7$ and $N = 4$, which were decided as the optimal value for parameters of (2) and (3).

## 3.5 Summary

In this chapter, we introduced the second framework of the proposed algorithm which is integrated from two tasks of feature extraction and SVM classifier for CLS classification. We

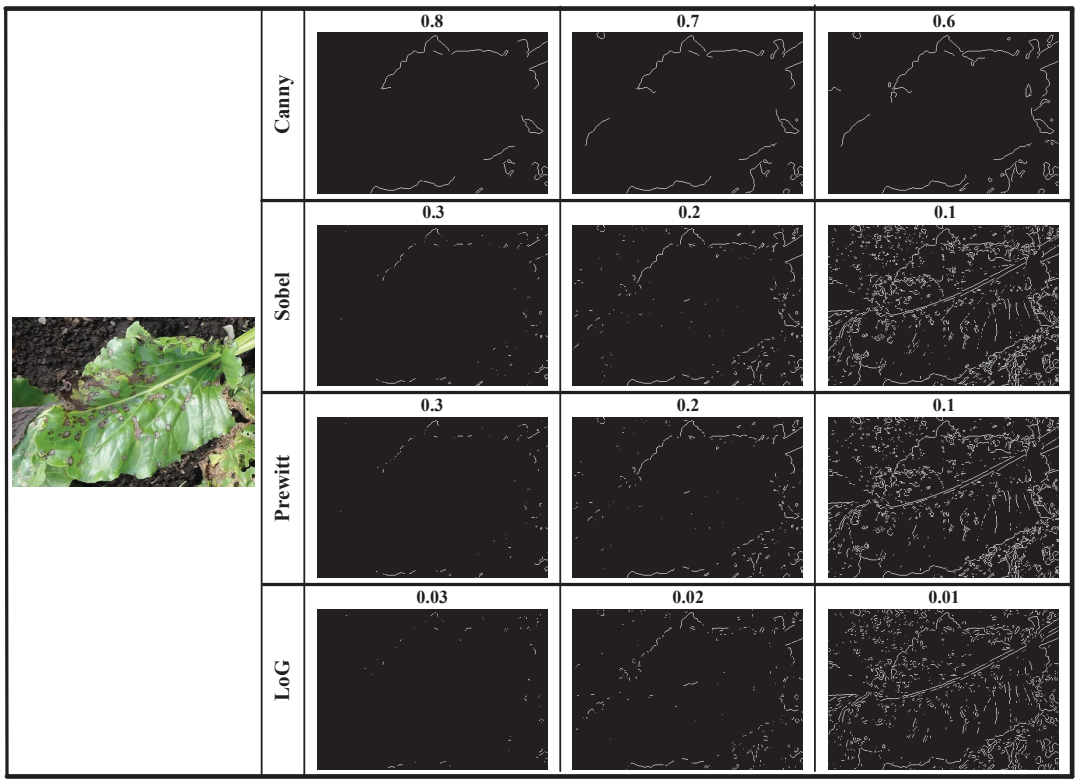



Figure 3.10: Comparative results for edge detection of leaf by different detectors with various thresholds.

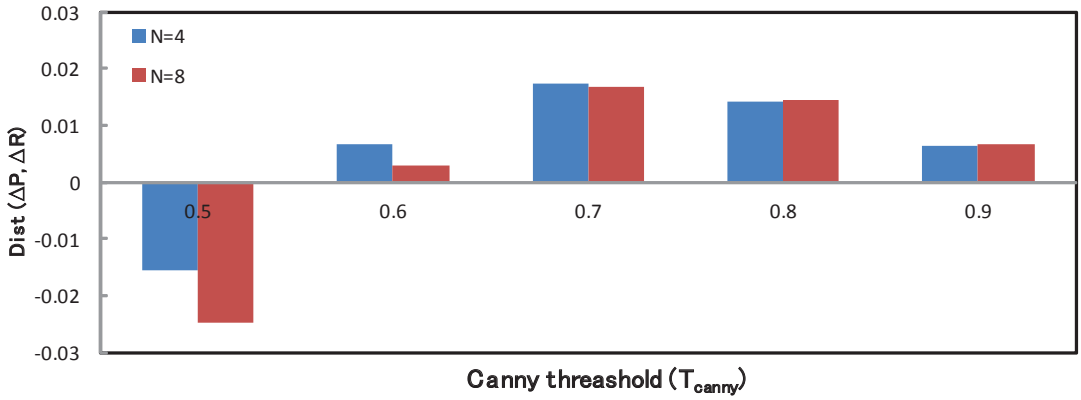



Figure 3.11: Distance value $dist(\triangle P, \triangle R)$ calculated from different $T_{Canny}$ and $N$ combinations for parameter optimization.

extracted two features for classifying CLS under two different conditions: one is a 2D feature of xy-color histogram for the condition without soil concern; the other is a 3D feature of $L^*$, $a^*$, Entropy $\times$ Density for the condition with soil concern.

The first feature is proposed based on color analysis for classifying CLS disease from other two visual pattens of healthy leaf and whitish background. Both components of the two-dimensional color distribution are luminance-independent, indicating robust CLS classification ability against illumination changes. Further, the feature was applied in both indoor and field experiments. The visualization of the 2D feature space showed its well discriminative power under both conditions.

The second feature is proposed based on color and orientation code histogram, for classifying CLS from more complex visual patterns in real field: healthy leaf, leaf stalk, specular reflection and sandy soil. The first two components are pixel-wise color based features which function as separating the visual patterns into counter-directional color distribution. The third component is a region-wise OC histogram based feature functioning as discriminating CLS from soil. It is notable that the Entropy $\times$ Density feature overcomes the challenging problem of CLS discrimination from sandy soil background in RGB color images. The visualization of the 3D feature space demonstrated its discriminative ability for CLS classification against complex real field backgrounds. After employing the SVM classifier, we further analyzed misclassified pixels in classified image, and an edge detection based post-processing was proposed to filter false positive noise in terms of their location property. Experimental results showed the effective performance of the post-processing for improving classification precision by the false positive noise reduction. In addition, parameters involved in the process of the feature extraction and post-processing are discussed and optimized.

# Chapter 4. Experimental treatments and results

This chapter firstly describes plant treatments (in section 4.1) and image acquisitions (in section 4.2) under indoor and field conditions, respectively. Then, the following sections shows experimental results by the proposed algorithm for CLS disease detection in sugar beet. We demonstrates the results into four parts for presenting the effectiveness and outperformance of the proposed algorithm. First, in section 4.3, a experiment was conducted for demonstration the robustness of OCM for searching foliage against various natural daylights. Comparative experimental results showed the superior robustness performance of the OCM compared to other three conventional template matching methods. Second, in section 4.4, as considering disease changes over time, we proposed adaptive OCM for tracking foliar disease. Comparative experiments were conducted for showing the superiority of the adaptive OCM for foliar disease tracking compared with original OCM. The third and fourth experiments are for showing the results of continuous CLS detection by the proposed two-framework algorithm. The third part (in section 4.5) shows experimental results for precise disease detection and quantification on local region scale without soil condition. Both indoor and field experiments were undertaken. The last part (in section 4.6) shows experimental results of disease detection on a single scale with clutter sandy soil condition in real field to approach practical field application.

## 4.1 Plant cultivation and pathogen inoculation

### 4.1.1 Indoor experiment

Sugar beet plants (cv. Amaibuki, 2004; Nippon Beet Sugar Manufacturing Co., Ltd., Japan) were cultivated in ceramic pots ($\phi$ 31cm) at 25° (day/night), 15% relative humidity (RH), and with the help of daily water spraying on the leaf surfaces to improve RH. The plants were watered as necessary and fertilized every two weeks with 200 ml of a 2% solution of fine powder HYPONeX (HYPONeX Co., Ltd., Japan).

In indoor experiment, *Cercospora beticola* was infected by manually sprinkling the infected leaf residual on the surfaces of healthy plant leaves at the vegetative stage of sugar beet plants. Subsequently, the infected plants were placed in a plastic greenhouse with 90% RH at 25° (day/night) for two weeks to produce conidiophores and experience the incubation period.

### 4.1.2 Field experiment

The field experiment was conducted in a test field which locates at Central Agricultural Experiment Station in Naganuma, Hokkaido, Japan. Sugar beet plants (cv. Amaibuki) were initially seeded on March 18th, 2013, and then transplanted into field on May 9, 2013. The plants were naturally cultivated under field environment. Meanwhile, the fungus of *C. beticola* was infected to beet plants naturally without artificially inoculation.

## 4.2 Experiment configuration

### 4.2.1 Indoor experiment

A weeklong experiment was conducted to assess disease changes in sugar beet leaves under indoor condition. The experimental system was placed next to a window to utilize natural daylight and simulate the outdoor sunlight conditions. The RGB plant images with $640 \times 480$ resolution were captured by a CMOS camera (CMOS130-USB2, Fortissimo Co., Japan), which was mounted on a horizontal beam supported by two vertical poles to achieve a constant camera height of 1.9 m above the plant. The top-view images were captured at 1-h intervals. An indoor fluorescent lamp (15 W, 5000 K, FL15EX-N-A, Hitachi Co., Japan) was used as the light resource when capturing plant images during night periods (17:00–6:00). Fig. 4.1 illustrates the experimental setup under the indoor condition.

### 4.2.2 Field experiment

A five-day experiment was implemented under natural field conditions from September 17 to 21 in 2013. Since our long-term target is to develop a cost-effective, easily-operated and portable disease evaluation system, which can be used in fields by both specialists and farmers. In the field experiment, a low-cost and portable experimental apparatus was equipped with minimum resources of one digital camera (DSC-HX30V, Sony Co., Japan) and a tripod. Fig. 4.2 shows graphic illustration of the field experiment setup. Plant canopy images with size of 1920×1080 pixels were captured in 'auto-focus' mode (without use of the zoom) at constant height and horizontal-top view from soil plane. During the experimental period, two blue sticks were used as markers to place the tripod so as to maintain same capturing position for plant each day. The plant-level image sequences were captured at one day intervals around 11:00 each day.

## 4.3 Robustness of OCM for foliage searching

To demonstrate the robustness of OCM with respect to illumination variations compared with that of SAD, SSD, and NCC, in this experiment, we use the time sequence images of a sugar beet plant captured over an entire day (01:00–24:00) under natural sunlight coming through the indoor window. To extract an initial template from the foremost plant image and better visualize its subsequent position shifts matched by OCM, an automatic gridding which divides the image

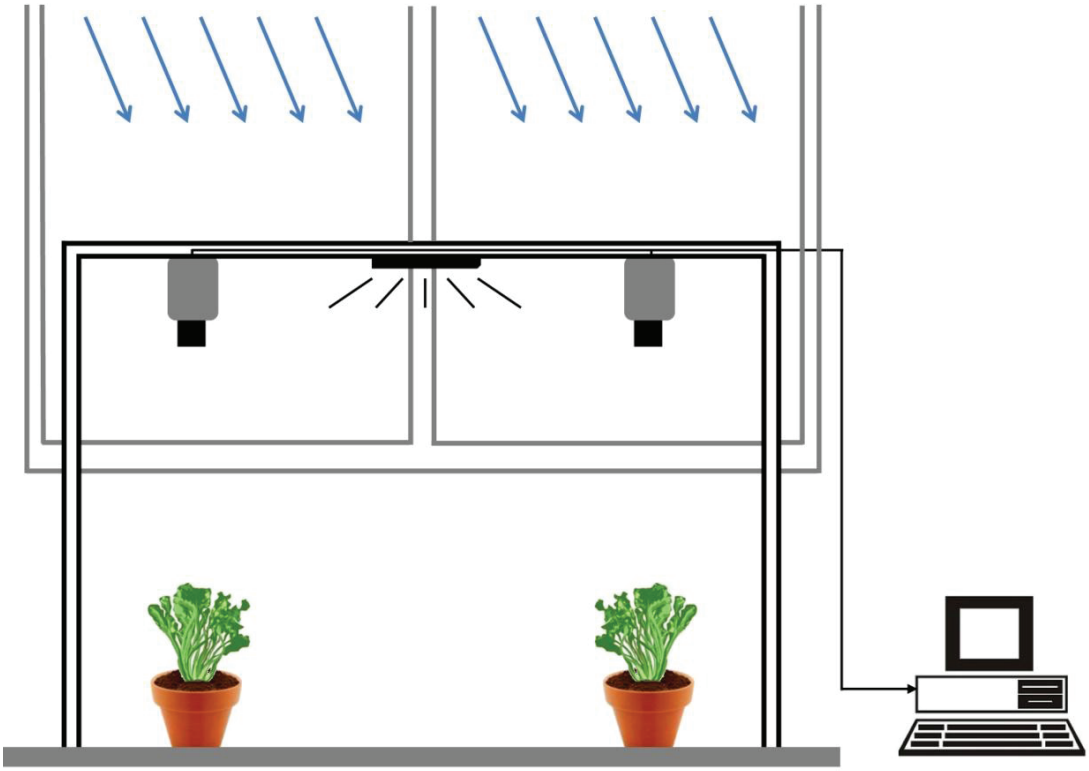


Figure 4.1: Graphic illustration of indoor experiment setup.



Figure 4.2: Graphic illustration of field experiment setup.

into several sub-blocks with a constant size (30 × 30 pixels) is applied as a position reference among the time sequence images. Thereafter, adaptive template matching is performed for the initial template between the adjacent image frames at each time step over all time sequence plant images by OCM, SAD, SSD, and NCC separately.

In this study, the correct matching and mismatching decisions are made by human naked eye visualization, and for the case of errors arising from subjective human eye observations, we set an error-tolerant range of two pixels in upper, bottom, left, and right between the matched results and human eyes. Fig. 4.3 shows the matching results and their relevant similarity values for one of the templates adaptively matched over the plant sequence images by different schemes throughout a day. OCM was successful for all time sequence images in the day, including the abrupt illumination change caused at daybreak (7:00) and in dark lighting conditions at nightfall (16:00). In contrast, SAD, SSD, and NCC failed to accurately match starting at daybreak (7:00), even for the first time (2:00) respectively. The reason for below-par matching results of NCC compared with those for SAD and SSD is that the template on the leaf chosen in this experiment contained specular reflection, and NCC is sensitive to local illumination fluctuations. Fig. 4.4 shows the comparative visualization results of the above procedure, where the time symbol in black indicates a correct matching, and the red color symbols represent false matches. Fig. 4.5 shows the example of the 3D plots for the similarity values around the best match position in the object scene at time 13:00. We observe that the contour of the similarity value for OCM obtains a distinct sharp peak that is a desirable characteristic for template matching compared with the three other methods. In general, good features for matching should meet the following demands: the high capability to distinguish an object from the background and high reliability in identifying the same object. From Fig. 4.5, we observe that OCM meets both requirements for reliable object matching.

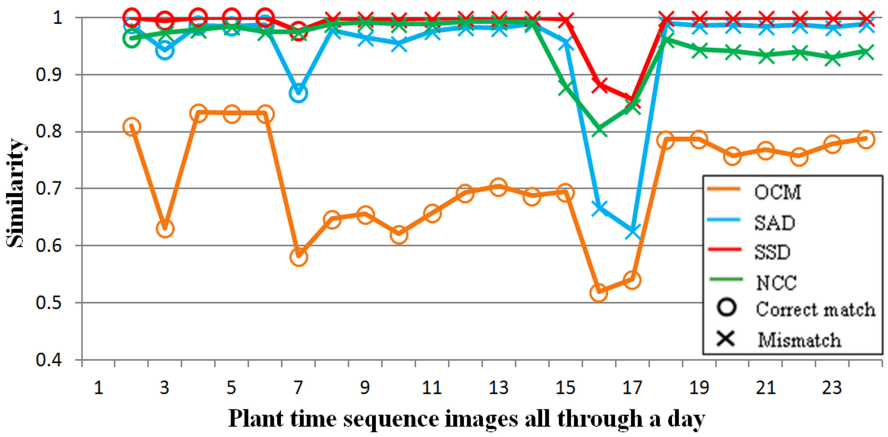
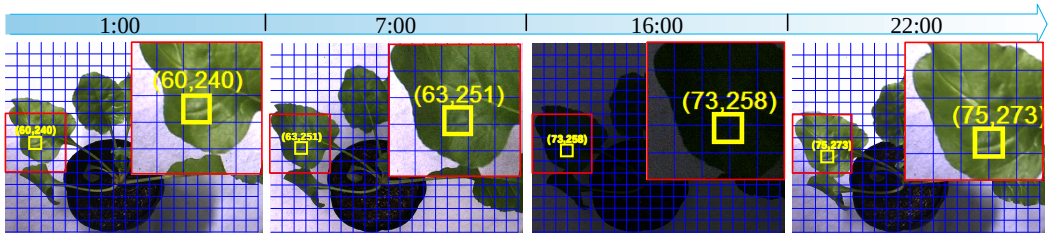
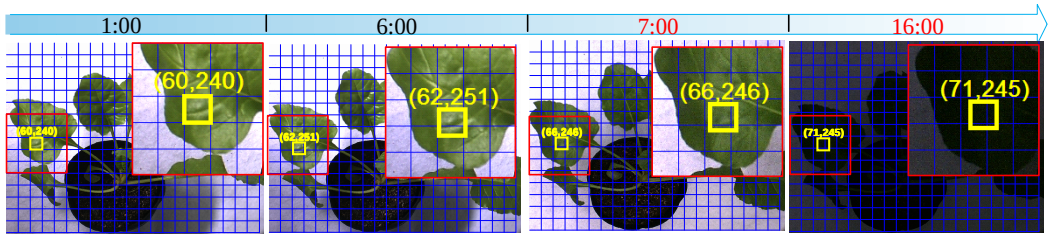


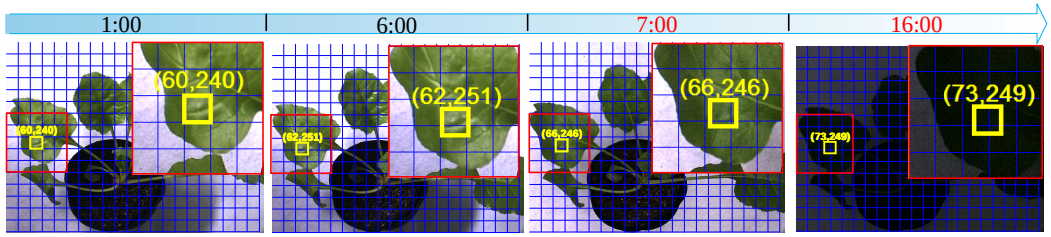

Figure 4.3: Comparation of matching results by OCM, SAD, SSD and NCC methods for time sequence plant images all through a day.



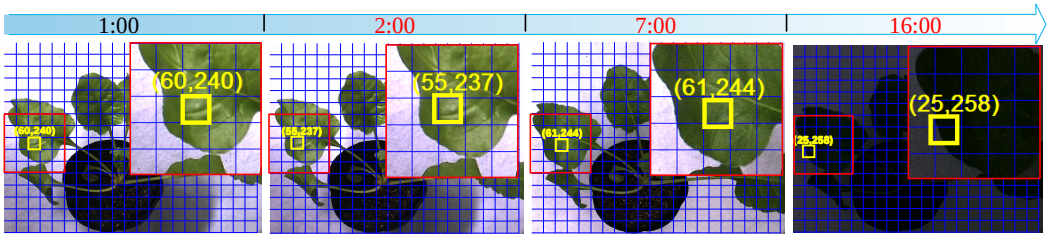

(a) OCM




(b) SAD




(c) SSD




(d) NCC

Figure 4.4: The comparative visualization results for the robustness of OCM against illumination changes.

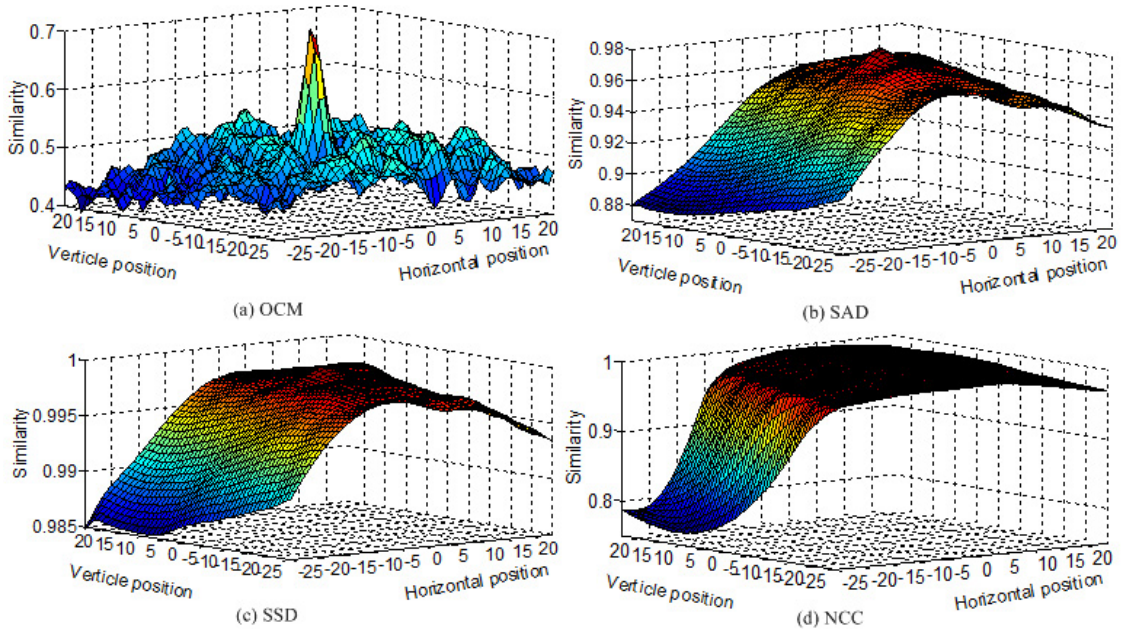



Figure 4.5: Comparative 3-D plots of the similarity values around the best match position in the object scene at time 13:00 by OCM, SAD, SSD and NCC methods respectively.

## 4.4 Effectiveness of adaptive OCM for foliar disease tracking

The experimental results in section above have demonstrated the robustness of OCM for foliage searching against illumination changes. However, when turning to issue of foliar disease observation, we extended the OCM into adaptive OCM to obtain more accurate disease tracking results with the regulation of following accumulated disease changes by adaptively replacing template over frames. For showing the effectiveness of the adaptive OCM compared to original OCM , we conducted two comparative experiments for tracking the CLS diseases at different development stages.

Fig. 4.6 shows comparative tracking results which extracted a template containing CLS disease at early stage. As disease develops, we see the early CLS spots get rapid changes in both color and shape aspects. Fig. 4.6 (a) shows the disease tracking results by the adaptive OCM, it can be seen that accurate positions of the template over frames can be aligned with the significant changes in the early spots. In contrast, OCM (Fig. 4.6 (b)) fails to track the early disease spots starting from the third day due to its inability of self-modification. The other comparative results are shown in Fig. 4.7 where the template with late-stage CLS spots was extracted. The disease at the late stage has relatively slower changes in color and shape than the early disease. But accumulated changes still exist along time. From the results by the adaptive OCM (Fig. 4.7 (a)), we see it can track the late spots with precisely accurate positions during the entire experimental period. In Fig. 4.7 (b), we see the OCM obtains similar tracking positions with the adaptive OCM due to the small changes of the late-stage disease over time. But more accurate disease tracking were obtained by the adaptive OCM through subtle position

comparisons. As a whole, we see the adaptive OCM shows its stability and accuracy for foliar disease tracking when disease develops with either fast or low speed. However, OCM is easy to loss reliability for tracking the disease with rapid changes.

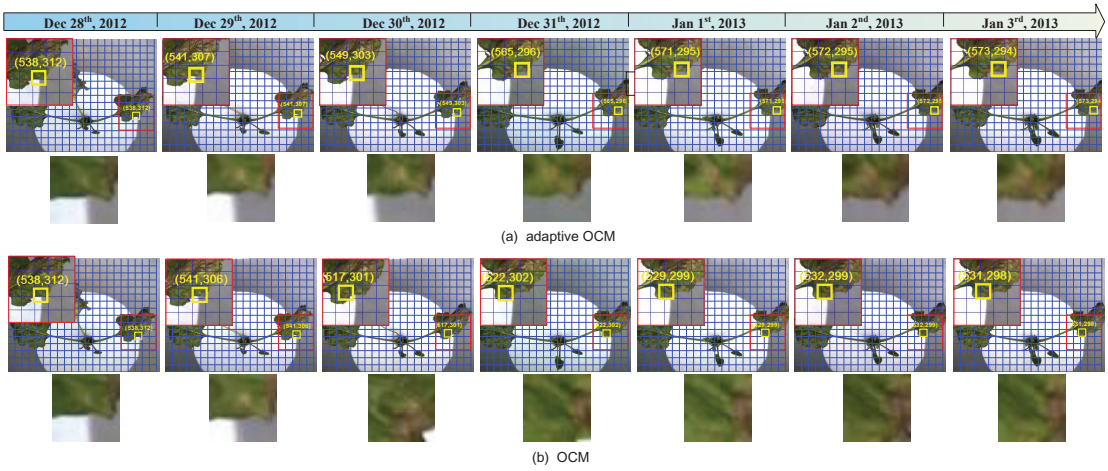



Figure 4.6: Comparative tracking results for foliar disease at early stage by adaptive OCM and OCM respectively.

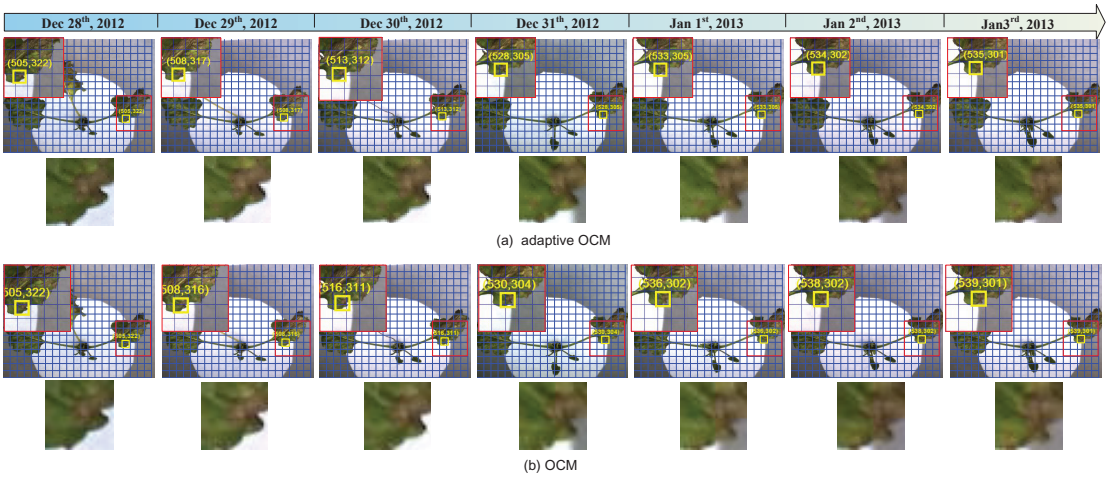


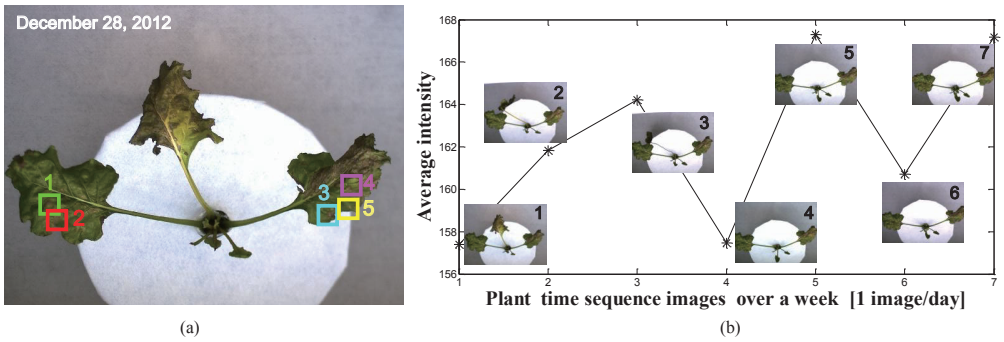

Figure 4.7: Comparative tracking results for foliar disease at late stage by adaptive OCM and OCM respectively.

## 4.5 Disease detection on local region scale without soil condition

### 4.5.1 Indoor experiment

#### Template extraction

In concurrence with the adaptive OCM applied for each frame among the plant sequence images, an SVM classifier was employed within the matched templates for classification and identification of disease pixels on the basis of the feature of color x and y intensities. In addition, to tentatively observe the relationship between disease processes and environmental RH, we chose one image per day during a one-week period from December 28, 2012 to January 3, 2013 (recorded as image frames: No.1–7) in this indoor experiments, and different amounts of water were sprayed on the plant leaves with a sprinkler each day at 1:00. Five manually chosen templates from the foremost plant frame on December 28, 2012 (shown in Fig. 4.8 (a)) were implemented by our proposed algorithm for continuous and site-specific disease development observation over time. For demonstrating the various illumination conditions of the seven plant frames, Fig. 4.8 (b) shows the average intensity of each frame. Obviously, illumination of each plant frame varies significantly and abruptly. Note that all the five templates were chosen from the leaf and right leaves of the plant rather than the middle one, it is because the middle leaf with heavy disease destruction was soon dying which can be visualized in the plant sequential images. This large leaf deformation makes template impossible to correspond its positions in subsequent images.




(a) (b)

Figure 4.8: Illustration of the five templates extraction and illumination conditions for seven plant frames over the experimental week period under indoor condition. (a) Extraction of five effective templates from the plant image frame on December 28, 2012 for disease development observation over time; (b) average intensity for each plant frame among all plant time sequence images.

#### Result visualization and disease quantification

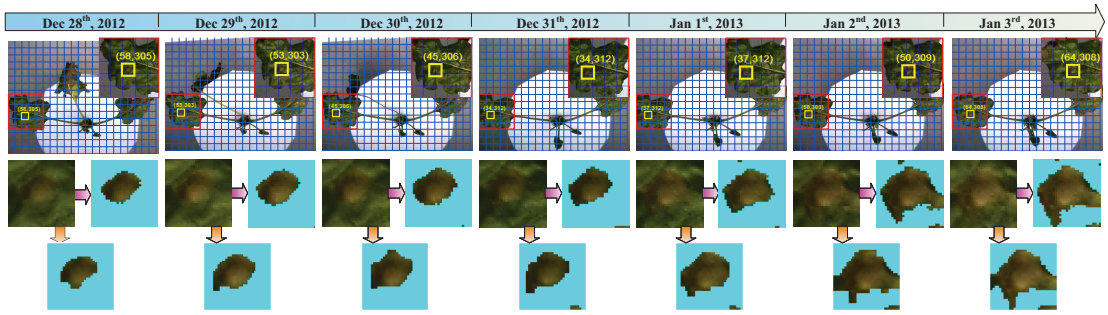
Fig. 4.9 shows the visual results for both continuous template matching by the adaptive OCM and further disease classification by the SVM classifier, for two different templates (template_

1 and template_ 3) of the five total templates (template_ 1–5) compared with manually classification results. For the images illustrated in each day, the first row shows the template matching results by the adaptive OCM. We can see that the selected initial template can be robustly and accurately tracked by the proposed matching method when illumination and plant movement changes. For the three subimages in the second row, the upper-left one indicates the matched template image, upper-right one is the corresponding disease classification result by the SVM, and lower-middle one is the result by manually classification. By comparation of the SVM with manually classification results, we can see that our proposed feature for the SVM classifier can keep robust performance for disease detection under environmental variation. Detailed results of the disease observation are as follows: (i) the disease in the first template (template_ 1) is an isolated spot, and this single spot expands in both size and shape over time, and diffuses more quickly in days with higher RH; (ii) the disease in the third template (template_ 3) initially started from one isolated large spot and two isolated small spots. As the disease progresses, individual spots coalesce and expand in size to heavily infect the leaf tissue. Therefore, site-specific disease quantization and expanding speed over time can be detected by the proposed method, providing information for precise disease mechanism observation and optimum fungicide-spraying decisions. However, from contrastive quantization and visualization results compared with manually classification, we observe that there is a distinct under-classification problem for the templates on December 31, 2012. It may be attributed to the darkest light conditions in that day's plant image frame, and is in a loss of prior information in the training data.

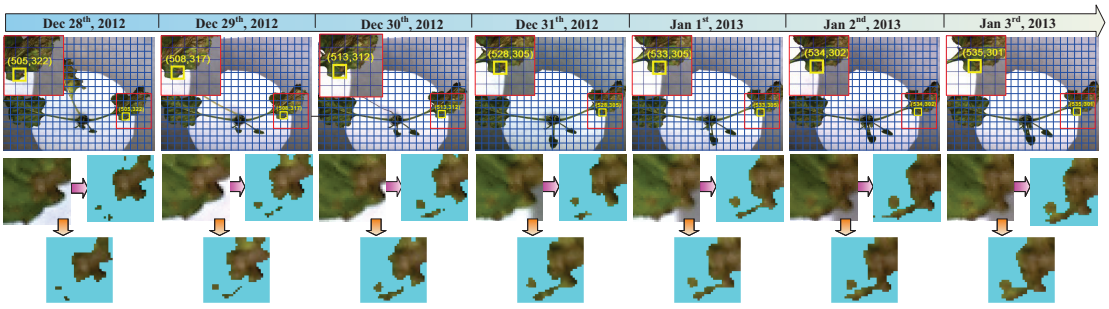
Fig. 4.10 (a) shows the disease classification and quantization results measured by the proposed algorithm for the five templates over the week in question. In addition, for evaluation and comparison of the disease classification algorithm performance employed in this study, a similar result was assessed with manual classification (Fig. 4.10 (b)) under the guidance of plant disease specialists. Using both our proposed algorithm and manual classification results, similar growth trends of the disease for all five effective templates over time were observed, which not only corresponds to the spread mechanism of the CLS disease but also shows the feasibility of our algorithm for predicting the spreading speed of the CLS. Meanwhile, the site-specific disease variances can also be observed by the template-based matching method. Moreover, the correlation between increasing speed of the CLS disease and environmental RH was revealed: the CLS disease grows faster in higher RH conditions than lower ones. This corresponds to the epidemiology of CLS because spores of *C. beticola* require moisture to germinate and infect leaves.

**Classification performance evaluation**

Correlated to the manual disease classification results, three statistical measurements, precision, recall, and $F$-measure, are utilized [68] in this study to analyze the temporal stability of the proposed method. Among these measurements, precision can be observed as a measure of exactness of fidelity, recall is a measure of completeness, and the $F$-measure considers both precision and recall in computing the score, where these can be interpreted and formulated as a weighted




(a) template_1




(b) template_3

Figure 4.9: Visualization results of adaptive template matching and disease classification for disease development observation with two different templates out of the five under indoor condition. (a) Result of template_1 and (b) result of template_3. (The blue areas correspond to the disease region. The gridding and red square are for position references of the template matching.)

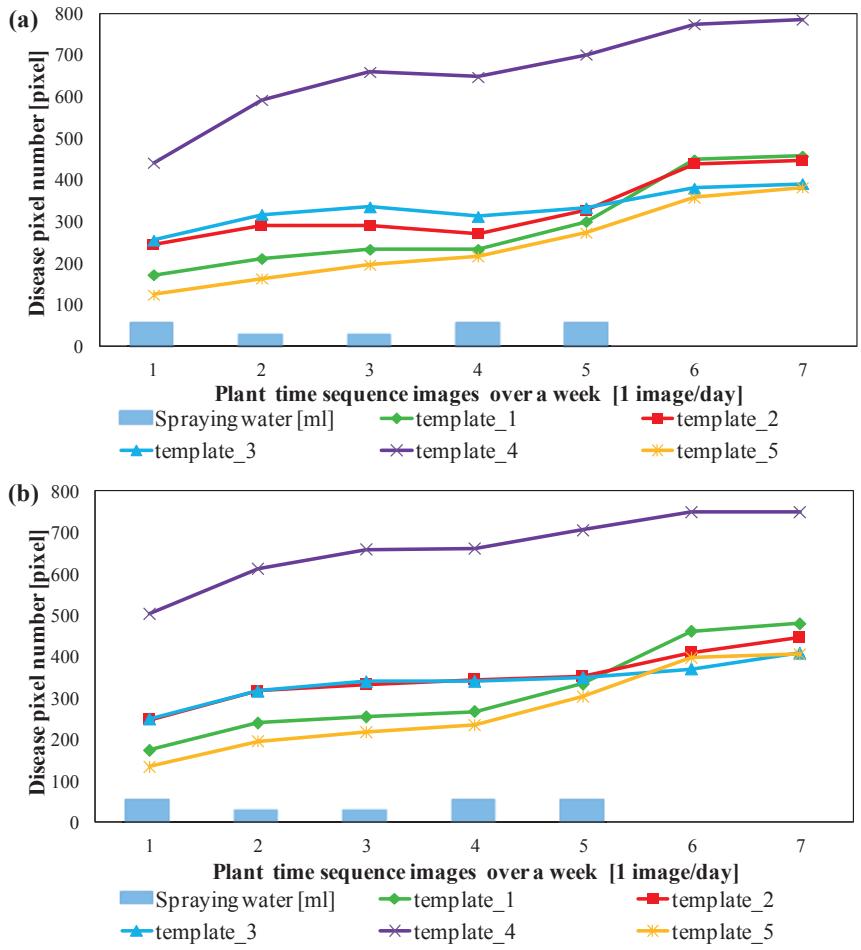



Figure 4.10: Quantitative results for the disease development of the five effective templates under indoor condition. (a) by our proposed method; (b) by manually classification.

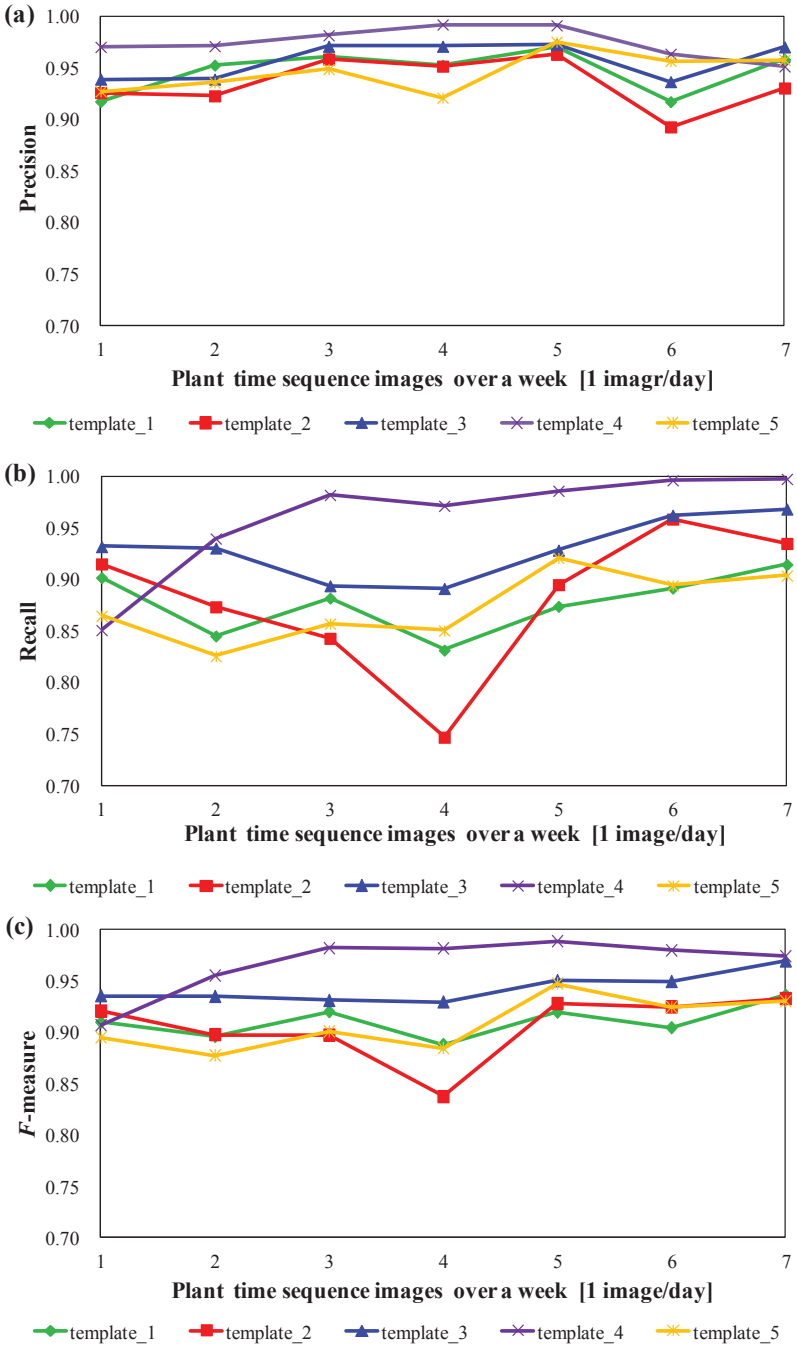



Figure 4.11: Performance evaluation of our proposed method by comparison with the manual classification results for (a) precision, (b) recall, and (c) *F*-measure under indoor condition.

harmonic mean of precision and recall. The formulas for the three statistical measurements are as follows:

$$\text{Precision} = \frac{\text{TruePositive}}{\text{TruePositive} + \text{FalsePositive}} \tag{4.1}$$

$$\text{Recall} = \frac{\text{TruePositive}}{\text{TruePositive} + \text{FalseNegative}} \tag{4.2}$$

$$F = 2 \cdot \frac{\text{Precision} \cdot \text{Recall}}{\text{Precison} + \text{Recall}} \tag{4.3}$$

The comparative results of precision, recall, and $F$-measure for the five templates of indoor experiments are shown in Fig. 4.11. We observe that the classification accuracies for precision, recall, and $F$-measure are consistent and greater than 0.74, indicating good performance and temporal stability of our proposed algorithm under indoor condition. However, again, the lowest value appears for all five templates on the fourth day (December 31, 2012) over the one-week period because of the darkest illumination condition. Furthermore, the mean values of the three statistical measurements for each template are recorded in Table 4.1, and all values were above 0.87, indicating good performance of the proposed method.

Table 4.1: Mean precision, recall, and $F$-measure values for the five templates under indoor condition.

| Template | Precision | Recall | $F$-measure |
|---|---|---|---|
| 1 | 0.9472 | 0.8772 | 0.9104 |
| 2 | 0.9353 | 0.8810 | 0.9054 |
| 3 | 0.9573 | 0.9294 | 0.9428 |
| 4 | 0.9747 | 0.9604 | 0.9668 |
| 5 | 0.9463 | 0.8738 | 0.9085 |

### 4.5.2 Field experiment

#### Template extraction

In field it contains more complex situations and variations comparing to relatively stable environment in indoor. The two main differences are: first, natural field involves the sandy soil background, which resembles CLS in color and is impossible to be eliminated by covering a whiteboard as we did in the indoor experiments; second, significant changes of ambient environment such as rainfall, wind and drought stress may result in large shape deformation of plant leaves, which is hardly to find the correspondences of leaf parts over frame. Therefore, to extend our proposed algorithm to field applications, we restrict the template selection process that the templates are chosen on the surface of leaves (within leaf edges) and preferentially from those leaves with less shape deformation over time. Fig. 4.12 (a) shows five chosen templates

from the foremost plant image on September 17, 2013 to demonstrate our five-day (September 17–21, 2013, recorded as image frame: No. 1–5) field experimental results. All of the five templates are chosen on the surface of three leaves which have less shape deformation over time. Furthermore, to demonstrate the illumination changes for the five frames in field experiments, we cannot simply use the same way as indoor experiments which regards the average intensity as a representative of illumination condition in each frame. Because the intensity value of soil background are affected not only by illumination intensity but also by soil moisture. Besides, illumination conditions in open field are not as uniform as that in indoor arising from specular reflection and shadows on leaves surfaces. Therefore, we use the average intensity of each template rather than the holistic plant image to indicate intensity changes for template series. Fig. 4.12 (b) shows the average intensity for each template. We can see that illumination conditions differ greatly in both intra-template and inter-template over time. It also can reflect the complexity of the illumination variations under natural day light condition.

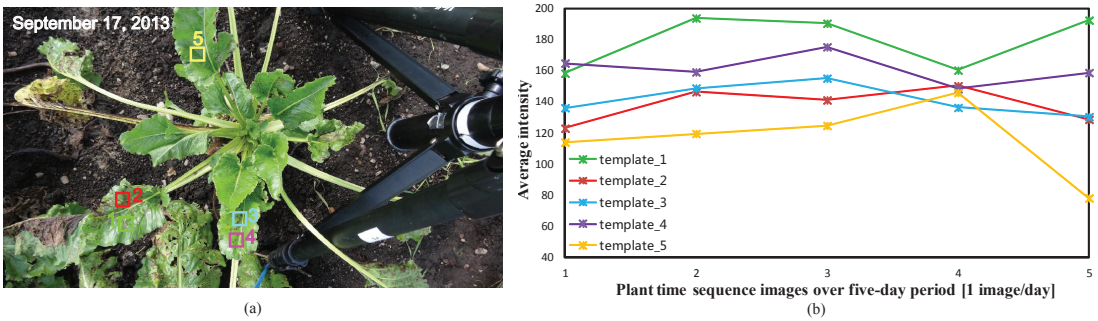



Figure 4.12: Illustration of the five templates extraction and local illumination conditions for the five templates during the five-day experimental period under field condition. (a) Extraction of five effective templates from the plant image frame on September 17, 2013 for disease development observation over time; (b) average intensity for each template during the five-day period.

**Result visualization and disease quantization**

Fig. 4.13 visualizes the results for three templates (template_1, template_3 and template_5) of the five ones (template_1–5). Fig. 4.14 shows the disease classification and quantization results for the five templates by the comparison of the proposed algorithm (Fig. 4.14 (a)) with manual classification (Fig. 4.14 (b)). From the aspect of disease growth tendency, we can see that large fluctuations occur in both manual classification and image detection results at the second day of the experimental period. This mainly results from overcast weather and drought soil at that day, which causes off-white image and downward wilting of leaves, and leads to inconsistent disease number of manual classification and under-classification problem of SVM classifier. But from the first row of Fig. 4.13, we can see that the OCM method can still correctly match the corresponding position for the templates under these severe changes at the second day. More-

over, if without regard to the second day's influence, CLS quantization results by the proposed method can generally have the similar growth trend comparing with those of manually classifications. But some expectations to the general growing tendency exist: first, the quantization result of the first template (template_1) shows a bigger slope at the fifth day by the proposed method compared with that of manual classification. This arises from specular reflection contained in this template and misclassified as CLS, as visualized in Fig. 4.13 (a); second, there is a large fluctuation in the third template (template_3) during last three days of the experiment period. This misclassification is because the contained leaf midrib and upper-left corner of the leaf part in the template resembling light brown color with CLS spots, which can be seen in Fig. 4.13 (b); Thirdly, the fifth template (template_5, visualized in Fig. 4.13 (c)), which shows a case of early detection for a single CLS spot, has a slight under-classification problem in early three days. However, we could see that our proposed template matching method of OCM can be robustly and successfully match the right positions for all five templates in time series images under such challengeable field condition. And also, our proposed feature of 2D xy-color histogram can be generally robust for CLS classification in field application, though some expectations exist under some extreme variations.

**Classification performance evaluation**

Fig. 4.15 shows a comparison of precision, recall and $F$-measure in field experiments. Repeatedly, as same as results in Fig. 4.14, all of the three measurements are in lower values at the second day than the rest four days over the experimental period, due to the severe under-classification problem caused by overcast weather and soil drought at that day. Additionally, if without considering the extreme cases of the third template (template_3, leaf midrib and yellow leaf part) and the fifth template (template_5, single-early CLS spot), the precision, recall and $F$-measure for the rest of three templates are greater than 0.57 under complex field condition. It is noticed that the third template (template_3) for detection of CLS in an early phrase, does not perform as well as the later stage in other templates. But we can see that the performance improves with disease growth. Table 4.2 further records the mean values of the three statistical measurements for all five templates during the experiment period.

Compared with lab experiment, the results from field experiments give slightly lower performance due to a variety of challenging situations in natural open field, but still show its capability and possibility of our proposed algorithm for robust CLS observation under complex field condition. Note that we did not apply any post-processing to our results for keeping independence and robustness of our algorithm, so some dispersed noise may appear. Thus the results could be improved by using some simple post-processing methods (such as morphological operation) to remove the noise according different application purposes.

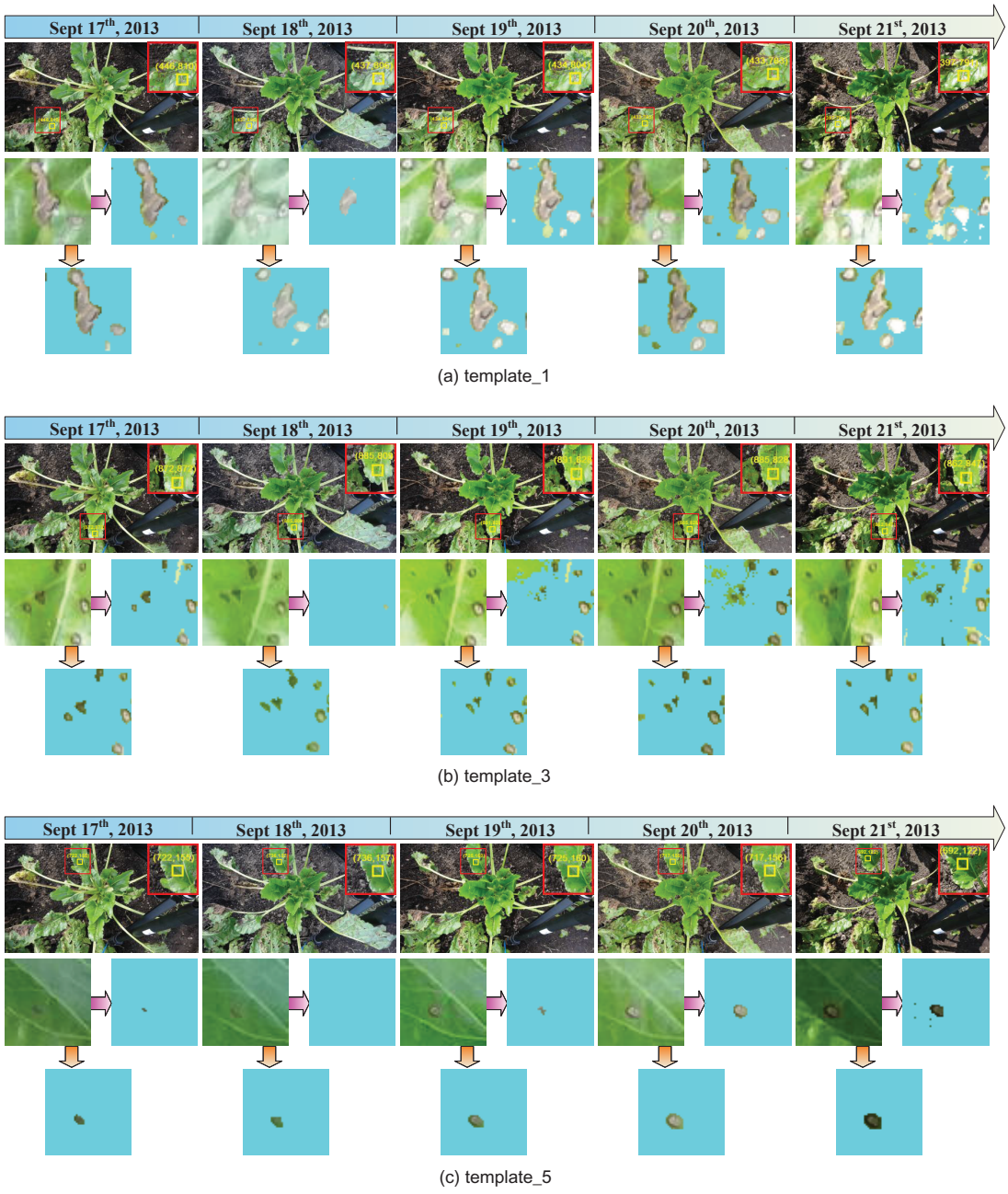



Figure 4.13: Visualization results of adaptive template matching and disease classification for disease development observation with three different templates out of the five under field condition. (a) Result of template_1, (b) result of template_3 and (c) result of template_5. (The blue areas correspond to the disease region. The red square is for position references of the template matching.)

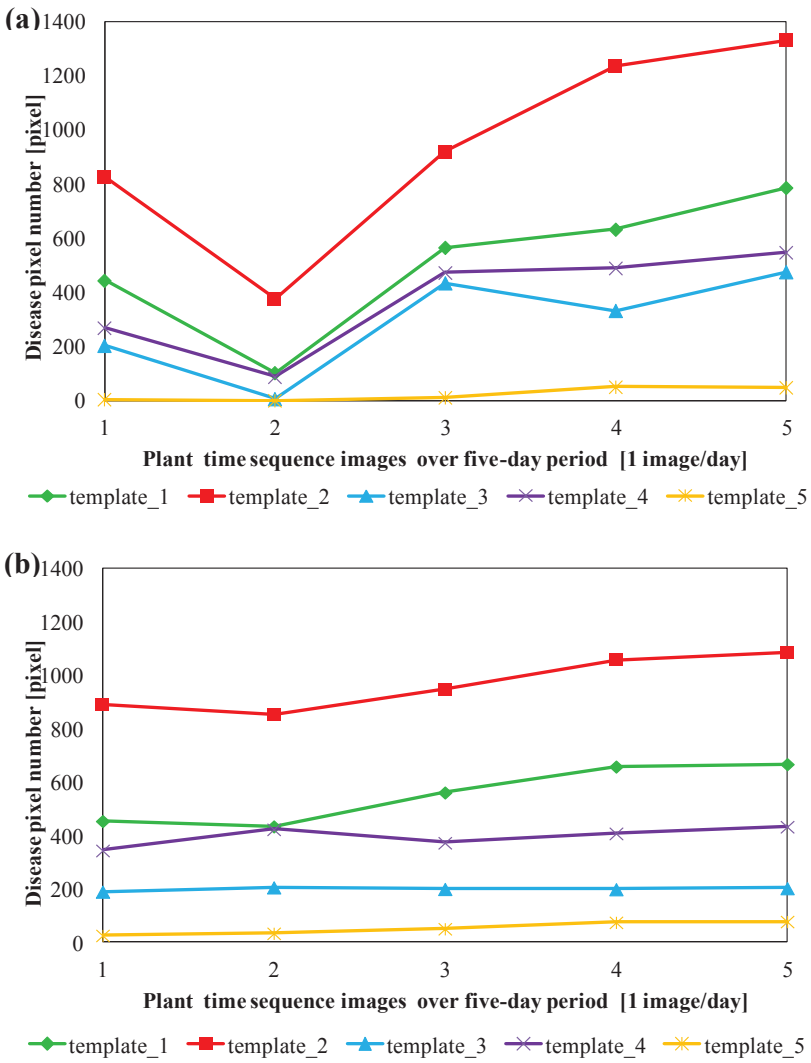



Figure 4.14: Quantitative results for the disease development of the five templates by both (a) our proposed method and (b) manually classification under field condition.

Table 4.2: Mean precision, recall, and $F$-measure values for the five templates under field condition.

| Template | Precision | Recall | $F$-measure |
|---|---|---|---|
| 1 | 0.8670 | 0.7259 | 0.7484 |
| 2 | 0.8509 | 0.7858 | 0.7945 |
| 3 | 0.5908 | 0.6409 | 0.4839 |
| 4 | 0.7199 | 0.6473 | 0.6403 |
| 5 | 0.7833 | 0.3254 | 0.4294 |

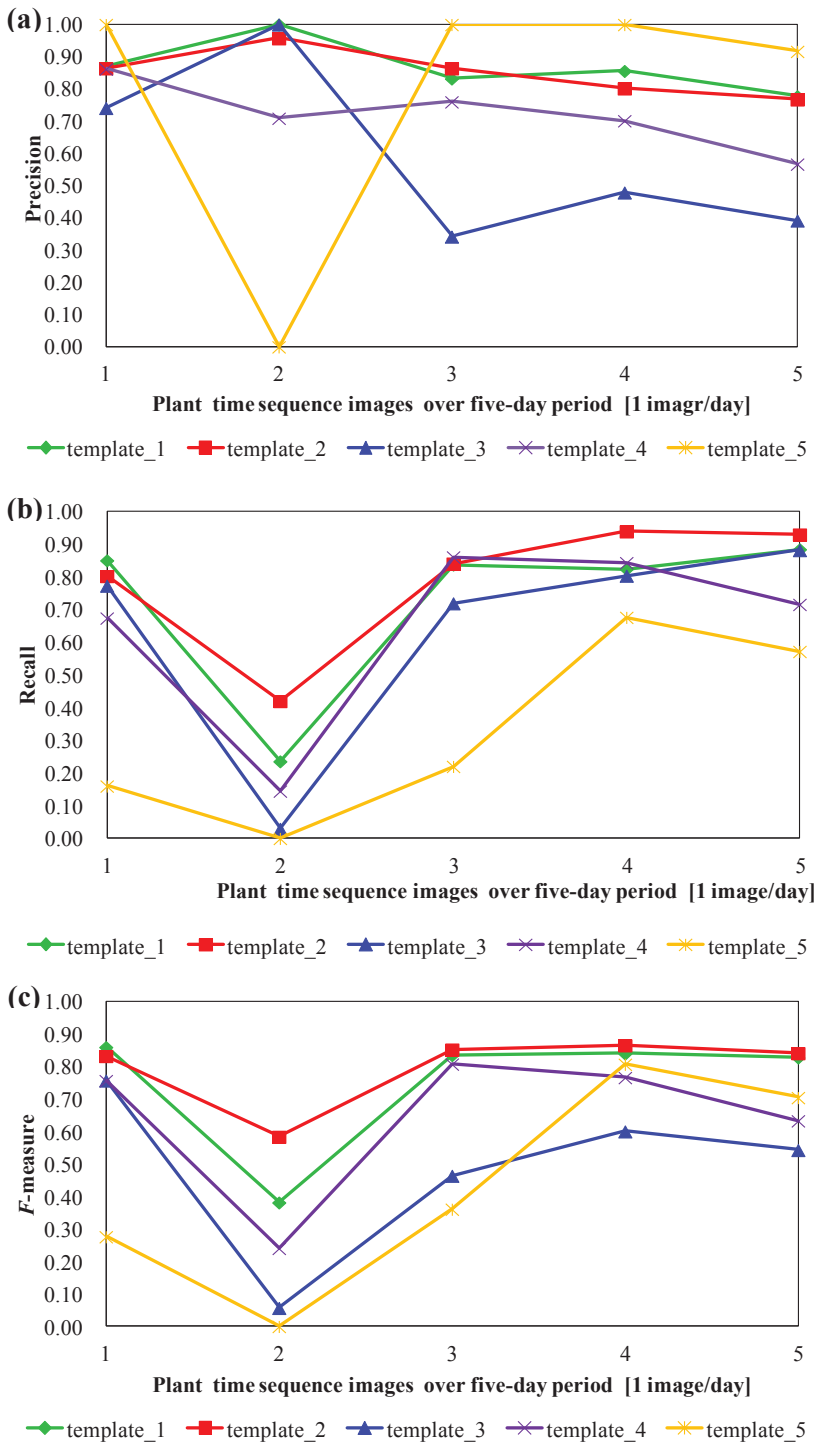



Figure 4.15: Performance evaluation of our proposed method by comparison with the manual classification results for (a) precision, (b) recall, and (c) *F*-measure under field condition.

## 4.6 Disease detection on single leaf scale with soil condition

### 4.6.1 Field experiment

#### Template extraction

Since the proposed algorithm is for disease observation on single leaf scale, a single leaf should be selected in advance for the observation. Due to the complex field conditions, however, not every single leaf is proper to be chosen as a template for its tracking by the adaptive OCM. If a leaf has a large shape deformation or moves out of the camera view, it could hardly be tracked successfully. Therefore, we suggest it is preferable to select those leaves with relatively stable movements and within the range of camera view among plant image sequences.

#### Result visualization

Fig. 4.16 demonstrates the experiment results by the proposed algorithm for two selected single leaves which are contained in each rectangular temple: one is an older leaf (upper part) and the other is a younger leaf (lower part) from the beet plant. Weather information (Temperature/T, relative humidity/RH, and insolation) at each day during the five-day experimental period is shown at the top row of the figure. From the weather information as well as plant-level image sequences, we can see that illumination differs greatly over frames due to natural daylight conditions, and the soil chromaticity which is not only affected by the illumination but also by soil moisture also varies a lot over time in the open field. For each part of the figure, the first row shows tracking results of the single leaf by the adaptive OCM framework, the second row shows further disease classification results for each matched template at each day by the SVM classification framework in conjunction with post-processing, the third row are the manually classification for the classification comparation. Firstly, from the matching results, we can see that both single leaves can be robustly and correctly tracked and observed by the first framework while illumination and non-rigid plant movement varying significantly under the field conditions. Secondly, from the classification results, it can be seen that CLS disease can be clearly detected against the clutter background with difficulties of sandy soil and specular reflection by the second framework. As a whole, we can see the effectiveness of the proposed algorithm for a single leaf scale based CLS developmental observation, by which automatic disease monitoring and detailed analysis can be achieved and facilitated during pathogenesis. Moreover, the observation of the disease development can also assist in judging fungicide efficiency.

Compared with the manual classification results, however, we could also see some misclassification problems existing in the experimental results. We categorized the misclassifications as over-classification and under-classification along with their causing reasons into three parts. First is an under-classification problem for the heavily destroyed leaf parts aroused from the feature of Entropy $\times$ Density, which fails to classify the heavily destroyed CLS pixels and misclassified them as soil pixels (discussed in Fig. 3.7 (b)). This under-classification for the heavily destroyed leaf parts can be obviously seen at the upper-left part of the older leaf at each day. Second is also a matter of under-classification but caused by the overcast weather at the second

day, which leaded to a fuzzy and off-white image for the low classification performance. We can see the sever under-classification problem in both classification results of older and younger leaves at that day. Third is an over-classification problem due to the intensive luminance at the fifth day of the experiment, in which some highlighted soil and shadowing leaf pixels were misclassified as CLS. But even with limitations of the misclassifications, the proposed method of adaptive OCM demonstrates its strong robustness for successful single leaf tracking among time series images under such various field conditions. Besides, the SVM classifier based on the proposed 3D feature combination also shows its discriminative power for the challenging CLS classification against the clutter field background. Furthermore, by utilizing the experimental results, individual difference of leaves within a whole plant (leaf-to-leaf variation) can also be observed: the older leaf suffers more serious disease destruction than the younger one in this experiment. In addition, the disease distribution within each single leaf could be possibly used for judging where fungus comes from by analyzing the spatial disease density.

**Classification performance evaluation**

Compared with the manual classification results, we implemented quantitative evaluation of the performance for the proposed method. Fig. 4.17 shows the comparative results of the precision (Fig. 4.17 (a)), recall (Fig. 4.17 (b)) and $F$-measure (Fig. 4.17 (c)) for the two selected single leaves during the five-day experiment period. The three metrics for the older leaf vary in a range of values from 0.53 to 0.83, and from 0.33 to 0.74 for the younger leaf. There are similar tendencies for both single leaves that more stable and greater results are obtained at the first, third, and fourth day compared with lower performances at second and fifth day. This is because the overcast weather at the second day and the intensive luminance at the fifth day caused severe the under-classification and over-classification problems. Furthermore, the mean values of the three metrics for each single leaf are shown in Table 4.3, and all value were above 0.53 which indicates the good performance and applicability of our proposed algorithm in the challenging field conditions. Note that the performance is obtained from a small number of training dataset extracted from a plant image capturing in one day. Furthermore, as can be seen from the comparison of the two single leaves, the older leaf obtained superior performance than the younger one. This is possibly because the older leaf surface with dark green color gets more distinct color difference against light brown CLS disease, while smaller contrast presents in the younger leaf with light green surface.

Table 4.3: Mean precision, recall, and $F$-measure values for the two templates of the older and younger single leaves over the five-day field experiment period.

| Template | Precision | Recall | $F$-measure |
|---|---|---|---|
| 1 | 0.7034 | 0.7521 | 0.7228 |
| 2 | 0.5272 | 0.5989 | 0.5545 |

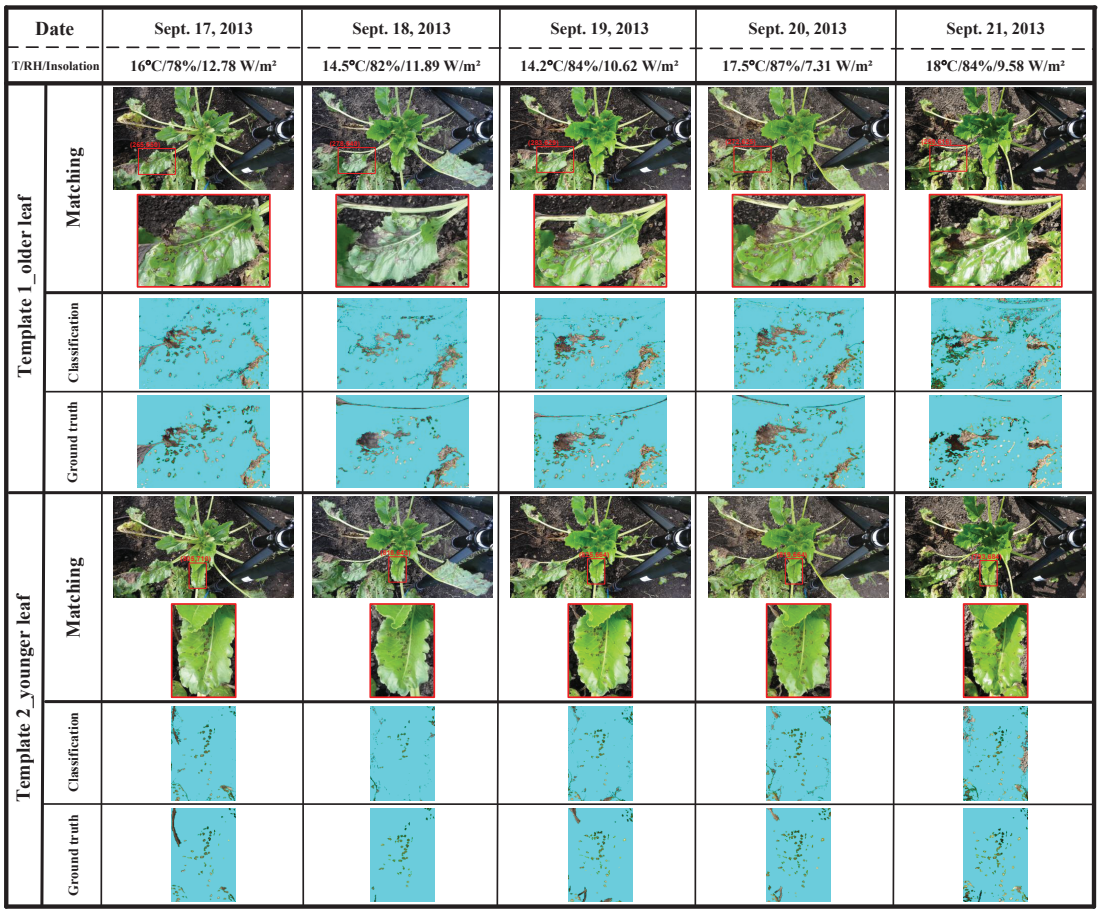
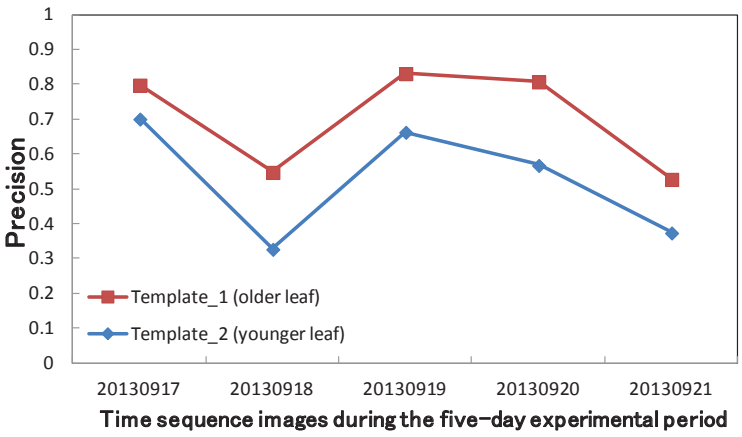
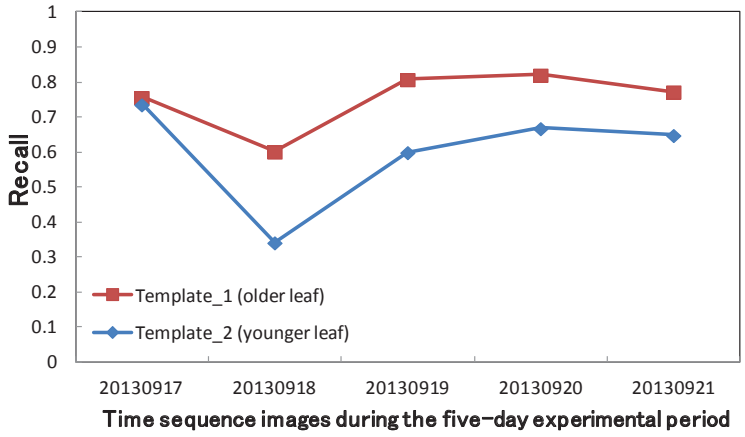


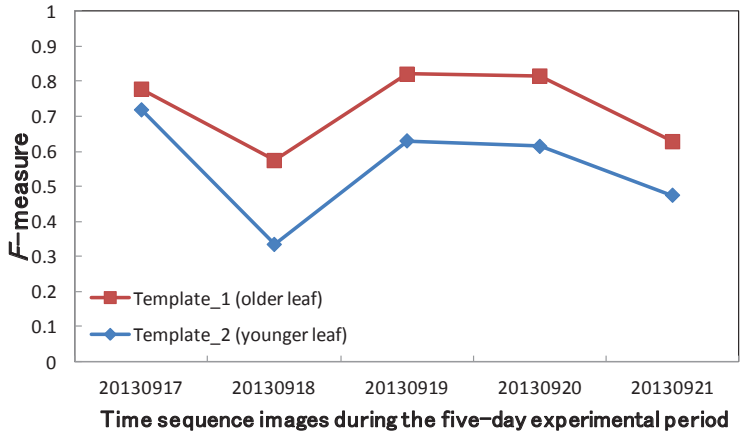

Figure 4.16: Visualization for single leaf based continuous CLS observation for two selected single leaves over five-day period. The upper part is for an older leaf and lower one if for a younger leaf. (The blue areas correspond to the background region.)




(a)




(b)




(c)

Figure 4.17: Visualization for single leaf based continuous CLS observation for two selected single leaves over five-day period. The upper part is for an older leaf and lower one if for a younger leaf. (The blue areas correspond to the background region.)

**Comparative results for the effectiveness of Entropy × Density**

For the proposed 3D feature L*, a*, Entropy × Density, the third feature is an integration of Entropy and Density by a multiplicative operation for exaggerating the discrimination between CLS and soil (the theoretical derivation is described in section 3.4.1). For demonstrating the effectiveness of the Entropy × Density compared with only employing a singular feature of Entropy or Density, a comparative experiment was implemented for disease classification by three different feature combination: (1) the proposed feature combination: L*, a*, Entropy × Density; (2) a feature combination with singular Entropy: L*, a*, Entropy; (3) a feature combination with singular Density: L*, a*, Density. Fig. 4.18 shows the comparative classification results of the three statical measurements for the selected two single leaves: the older leaf (Fig. 4.18 (a)) and younger leaves (Fig. 4.18 (b)), respectively. Meanwhile, Table 4.4 shows the mean value of the comparative results. Through the comparative results, it can be seen that all three feature combinations get close performances in the three evaluation measurements. However, the proposed feature L*, a*, Entropy × Density shows better performances in precision and *F*-measure for the both leaves compared with the other two feature combinations with the singular Entropy or Density.

Table 4.4: Mean precision, recall, and *F*-measure values for the comparative classification results for showing the effectiveness of Entropy × Density over the five-day field experiment period.

| Template | | Precision | Recall | *F*-measure |
|---|---|---|---|---|
| 1 | L*, a*, E×D | 0.7034 | 0.7521 | 0.7228 |
| | L*, a*, E | 0.6584 | 0.7532 | 0.6992 |
| | L*, a*, D | 0.6575 | 0.7706 | 0.7056 |
| 2 | L*, a*, E×D | 0.5272 | 0.5989 | 0.5545 |
| | L*, a*, E | 0.4723 | 0.6067 | 0.5249 |
| | L*, a*, D | 0.4629 | 0.6024 | 0.5147 |

**Comparative results of different feature combinations**

For the proposed 3D feature combination of L*, a*, Entropy × Density as inputs into the SVM classifier, the first feature of L* is a luminance-dependent color component indicating as lightness in L* a* b* color space. Usually, for achieving robust classification performance under various illuminations, features should be proposed with irrelevant lightness. However, we use L* as a necessary component in the proposed 3D feature combination because it is capable to separate the pixels belonging to the highlighted leaf/stalk and specular reflection from CLS, to enhance the discriminative power associating with a* in the color distribution. In this section, for demonstrating the effectiveness and necessity of L*, we implemented a comparative experiment which compared the classification results from four different feature combinations as inputs for SVM classifier: (1) the proposed feature combination: L*, a*, Entropy × Density; (2) a feature

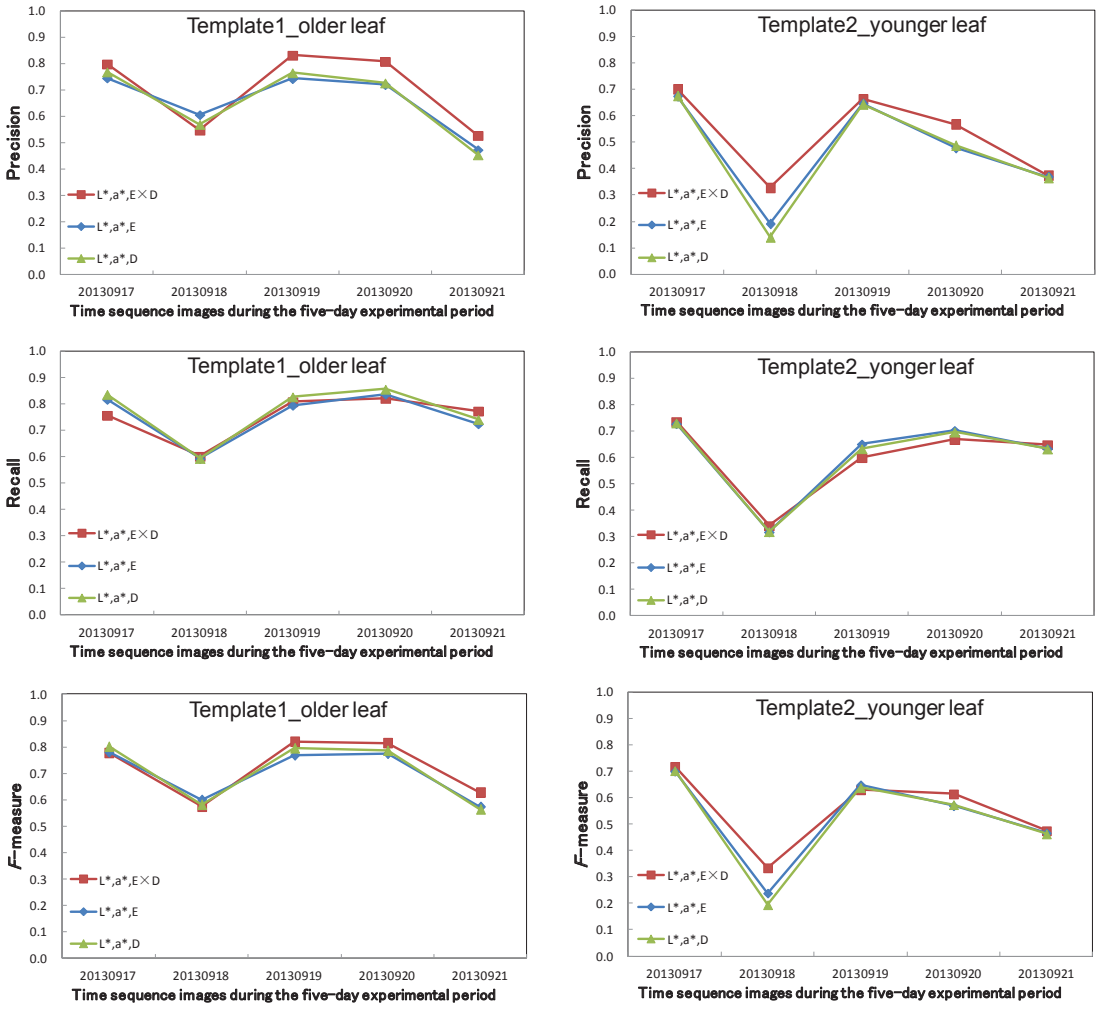



Figure 4.18: Comparative classification results of precision, recall, and *F*-measure for showing the effectiveness of $L^*$, $a^*$, Entropy × Density compared with $L^*$, $a^*$, Entropy and $L^*$, $a^*$, Density. (a) Results of the older leaf; (b) results of the younger leaf.

combination without $L^*$ component: $a^*$, Entropy × Density; (3) a feature combination with other two luminance-independent components in $L^*$ $a^*$ $b^*$ color space: $a^*$, $b^*$, Entropy × Density; (4) also a feature combination with other two luminance-independent components but in xyY color space: x, y, Entropy × Density. Fig. 4.19 shows the comparative classification results of the precision, recall, and *F*-measure from the different feature combinations for the selected older (Fig. 4.19 (a)) and younger leaves (Fig. 4.19 (b)), respectively. Meanwhile, Table 4.5 shows the mean value of the comparative results. From the comparison, we can see that the proposed feature combination of $L^*$, $a^*$, Entropy × Density excels in the classification performances of all three metrics compared with other three feature combinations, by which the effectiveness and necessity has been quantitatively verified.

Table 4.5: Mean precision, recall, and *F*-measure values for the comparative classification results from different feature combinations over the five-day field experiment period.

| Template | | Precision | Recall | *F*-measure |
|---|---|---|---|---|
| 1 | $L^*$, $a^*$, E×D | 0.7034 | 0.7521 | 0.7228 |
| | $a^*$, E×D | 0.5820 | 0.6413 | 0.5956 |
| | $a^*$, $b^*$, E×D | 0.7358 | 0.6483 | 0.6710 |
| | x, y, E×D | 0.5984 | 0.6245 | 0.5639 |
| 2 | $L^*$, $a^*$, E×D | 0.5272 | 0.5989 | 0.5545 |
| | $a^*$, E×D | 0.1637 | 0.2534 | 0.1910 |
| | $a^*$, $b^*$, E×D | 0.2300 | 0.3970 | 0.2694 |
| | x, y, E×D | 0.3616 | 0.4863 | 0.3754 |

**Comparative results of different types of datasets**

The comparative experiment in section above has demonstrated the necessity of the luminance-dependent component $L^*$ for the effective CLS classification. However, to what degree does the component $L^*$ affect the results for disease classification with respect to illumination changes?

We attempted to design robust features for CLS classification, thus the current dataset used for SVM classifier was extracted from the plant image captured in one day. In this study, we used the image from the first day of experimental period. We name the current dataset as constant dataset. However, since the existence of the $L^*$, the differences of the classification performances between the constant dataset and adaptive dataset (i.e., dataset was adaptively extracted from each day) need to be evaluated. In practice, making the adaptive dataset at each day is time-consuming to disturb automatic and real-time application of the proposed algorithm. Therefore, if the performance differences between the two types of datasets are smaller than a tolerant value, the relative robustness of the proposed $L^*$, $a^*$, Entropy × Density feature is ensured, thereby the applicability of the constant dataset for multi-day disease classification can be confirmed.

On the basis of the above analysis, the adaptive dataset was additionally made for evaluating the differences. Differing from the constant dataset described in section 3.4.3, the adaptive dataset was made by extracting 500 pixels from the plant image captured at each day, and then

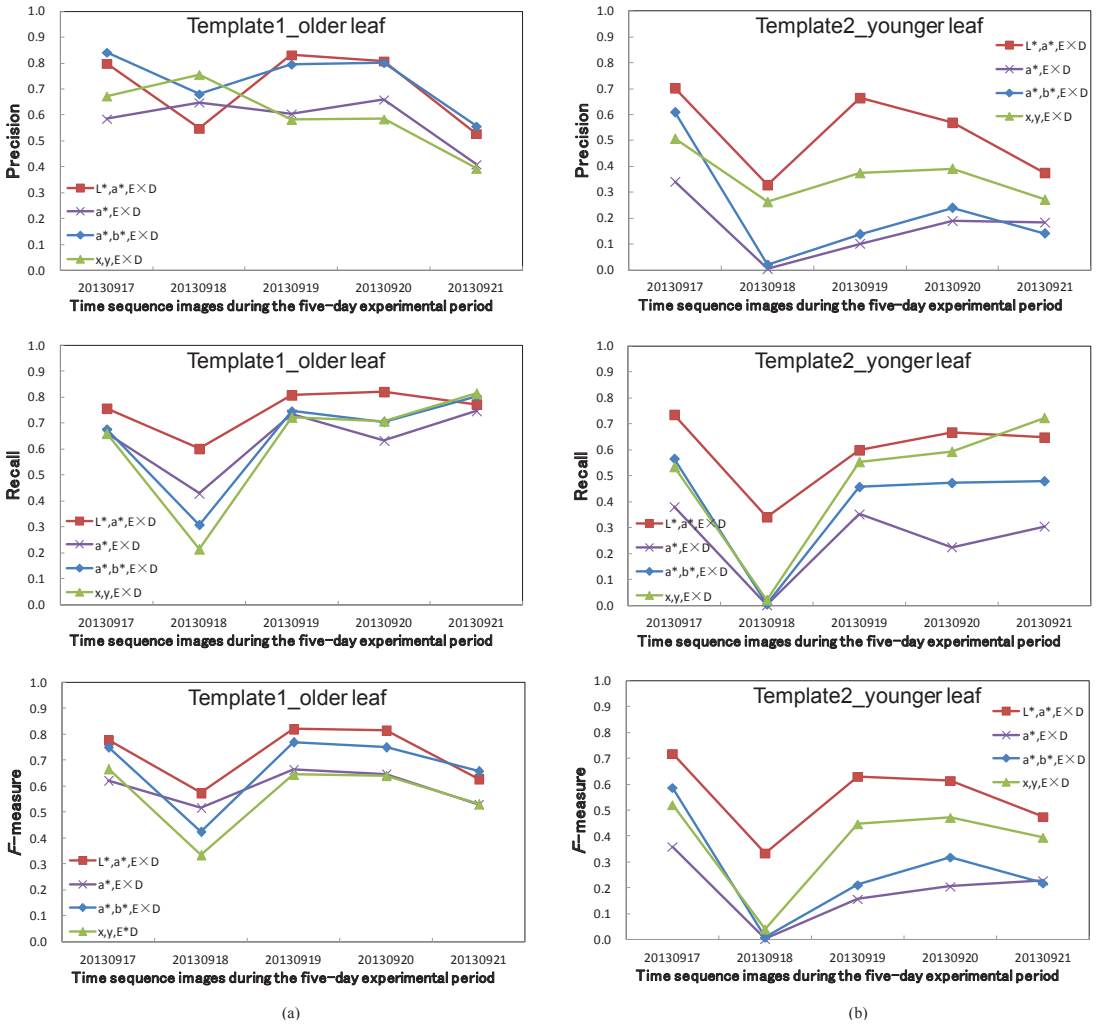



Figure 4.19: Comparative classification results of precision, recall, and $F$-measure from different feature combinations. (a) Results of the older leaf; (b) results of the younger leaf.

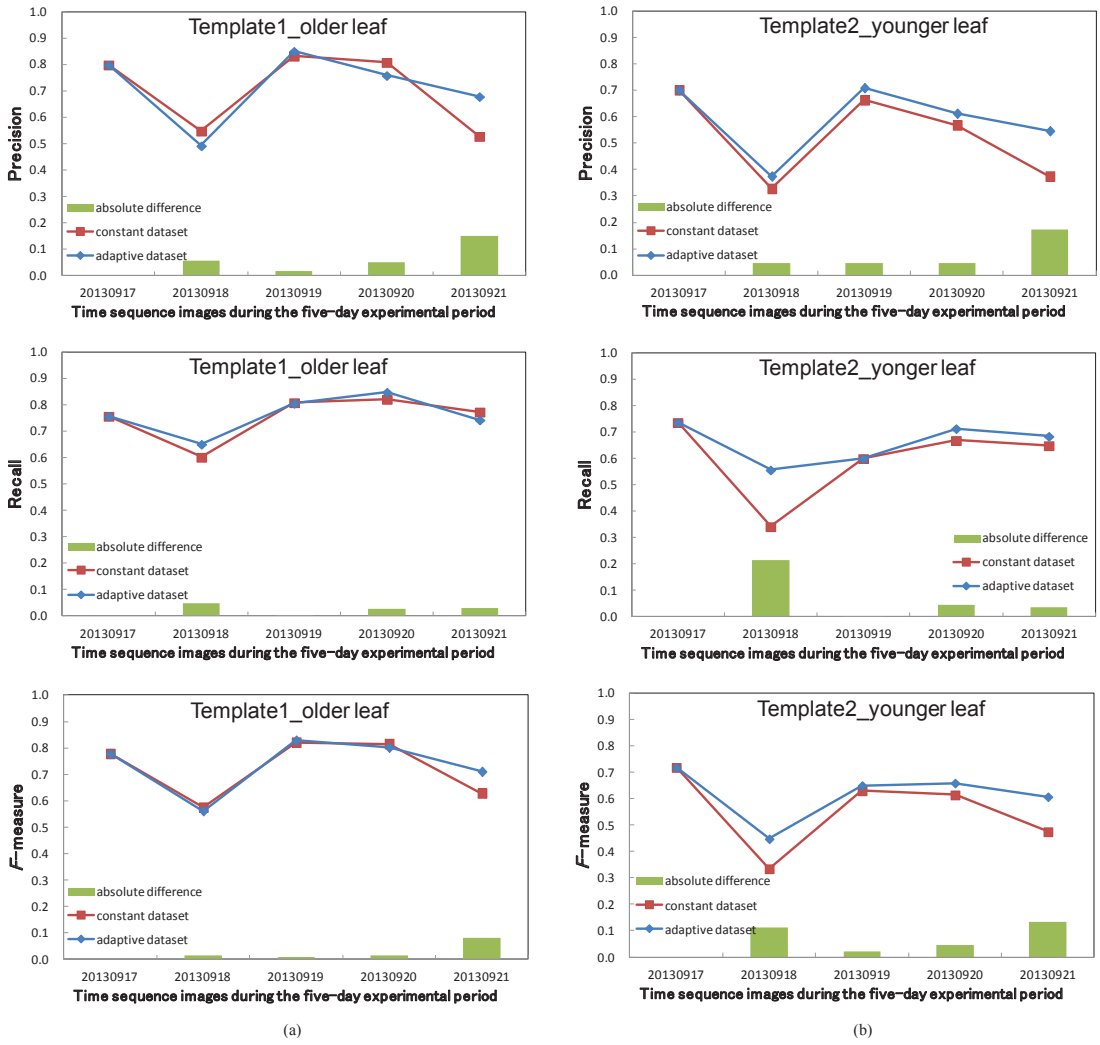



Figure 4.20: Comparative classification results of precision, recall, and *F*-measure from two types of datasets. (a) Results of the older leaf; (b) results of the younger leaf.

only apply the each day's dataset for the intra-day disease classification. Fig. 4.20 shows the comparative classification results for the two single leaves from the two types of datasets. From the comparison, we see the differences of the results between the two types of datasets are small. Both datasets get downward performances at the second and fifth day, and close performances are obtained in the rest three days due to similar light conditions. Meanwhile, Table. 4.6 shows the average value of the performance measurements, the mean differences between the two datasets are less than a small value of 0.062, by which the relatively robust performance of the proposed feature as well as the applicability of the constant dataset were quantitatively verified.

Table 4.6: Mean precision, recall, and *F*-measure values for the comparative classification results from different types of datasets over the five-day field experiment period.

| Template | | Precision | Recall | *F*-measure |
|---|---|---|---|---|
| 1 | Constant dataset | 0.7034 | 0.7521 | 0.7228 |
| | Adaptive dataset | 0.7161 | 0.7608 | 0.7353 |
| | Absolute difference | 0.0127 | 0.0086 | 0.0125 |
| 2 | Constant dataset | 0.5272 | 0.5989 | 0.5545 |
| | Adaptive dataset | 0.5891 | 0.6578 | 0.6166 |
| | Absolute difference | 0.0619 | 0.0589 | 0.0621 |

## 4.7 Summary

This chapter initially described the experimental treatments for both indoor and field experiments. Then, corresponding experimental results by the proposed algorithm was shown. First, the superior robustness of the OCM for searching foliar object compared with other three conventional method was demonstrated visually and quantitatively. Then, comparative experiments demonstrated the effectiveness of the adaptive OCM for leaf disease tracking comparing to the original OCM. The adaptive OCM showed its stable and accurate disease tracking performance in both early and late disease development stages. The third and fourth experiments presented CLS disease detection results by the proposed algorithm on two scales and two conditions. One is detecting disease on local region scale without soil condition by small-scaled template tracking and the 2D xy-color histogram feature, both indoor and field experiments showed the proposed algorithm can obtain precise and quantitative disease observation. The other is detecting disease on a single leaf scale with soil condition by leaf-scaled template tracking and the $L^*$, $a^*$, Entropy $\times$ Density feature, the field experimental results showed the effectiveness the proposed algorithm for CLS observation in the complex and natural field conditions.

# Chapter 5. Conclusions

In this chapter, we first present the contribution of this thesis, then outline future research needs and possibilities, finally a brief conclusion of this study.

## 5.1 Thesis contributions

This study proposed a novel and robust algorithm for continuous CLS disease detection in sugar beet against various changes. Both indoor and field experiments were implemented. The main contributions of this thesis are concluded by taking both insights on algorithm designing and related experiment results:

- Adaptive OCM was proposed for robust and effective foliar disease tracking in Chapter 2. The adaptive OCM was proposed on the basis of a template matching method of OCM. Notably, this is the first study that introduces the OCM into agricultural application for foliage searching. We first explained the robustness of OCM theoretically. Meanwhile, the excellent properties of OC image for extracting illumination irrelevant features and representing fine leaf edge information were demonstrated in Section 2.2. Furthermore, a comparative results in Section 4.3 shows the superior robustness of the OCM for non-rigid foliage searching against server natural daylight changes. Then, we extended the OCM into adaptive OCM as a object tracking scheme for accommodating the changes of disease progress in Section 2.3. Comparative experiments in Section 4.4 showed the necessity and effectiveness of the adaptive OCM for foliar disease tracking from the original OCM.

- Foliar disease tracking was applied for observing disease progresses at variant scales in Section 2.3. In practical application, both small-scale disease understanding and comprehensive disease analysis are required for precise plant protection. The flexibility of the template-based adaptive OCM leads resizable template selection for tracking foliar disease at variant scales. In this study, we employed two scales' disease tracking, one is on local region scale for detailed description of disease pigment and morphological changes; the other is on a single leaf scale for corresponding one of the actual used disease evaluation system and aiming for real field application. Furthermore, multiple templates can be extracted and tracked by the adaptive OCM simultaneously which makes site-specific reflection of inter- and intra-variances of disease progresses within a whole plant available. In this study, experiments were implemented to observe disease variations in region-based (in Section 4.5) and leaf-based (in Section 4.6) aspects.

- Novel feature extraction: a 2D xy-color histogram feature was proposed for CLS classification without soil condition in Section 3.3. We proposed the 2D xy-color histogram feature to classify CLS in environments without soil concern, such as sheltering soil background or concentrating disease observation on leaf surfaces, for obtaining high precision in disease classification and quantification without the interference of soil. The feature characters low dimensionality, non-parametric, luminance-independent, by which reliable and robust disease classification and quantification results were accessed in both indoor experiment and real field conditions (in Section 4.5).

- Novel feature extraction: a 3D $L^*$, $a^*$, Entropy $\times$ Density feature was proposed for CLS classification with soil condition in Section 3.4. For field application, sandy soil background in natural field is impossible to be eliminated. However, resembling in color between CLS and soil is a great challenge for their discrimination in RGB color images. In this study, we proposed a novel 3D feature space of the $L^*$, $a^*$, Entropy $\times$ Density, by which the difficulty of the discrimination between CLS and soil was attacked. Additionally, the feature space can classify the CLS disease from more clutter and complex visual patterns in real field conditions containing disease, healthy leaf, leaf stalk, specular reflection and soil. Field experiment results (in Section 4.6) demonstrated the effectiveness of the feature for CLS classification against the complex backgrounds. Moreover, a comparative experiment was implemented and indicated the superior performance of the proposed feature for disease classification compared with other feature combinations. Meanwhile, the other comparative experiment results additionally demonstrated the relative robustness of the proposed feature space. As a whole, it showed great promise of the proposed 3D feature for image-based CLS monitoring in sugar beet under real field conditions.

- Experiment systems with minimum equipment requirements were designed for both indoor and field conditions in Section 4.2. Both systems mainly consist of two components: a digital camera and a support. Any artificial illumination and plant growth interference were not needed (note that the fluorescent lamp in indoor experiment was placed only for providing light resource of image capturing during dark night rather than keeping uniform illumination). The simple construction makes the experimental system easily-accessed, low-cost, portable and easily-operated, which leads the practicality of the proposed algorithm for further large-scale field application.

## 5.2 Discussion and future work

In this section, we firstly concentrate on discussing possibilities to improve the proposed algorithm for better experiment performances and real applications. Because we employed the proposed algorithm for foliar disease detection on two scales under two different conditions, we discuss the relevant algorithm designing along with their experimental results separately as follows:

- First is detecting foliar disease on local region scale without soil condition for precise disease quantification. The small-scale adaptive OCM tracking (in Section 2.3.1) and 2D feature extraction of xy-color histogram (in Section 3.3.1) were utilized. Both indoor and field experiments were conducted in Section 4.5. From the experimental results, we see successful and robust matching results was achieved for local disease tracking against various illuminations by the adaptive OCM. However, an slight under-classification problem was revealed. The under-classification occurred in largely changed illumination conditions such as dark illumination in indoor experiments and overcast weather in field experiments. The problem appears to arise from two aspects: (1) the training sample for the SVM classifier in this study was only constructed from one day, and thus, they may be insufficient to capture all types of illumination under different weather conditions; and (2) a single feather of the 2D xy-color histogram was used rather than integrating multiple features that might remedy the defects observed by use of only one feature. These problems could potentially be improved by a combination of other features to improve robustness and discriminative capability of the SVM classifier, such as the use of texture feature and local homogeneity. Furthermore, color calibration for compensation of plant images under various illumination changes may prove another effective way.

- Second is the foliar disease detection on a single leaf scale with soil condition for further practical application. The leaf-scale adaptive OCM tracking (in Section 2.3.2) and 3D $L^*$, $a^*$, Entropy $\times$ Density (in Section 3.4.1) were employed. The field experiment results were showed in Section 4.6. We see the proposed algorithm can successfully track the single leaf with relatively dramatic movements and clearly classify the CLS disease against complex field backgrounds. However, accurate quantification of the disease progress can not be provided for further disease severity evaluation. There are some reasons for the inability in quantification: (1) the under-classification and over-classification exist in the largely changed weather conditions; (2) uneven soil ground causes slight view changes between camera and leaves over time; (3) large leaf deformation occurs due to internal circadian clock movements and external environment interactions. The problem aroused from the third reason is impossible to be handled by human operation. However, the first two problems might be improved through adjusting the robustness of the classification feature/model and the stabilization of the experimental system, to accommodate complex changes in real field environments for reliable quantification. Furthermore, a criterion for quantitatively evaluating image-based CLS severity index which corresponds with the practical one is also taken into account in our future work to promote the current study for the guidance of fungicide spraying .

In addition, the open problem of the initial template selection (size and position) as mentioned in Section 2.3.3 needs to be further experimentally investigated and theoretically analysed for different application purposes and environmental conditions. Correlation models should be built for analyzing the effect of initial template selections and specific purposes so as to develop ideal scales for different application intentions.

## 5.3 Conclusion

This thesis established a novel image algorithm for continuously detecting foliar disease against variations in natural and complex environments. The main content of the thesis is the proposed algorithm which mainly involves of two frameworks for tracking and classifying the foliar disease from plant-level image sequences, respectively. The algorithm was applied under double scales and conditions. Both indoor and field experiments were implemented. The experimental results indicated the feasibility and potential of the algorithm as a fundamental measurement method for consistent, site-specific and quantitative observation of disease progresses in plant, thus facilitating precise plant protection. Notably, the proposed algorithm might be generally applicable and suitable to other leafy plant varieties infected by monochromatic leaf diseases.

# Acknowledgements

I would like to express my heartfelt gratitude to my supervisor Professor Shun'ichi Kaneko. He led me to the research field of image processing with simultaneously kind consideration of my agriculture-oriented research background. I have been motivated by his extensive knowledge, logical thinking and unceasing self-improvement will. Meanwhile, his respect, patient and understanding are also as the fertilizer for this study. Through many times of research discussions, he guided me to analysis problem and develop new ideas logically and mathematically, which assist me to learn and describe the intrinsic property of the problem. Besides, He taught me many principles and excellent algorithms of image processing, which inspired the algorithm designing for this study. Moreover, I have learned how to effectively present, express and communicate problems with other researchers. All of these will benefit for my life-long research career.

I would like to extend my deep thanks to Dr. Fumio Tanaka, Dr. Miyuki Kayamori, and Dr. Motoshige Shimizu from Central Agricultural Experiment Station of Hokkaido Research Organization, who are cooperators of this research work. They introduced the agricultural problem to this study, and provide knowledges, suggestions and discussions from the view of agriculture applications. Furthermore, they assisted this study in many ways such as plant cultivation, fungus inoculation and test field management.

I would like to thank Associate Professor Takayuki Tanaka for his encouragement and useful comments for this study. And Dr. Isao Ohmura of Hokkaido Research Organization for his explanation and discussion of stereo vision calculation. And Associate Professor Hedenori Takauji of Muroran Institude of Technology for inspiriting me the feature extraction process of this research.

I wish to thank Dr. Yutaka Satoh of the National Institute of Advanced Industrial Science and Technology (AIST) for his meticulous preparation and work to assist my research and smooth my life during the one-month internship in AIST.

I also want to thank entire stuff and lab members along with the graduated students in Human-centric Engineering Laboratory for their friendly and kind help in both study and life aspects during my doctoral study.

This work is supported in part by the China Scholarship Council (CSC) under the grant No. 2011635044, which I gratefully acknowledge.

Finally, special thanks to my loving families: my grandmother, my parents, younger sister, my husband and his parents. Their endless love has always supported and encouraged me. Without their supports and understanding, this thesis would not be finished. I dedicate this thesis to them.

# References


[1] G. Agrios, Significance of plant diseases, Plant pathology (1997) 25–37.

[2] C. E. Windels, H. A. Lamey, D. Hilde, J. Widner, T. Knudsen, A cerospora leaf spot model for sugar beet: In practice by an industry, Plant disease 82 (7) (1998) 716–726.

[3] R. Jones, C. Windels, A management model for cercospora leaf spot of sugar beets, Tech. rep., Minnesota Extension Service, University of Minnesota. (1991).

[4] H.-E. Nilsson, Remote sensing and image analysis in plant pathology, Canadian Journal of Plant Pathology 17 (2) (1995) 154–166.

[5] E. Kerr, A. Weiss, et al., Fungicide efficacy and yield responses to fungicide treatments based on predictions of cercospora leaf spot of sugar beet, J. Sugar Beet Res 27 (1990) 58–71.

[6] Food, A. O. of the United Nations (FAO), Agribusiness Handbook: Sugar beet white sugar, FAO, 2009.

[7] B. Holtschulte, M. Asher, M. Molard, F. Rosso, G. Steinrücken, R. Beckers, et al., Cercospora beticola-worldwide distribution and incidence, Cercospora beticola Sacc. biology, agronomic influence and control measures in sugar beet. (2000) 5–16.

[8] M. Robert, E. plant pathologist, Cercospora leaf spot of sugar beet, University of Nebraska-Lincoln,Institute of Agriculture and Natural Resources, 2013.

[9] P. Ioannidis, G. Karaoglanidis, Control of Cercospora leaf spot and powdery mildew of sugar beet with fungicides and tolerant cultivars, The American Phytopathological Society, St. Paul, Minnesota, 2010, Ch. 3, pp. 189–211.

[10] W. C. James, Assessment of plant diseases and losses, Annual Review of Phytopathology 12 (1) (1974) 27–48.

[11] F. W. Nutter Jr, P. D. Esker, R. A. C. Netto, Disease assessment concepts and the advancements made in improving the accuracy and precision of plant disease data, in: Plant disease epidemiology: facing challenges of the 21st Century, Springer, 2006, pp. 95–103.

[12] J. Vereijssen, J. Schneider, A. Termorshuizen, M. Jeger, Comparison of two disease assessment methods for assessing cercospora leaf spot in sugar beet, Crop Protection 22 (1) (2003) 201–209.

[13] C. Bock, G. Poole, P. Parker, T. Gottwald, Plant disease severity estimated visually, by digital photography and image analysis, and by hyperspectral imaging, Critical Reviews in Plant Sciences 29 (2) (2010) 59–107.

[14] G. J. Holmes, E. A. Brown, G. Ruhl, What's a picture worth? the use of modern telecommunications in diagnosing plant diseases, Plant disease 84 (12) (2000) 1256–1265.

[15] A.-K. Mahlein, E.-C. Oerke, U. Steiner, H.-W. Dehne, Recent advances in sensing plant diseases for precision crop protection, European Journal of Plant Pathology 133 (1) (2012) 197–209.

[16] S. Sankaran, A. Mishra, R. Ehsani, C. Davis, A review of advanced techniques for detecting plant diseases, Computers and Electronics in Agriculture 72 (1) (2010) 1–13.

[17] H.-E. Nilsson, Remote sensing and image processing for disease, Protection Ecology 2 (1980) 271–274.

[18] T. Price, R. Gross, W. J. Ho, C. Osborne, A comparison of visual and digital image-processing methods in quantifying the severity of coffee leaf rust (hemileia vastatrix), Animal Production Science 33 (1) (1993) 97–101.

[19] J. Garling, R. Rimelspach, M. Boehm, A comparisoin of four methods to accurately measure dollar spot severity of turfgrass, Phytopathology 89 (1999) S26.

[20] C. Bock, P. Parker, A. Cook, T. Gottwald, Visual rating and the use of image analysis for assessing different symptoms of citrus canker on grapefruit leaves, Plant Disease 92 (4) (2008) 530–541.

[21] G. Polder, G. van der Heijden, H. Jalink, J. Snel, Correcting and matching time sequence images of plant leaves using penalized likelihood warping and robust point matching, Computers and electronics in agriculture 55 (1) (2007) 1–15.

[22] A. Camargo, J. Smith, An image-processing based algorithm to automatically identify plant disease visual symptoms, Biosystems Engineering 102 (1) (2009) 9–21.

[23] A. Camargo, J. Smith, Image pattern classification for the identification of disease causing agents in plants, Computers and Electronics in Agriculture 66 (2) (2009) 121–125.

[24] Y. Tian, C. Zhao, S. Lu, X. Guo, Svm-based multiple classifier system for recognition of wheat leaf diseases, in: World Automation Congress (WAC), 2012, IEEE, 2012, pp. 189–193.

[25] K.-Y. Huang, Application of artificial neural network for detecting phalaenopsis seedling diseases using color and texture features, Computers and electronics in agriculture 57 (1) (2007) 3–11.

[26] I. S. Ahmad, J. F. Reid, M. R. Paulsen, J. B. Sinclair, Color classifier for symptomatic soybean seeds using image processing, Plant disease 83 (4) (1999) 320–327.

[27] J. G. A. Barbedo, Digital image processing techniques for detecting, quantifying and classifying plant diseases, SpringerPlus 2 (1) (2013) 660.

[28] A. F. Goetz, G. Vane, J. E. Solomon, B. N. Rock, Imaging spectrometry for earth remote sensing, Science 228 (4704) (1985) 1147–1153.

[29] C. Bravo, D. Moshou, J. West, A. McCartney, H. Ramon, Early disease detection in wheat fields using spectral reflectance, Biosystems Engineering 84 (2) (2003) 137–145.

[30] L. Chaerle, D. Van Der Straeten, Imaging techniques and the early detection of plant stress, Trends in plant science 5 (11) (2000) 495–501.

[31] T. Kobayashi, E. Kanda, K. Kitada, K. Ishiguro, Y. Torigoe, Detection of rice panicle blast with multispectral radiometer and the potential of using airborne multispectral scanners, Phytopathology 91 (3) (2001) 316–323.

[32] T. Rumpf, A.-K. Mahlein, U. Steiner, E.-C. Oerke, H.-W. Dehne, L. Plümer, Early detection and classification of plant diseases with support vector machines based on hyperspectral reflectance, Computers and Electronics in Agriculture 74 (1) (2010) 91–99.

[33] A.-K. Mahlein, U. Steiner, C. Hillnhütter, H.-W. Dehne, E.-C. Oerke, Hyperspectral imaging for small-scale analysis of symptoms caused by different sugar beet diseases, Plant methods 8 (1) (2012) 3.

[34] R. Oberti, M. Marchi, P. Tirelli, A. Calcante, M. Iriti, A. N. Borghese, Automatic detection of powdery mildew on grapevine leaves by image analysis: Optimal view-angle range to increase the sensitivity, Computers and Electronics in Agriculture 104 (2014) 1–8.

[35] G. Polder, G. Van der Heijden, J. Van Doorn, J. Clevers, R. Van der Schoor, A. Baltissen, Detection of the tulip breaking virus (tbv) in tulips using optical sensors, Precision Agriculture 11 (4) (2010) 397–412.

[36] D. Moshou, C. Bravo, R. Oberti, J. West, L. Bodria, A. McCartney, H. Ramon, Plant disease detection based on data fusion of hyper-spectral and multi-spectral fluorescence imaging using kohonen maps, Real-Time Imaging 11 (2) (2005) 75–83.

[37] A.-K. Mahlein, C. Hillnhütter, T. Mewes, C. Scholz, U. Steiner, H.-W. Dehne, E.-C. Oerke, Disease detection in sugar beet fields: A multi-temporal and multi-sensoral approach on different scales, in: SPIE Europe Remote Sensing, International Society for Optics and Photonics, 2009, pp. 747228–747228.

[38] C. Bravo, D. Moshou, R. Oberti, J. West, A. McCartney, L. Bodria, H. Ramon, Foliar disease detection in the field using optical sensor fusion.

[39] F. Ullah, S. Kaneko, S. Igarashi, Orientation code matching for robust object search, IEICE transactions on information and systems 84 (8) (2001) 999–1006.

[40] F. Ullah, S. Kaneko, Using orientation codes for rotation-invariant template matching, Pattern recognition 37 (2) (2004) 201–209.

[41] S. Hutchinson, G. D. Hager, P. I. Corke, A tutorial on visual servo control, Robotics and Automation, IEEE Transactions on 12 (5) (1996) 651–670.

[42] N. P. Papanikolopoulos, P. K. Khosla, T. Kanade, Visual tracking of a moving target by a camera mounted on a robot: a combination of control and vision, Robotics and Automation, IEEE Transactions on 9 (1) (1993) 14–35.

[43] E. Bardinet, L. Cohen, N. Ayache, Tracking medical 3d data with a deformable parametric model, in: Computer Vision–ECCV'96, Springer, 1996, pp. 315–328.

[44] R. Howarth, H. Buxton, Visual surveillance monitoring and watching, in: Computer Vision–ECCV'96, Springer, 1996, pp. 321–334.

[45] T. Frank, M. Haag, H. Kollnig, H.-H. Nagel, Tracking of occluded vehicles in traffic scenes, in: Computer Vision–ECCV'96, Springer, 1996, pp. 485–494.

[46] F. Ullah, S. Kaneko, Robust computation of optical flow using orientation code matching., IEEJ T. Electron. Inf. Syst. 123 (2) (2003) 301–308.

[47] I. Ohmura, T. Mitamura, H. Takauji, S. Kaneko, A real-time stereo vision sensor based on fpga realization of orientation code matching, in: Optomechatronic Technologies (ISOT), 2010 International Symposium on, IEEE, 2010, pp. 1–5.

[48] V. N. Vapnik, V. Vapnik, Statistical learning theory, Vol. 2, Wiley New York, 1998.

[49] http://www.visiondummy.com/2014/04/curse-dimensionality-affect-classification/.

[50] M. Verleysen, D. François, The curse of dimensionality in data mining and time series prediction, in: Computational Intelligence and Bioinspired Systems, Springer, 2005, pp. 758–770.

[51] S. Vassiliadis, E. A. Hakkennes, J. Wong, G. G. Pechanek, The sum-absolute-difference motion estimation accelerator, in: Euromicro Conference, 1998. Proceedings. 24th, Vol. 2, IEEE, 1998, pp. 559–566.

[52] N. N. Dawoud, Fast template matching method based optimized sum of absolute difference algorithm for face localization., International Journal of Computer Applications 18.

[53] K. Briechle, U. D. Hanebeck, Template matching using fast normalized cross correlation, in: Aerospace/Defense Sensing, Simulation, and Controls, International Society for Optics and Photonics, 2001, pp. 95–102.

[54] T. Dornbusch, O. Michaud, I. Xenarios, C. Fankhauser, Differentially phased leaf growth and movements in arabidopsis depend on coordinated circadian and light regulation, The Plant Cell Online 26 (10) (2014) 3911–3921.

[55] V. Vapnik, Universal learning technology: Support vector machines, NEC Journal of Advanced Technology 2 (2) (2005) 137–144.

[56] P. Dollár, Z. Tu, H. Tao, S. Belongie, Feature mining for image classification, in: Computer Vision and Pattern Recognition, 2007. CVPR'07. IEEE Conference on, IEEE, 2007, pp. 1–8.

[57] K. T., Auto-correlation based feature extraction and recognition methods and their applications, Ph.D. thesis, Tsukuba University (2009).

[58] J. Van De Weijer, C. Schmid, Coloring local feature extraction, in: Computer Vision–ECCV 2006, Springer, 2006, pp. 334–348.

[59] Y. Domae, H. Takauji, H. Stier, S. Kaneko, T. Tanaka, Extraction and tracking of orientation coded features being robust against illumination changes, in: Proceedings of the ISPRS Commission V Symposium, Vol. 36, Citeseer, pp. 2006–9.

[60] A. Biem, S. Katagiri, B.-H. Juang, Pattern recognition using discriminative feature extraction, IEEE transactions on signal processing 45 (2) (1997) 500–504.

[61] S. Knerr, L. Personnaz, G. Dreyfus, Single-layer learning revisited: a stepwise procedure for building and training a neural network, in: Neurocomputing, Springer, 1990, pp. 41–50.

[62] H. Yu, T. Xie, S. Paszczynski, B. M. Wilamowski, Advantages of radial basis function networks for dynamic system design, Industrial Electronics, IEEE Transactions on 58 (12) (2011) 5438–5450.

[63] D. A. Kerr, The CIE XYZ and xyY color spaces (2010).

[64] C. Ying, P. Hao, Optimal transform in perceptually uniform color space and its application in image retrieval, in: Signal Processing, 2004. Proceedings. ICSP'04. 2004 7th International Conference on, Vol. 2, IEEE, 2004, pp. 1107–1110.

[65] T. H, K. SI, T. T, Scalable image searching method based on orientation code density, Journal of the Japan Society for Precision Engineering 72 (4) (2006) 487–493.

[66] B. Scholkopft, K.-R. Mullert, Fisher discriminant analysis with kernels, Neural networks for signal processing IX.

[67] C.-C. Chang, C.-J. Lin, Libsvm: a library for support vector machines, ACM Transactions on Intelligent Systems and Technology (TIST) 2 (3) (2011) 27.

[68] J. Makhoul, F. Kubala, R. Schwartz, R. Weischedel, et al., Performance measures for information extraction, in: Proceedings of DARPA broadcast news workshop, 1999, pp. 249–252.

[69] http://en.wikipedia.org/wiki/Precision_and_recall.

# Appendix A Publication lists

## A.1 Journal Papers

Rong Zhou, Shun'ichi Kaneko, Fumio Tanaka, Miyuki Kayamori, Motoshige Shimizu: Disease Detection of Cercospora Leaf Spot in Sugar Beet by Robust Template Matching. Computers and Electronics in Agriculture, Vol.108, pp.58-70, 2014.

## A.2 International Conferences

1. Rong Zhou, Shun'ichi Kaneko, Fumio Tanaka, Miyuki Kayamori, Motoshige Shimizu: Robust Detection of Cercospora Leaf Spot in Sugar Beet Using Orientation Code Matching. The 11th International Conference on Quality Control by Artificial Vision (QCAV2013), pp.99-106, Fukuoka, Japan, May 30 - June 1, 2013.

2. Rong Zhou, Shun'ichi Kaneko, Fumio Tanaka, Miyuki Kayamori, Motoshige Shimizu: Matching-Based Cercospora Leaf Spot Detection in Sugar Beet.The 7th International Conference on Agricultural, Biotechnology, Biological and Biosystems Engineering (ICABBE2013), pp.2014-2020, Switzerland, Zurich, July 30-31, 2013.

3. Rong Zhou, Shun'ichi Kaneko, Fumio Tanaka, Miyuki Kayamori, Motoshige Shimizu: Early Detection and Continuous Quantization of Plant Disease Using Template Matching and Supporter Vector Machine Algorithms. The 1st International Workshop on BioImage Recognition (BIR2013), pp.300-304, Matsuyama, Japan, December 4-6, 2013.

4. Rong Zhou, Shun'ichi Kaneko, Fumio Tanaka, Miyuki Kayamori, Motoshige Shimizu: Robust Detection of Cercosporo Leaf Spot of Sugar Beet in Real Field. 2014 ASABE and CSBE/SCGAB Annual International Meeting (ASABE2014), pp.1-6, Montreal, Canada, July 13-16, 2014.

## A.3 Japan Conferences

1. Rong Zhou, Shun'ichi Kaneko, Fumio Tanaka, Miyuki Kayamori, Motoshige Shimizu: Detecting Cercospora Leaf Spot in Sugar Beets Based on Robust Matching Algorithm. Hokkaido University Symposium on Alliance of Young Researchers in Information Science and Technology, pp.222-224, Sapporo, Japan, March 7-8, 2013.

2. Rong Zhou, Shun'ichi Kaneko, Fumio Tanaka, Miyuki Kayamori, Motoshige Shimizu: Detecting Cercospora Leaf Spot in Sugar Beets Based on Robust Matching Algorithm. The 19th symposium on Sensing via Image Information (SSII2013), IS3-03, pp.1-7, Yokohama, Japan, June 12-14, 2013.

3. Rong Zhou, Shun'ichi Kaneko, Fumio Tanaka, Miyuki Kayamori, Motoshige Shimizu: Early Detection of Cercospora Leaf Spot in Sugar Beet By Matching-based Method. Hokkaido University Symposium on Alliance of Young Researchers in Information Science and Technology, pp.131-132, Sapporo, Japan, November 28-29, 2013.

4. Rong Zhou, Shun'ichi Kaneko, Fumio Tanaka, Miyuki Kayamori, Motoshige Shimizu: Robust Matching and Segmentation Algorithm for Detecting Cercosporo Leaf Spot in Sugar Beet under Real Field Conditions. The Annual Meeting of Phytopathological Society of Japan (PSJ), abstract (no.474) in page 122, Sapporo, Japan, June 2-4, 2014.